STEM CELLS, SCAFFOLDS AND SMALL MOLECULES FOR ORTHOPEDIC TISSUE REGENERATION

by
Okhee Jeon

A dissertation submitted to Johns Hopkins University in conformity with the requirements for the degree of Doctor of Philosophy

Johns Hopkins University
Baltimore, Maryland
May, 2017

Abstract

Orthopedic tissue regeneration would benefit the aging population or patients with large osteoporotic large bone fracture and degenerative cartilage diseases, especially osteoarthritis (OA). Despite progress in surgical and pharmacological interventions, new regenerative approaches are needed to meet the challenge of restoring bone and articular cartilage tissues that are not only structurally sound but also functional. The following work explores two promising therapeutic strategies for orthopedic tissue regeneration: "*ex vivo* tissue engineering" to engineer bone tissue constructs with smart combinations of stem cells and biomaterials and "small molecule-based *in vivo* regenerative approach" to i) promote the chondrogenic potential of endogenous progenitor cells and ii) eliminate abnormal cells – senescent cells (SnCs) – that develop with OA.

The *ex vivo* tissue engineering focused on the development of functional bone like-tissue by co-culturing human induced pluripotent stem cells-derived osteoblasts (OB) and osteoclasts (OC) in hydroxyapatite (HA)-based three dimensional scaffolds. Results showed 3D bone model comprising both cell types promote bone formation compared to OB only cultures in a HA-dose dependent manner via coupling signals coordinating osteoblast and osteoclast activity and finely tuned expression of inflammatory molecules. The first small molecule approach for cartilage regeneration that was explored involved carbohydrate-based OA drug, tri-butanoylated N-acetyl-D-galactosamine analog, as a inducer of chondrogenic differentiation of hMSCs and inhibitor of inflammation. The second drug-based therapy is intra-articular (IA) injection of a senolytic molecule that selectively killed SnCs. This work explores the role of SnCs in the disease progression of post-traumatic and naturally-occurring OA and how eliminating SnCs can slow OA

development. It was found SnCs accumulate in the articular cartilage after anterior cruciate ligament transection (ACLT) and selective elimination of these cells attenuated the development of OA, reduced pain, and increased cartilage development. The three therapies presented in this dissertation represent viable strategies for bone and articular cartilage regeneration.

Thesis Committee:

Jennifer Elisseeff, Ph.D. (Advisor, Reader)

Professor, Biomedical Engineering, Director, Translational Tissue Engineering Center,

Johns Hopkins University School of Medicine

Jordan Green, Ph.D. (Thesis chair, Reader)

Associate Professor of Biomedical Engineering, Ophthalmology, Oncology,

Neurosurgery, and Materials Science & Engineering, Johns Hopkins University School of Medicine

Patrick Cahan, Ph.D.

Assistant Professor of Biomedical Engineering, Institute of Cell Engineering

Johns Hopkins University School of Medicine

Judith Campisi, Ph.D.

Professor of Buck Institute for Research on Aging and Lawrence Berkeley National

Laboratory

Acknowledgements:

I want to thank Dr. Jennifer Elisseeff for all her guidance in research in tissue engineering and small molecules for orthopedic regeneration and industry and clinical outlook. It was a great honor to be able to work with her and learn about collaborations between industry and academia. I would also like to thank Dr. Green and Dr. Cahan for giving me valuable comments on my thesis project. Lastly, I want to thank Dr. Campisi for providing me wonderful insight into cellular senescence, which is helpful for me to proceed my thesis project regarding targeting senescent cells for osteoarthritis treatment. I also really appreciate my wonderful mentors and members in the Elisseeff Lab: Chaekyu Kim, Nicole Lu and Jeremy Chae. The work presented in this dissertation would not have been possible without Dr. Feldman in university of Maryland school of medicine, Dr. Yarema in Johns Hopkins University, Remi Laberge, Alain Vasserot and Nathaniel David at Unity Biotechnology in San Francisco, Marco Demaria at Buck institute, Dr. Baker and Dr. van Deursen at Mayo clinic and Dr. Santambrogio and Dr. Clement at Albert Einstein medical school. These all people inspired and challenged me to always be better than myself, scientifically and I am incredibly grateful for this.

During the past five years at Hopkins, I have made amazing friends that have emotionally supported me and I appreciate for this. Lastly, I want to thank my mom, dad and younger sister to have provided encouragement, love and continuous emotional support and have been a constant source of my determination. 엄마 아빠 그리고 동생 민정이 너무 감사합니다!

Table of Contents:

List of Tables:

Table 1. List of human primer sequences used for gene expression in RT-PCR analysis

Gene *(Human)*	Forward Sequence (5'-3')	Reverse Sequence (5'-3')
nfatc1	TCTCAGGAGTGAAAGCATTGCACATA	AATGCTATGACCGAATGCAGCAGTTA
rankl	CCAAGATCTCCAACATGACT	TAC ACCATTAGTTGAAGATACT
catk	CAGTGAAGAGGTGGTTCAGA	AGAGTCTTGGGGCTCTACCTT
ctr	TCTCAGGAGTGAAAGCATTGCACATA	AATGCTATGACCGAATGCAGCAGTTA
trap5b	TTCTACCGCCTGCACTCCAA	AGCTGATCTCCACATAGGCA
col10a1	GGAATGCCTGTGTCTGCTTT	TGGGTCATAATGCTGTTGCC
col1a1	GCTGGTCACCATGGTGATCAAGG	TACCAGGATGTCCAGTGCGAC
runx2	CTTCACAAATCCTCCCAGTAGCTA	GGTTTAGAGTCATCAAGCTTCTGTCT
ocn	GTGACGAGTTGGCTGACC	TGGAGAGGAGCAGAACTGG
alp	CACGGGCACCATGAAGGAAAA	ATTCTCTCGTTCACCGCCCAC
sox9	GCATGAGCGAGGTGCACTC	TCTCGCTTCAGGTCAGCCTTG
acan	TGGGAACCAGCCTATACCCCAG	CAGTTGCAGAAGGGCCTTCTGTAC
c/ebp α	TCACCGCTCCAATGCCTA	CCTGCTCCCCTCCTTCTCTCA
fabps	ACAGGAAAGTCAAGAGCACCATAA	TGACGCATTCCACCACCAGTT
lpl	GTCAGAGCCAAAAGAAGCAGC	GGGTTTCACTCTCAGTCCCAG
il6	CCCCTGACCCAACCACAAAT	ATTTGCCGAAGAGCCCTCAG
il1β	GGACAAGCTGAGGAAGATGC	TCGTTATCCCATGTGTCGAA
tnf α	GGACAAGCTGAGGAAGATGC	TCGTTATCCCATGTGTCGAA
opg	GCTAACCTCACCTTCGAG	TGATTGGACCTGGTTACC
opn	GACACATATGATGGCCGAGGTGATAG	GGTGATGTCCTCGTCTGTAGCATC
cdkn2a	AATCTCCGCGAGGAAAGC	GTCTGCAGCGGACTCCATS
mmp3	TTCTGGGCTATACGAGGGCA	CTTCTTCACGGTTGCAGGGA
il6	GCTACCAAACTGGATATAATCAGGA	CCAGGTAGCTATGGTACTCCAGAA
mmp13	GGAGCCCTGATGTTTCCCAT	GTCTTCATCGCCTGGACCATA
il1β	GTATGGGCTGGACTGTTTC	GCTGTCTGCTCATTCACG
sox9	ACCCACAGCTCCCCTGAAG	CTCACCTTCAGTGGCAAGAGC
COL II	CCTCCGTCTACTGTCCACTGA	ATTGGAGCCCTGGATGAGCA
Aggrecan	CGTTGCAGACCAGGAGCAAT	CGGTCATGAAAGTGGCGGTA
β-actin	CAACCGTGAAAAGATGACCC	GTAGATGGGCACAGTGTGGG

Table 2. List of mouse primer sequences used for gene expression in RT-PCR analysis

Gene ***(Mouse)***	**Forward Sequence (5'-3')**	**Reverse Sequence (5'-3')**
$p16^{INK4a}$ (cdkn2a)	AATCTCCGCGAGGAAAGC	GTCTGCAGCGGACTCCATS
p21 (cdkn1a)	ATTCCATAGGCGTGGGACCT	TCCTGGGCATTTCGGTCAC
mmp3	TTCTGGGCTATACGAGGGCA	CTTCTTCACGGTTGCAGGGA
il6	GCTACCAAACTGGATATAATCAGGA	CCAGGTAGCTATGGTACTCCAGAA
mmp13	GGAGCCCTGATGTTTCCCAT	GTCTTCATCGCCTGGACCATA
il1β	GTATGGGCTGGACTGTTTC	GCTGTCTGCTCATTCACG
sox9	ACCCACAGCTCCCCTGAAG	CTCACCTTCAGTGGCAAGAGC
Col2a1	CCTCCGTCTACTGTCCACTGA	ATTGGAGCCCTGGATGAGCA
Aggrecan (acan)	CGTTGCAGACCAGGAGCAAT	CGGTCATGAAAGTGGCGGTA
Runx2	GCCGGGAATGATGAGAACTA	GGTGAAACTCTTGCCTCGTC
Osteocalcin (bglap)	GGCGCTACCTTGGGTAAGTG	GACCACTCCAGCACAACTCC
ctsk	GCACCCTTAGTCTTCCGCTC	ACCCACATCCTGCTGTTGAG
rankl	GAGCACGAAAAACTGGTCGG	AGGGTTGGACACCTGAATGC
opg	CAGCCATTTGCACACCTCAC	TTAGAGATCTTGGCCCAGCC
β-actin	CAACCGTGAAAAGATGACCC	GTAGATGGGCACAGTGTGGG

List of Figures:

List of Abbreviations:

Human induced pluripotent stem cells (hiPSC)

Poly(lactic-co-glycolic acid) (PLGA)

Poly(L-lactic acid) (PLLA)

Hydroxyapatite (HA)

Mesenchymal stem cells (MSCs)

Osteoblasts (OB)

Osteoclasts (OC)

Calcium phosphate (CaP)

Embryonic body (EB)

Three dimensional (3D)

Human embryonic stem cells (hESC)

Osteoprotegerin (OPG)/ receptor activator of nuclear factor κB ligand (RANKL)

Interleukin (il)

Tumor necrosis factor α (TNFα)

alkaline phosphatase (ALP),

runt-related transcription factor 2 (RUNX2)

fatty acid binding protein (FABP)

lipoprotein lipase (LPL)

CCAAT-enhancer-binding proteins (C/EBPα)

macrophage colony-stimulating factor (M-CSF)

Tartrate-resistant acid phosphatase (TRAP)

nuclear factor-activated T cells c1 (NFATC1)

Calcitonin receptor (CTR)

Cathepsin K (CATK)

Osteopontin (OPN)

Basic fibroblast growth factor (b-FGF)

Osteoarthritis (OA)

Tri-butanoylated N-acetyl-D-galactosamine analog (3,4,6-*O*-Bu_3GalNAc)

Disease-modifying OA drugs (DMOADs)

Medial meniscal transection (MMT)

Osteoarthritis Research Society International (OARSI)

Nonsteroidal anti-inflammatory drugs (NSAID)

Intra-articular (IA)

Extracellular matrix (ECM)

Bone morphogenetic protein 7 (BMP-7)

Nuclear factor-κB (NF-κB)

Transforming growth factor-β1 (TGF-β1)

Glycosaminoglycans (GAG)

Immunohistochemistry (IHC)

Real-Time Polymer Chain Reaction (RT-PCR)

Complementary DNA (cDNA)

Post-traumatic OA (PTOA)

Senescent associated secretory phenotype (SASP)

Matrix metallopeptidases (MMP)

Synovial fluid (SF)

Senescent Cells (SnCs)

Non- Senescent Cells (non-SnCs)

Senescence-associated beta-galactosidase (SA-β-gal)

Renilla luciferasee (rLUC)

Monomeric red fluorescent protein (mRFP)

Herpes simplex virus thymidine kinase (HSV-TK)

Pharmokinetics (PK)

Anterior cruciate ligaments transection (ACLT)

Half-Maximal Inhibitory concentration (IC50)

Ganciclovir (GCV)

Phosphate-buffered saline (PBS)

Penicillin and streptomycin (Pen/Strep)

Dulbecco's modified Eagle's medium (DMEM)

Fetal bovine serum (FBS)

high-mobility group box 1 (HMGB1)

proliferating cell nuclear antigen (PCNA)

5-ethynyl-20-deoxyuridine (EdU)

sulfated glycosaminoglycans (sGAG)

Chapter 1: Introduction to Thesis

1.1 Introduction

Most of the current strategies in bone tissue engineering involve the cultivation of OB derived from human bone marrow MSCs on 3D alloplastic materials (primarily calcium phosphate, CaP) prior to re-implantation. However, this approach fails to emulate physiological bone regeneration involving a well-orchestrated series of cytokines and regulatory molecules secreted from immune cells, including monocytes, macrophages, and OC [1, 2]. We hypothesize that OB and OC—and their respective bone-building and -resorbing activities—must be balanced on bone-like synthetic scaffolds to create such bone substitutes. hiPSCs constitute an exciting prospective cell source for engineering bone [3], as they can generate patient- or disease-specific mesenchymal and monocyte/macrophage precursors that in turn differentiate into OBs and OCs, respectively. *The purpose of Aim 1 is to engineer functional bone like-tissue constructs by co-culturing hiPSC-MSC and -macrophages.* From a translational standpoint, our 3D tissue-engineered bone using patient-specific iPSCs could capture the functional interplay between osteoclastic and osteoblastic activities and thus, it could be used in understanding of bone cell phenotypes in the pathology of bone disease and in the testing of drugs regulating bone homeostasis.

OA is a chronic disease characterized by degeneration of cartilage tissue that lines articulating joint surfaces, leading to pain and physical disability [4]. Current pharmacologic OA treatment options are analgesics, non-steroidal anti-inflammatory drugs, and viscosupplementation (e.g. hyaluronic acid) with IA injections [5]. These

treatments focus on short-term symptomatic pain relief and care of joint function[6], however with advances in the understanding of the OA pathogenesis there is a focus now on disease-modifying OA drugs (DMOADs) designed to block or reverse OA progression by targeting specific OA catabolic pathways and pathophysiological signaling pathways [7, 8].

The inflammatory cytokines and catabolic regulators present in an OA joint disrupt the chondrogenic differentiation capabilities of the MSCs and reduce cartilage regenerative capacity[9, 10]. Therefore, there is a critical need for small-molecules drug to not only reduce inflammation in the local joint environments but also rebuild cartilage tissue by creating favorable conditions for drugs to act on endogenous MSCs on the cartilage tissue. *The goal of Aim 2 is to investigate a therapeutic effect of the new carbohydrate-based disease-modifying OA drug, tri-butanoylated N-acetyl-D-galactosamine analog (3,4,6-O-Bu3GalNAc), for cartilage repair by inducing cartilage tissue production by human MSCs and inhibiting inflammatory response of human OA chondrocytes.*

The incidence of OA correlates directly with aging and joint trauma, but the underlying mechanisms remain unclear, impeding the development of therapeutic interventions that might prevent or treat the disease. Cellular senescence, a mechanism that prevents proliferation of damaged and dysfunctional cells, protects against cancer development [11, 12] but also contributes significantly to cell and tissue deterioration that underlies age-related pathologies[13]. SnCs accumulate in tissues and organs with aging where they progressively disrupt organ structure and function, presumably through the secretion of a senescence-associated secretory phenotype (SASP) that includes

extracellular matrix proteases, pro-inflammatory molecules, and growth factors [14]. While the accumulation of SnCs has been associated with OA [15, 16], the underlying mechanisms and details of SnCs impact on the OA progression – whether or which tissues in the arthritic joints become senescent, their kinetics of accumulation, and the removal of SnCs to attenuate or reverse OA. *Thus, the goal of Aim 3 is to develop a novel pharmacological approach that aims to eliminate SnCs in a joint for cartilage regeneration.*

1.2 Specific Aims of thesis

To achieve these goals, we propose the follow aims **(Fig 1.1)**;

Aim 1: Engineering bone tissue from hiPSC-derived osteoblast and osteoclast lineages in 3D biomaterials

Hypothesis: *Incorporation of hiPSC-macrophage and osteoclast responsible for bone matrix remodeling to osteoblasts accelerates the maturation of bone compared with osteogenic cells alone.*

Aim 2: Promoting chondrogenesis by local delivery of a sugar analog for cartilage repair

Hypothesis: *The sugar analog 3,4,6-O-Bu3GalNAc promotes chondrogenesis of human MSC and reduces inflammation of human OA chondrocytes by modulating Wnt/β-catenin signaling.*

Aim 3: Targeting senescent cells in trauma-induced degenerative joints for cartilage repair

Hypothesis: *Trauma and aging induces SnCs in the articular joint and removal of SnCs in the model trauma-induced and aging-related OA reduces the disease progression of OA and related pain.*

1.3 Figures

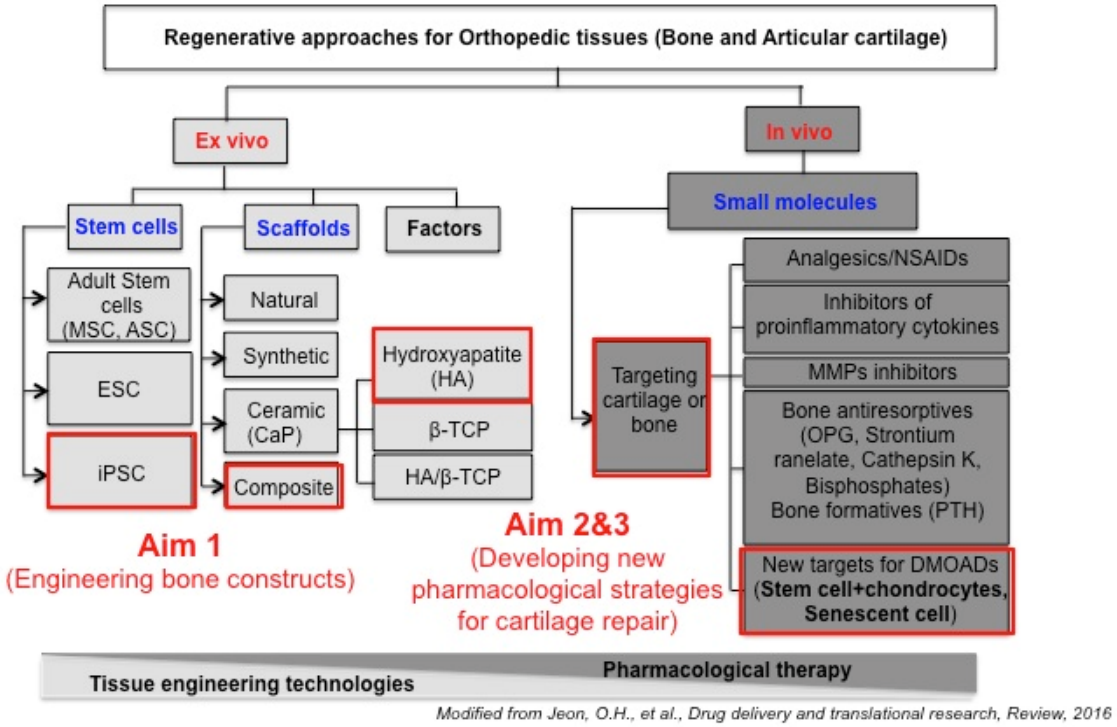

Figure 1.1 Schematic representation of two promising regenerative approaches for orthopedic tissues for bone and articular cartilage. *ex vivo* tissue engineering uses smart combination of stem cells, scaffold-based biomaterials and growth and differentiation factors (in Aim 1 in this dissertation) and small molecule-based *in vivo* regenerative approaches include targeting endogenous chondrocyte progenitor cells located in articular cartilage (in Aim 2) or another cell type, senescent cells (in Aim 3).

1.4 References

[1] R.P. Pirraco, A.P. Marques, R.L. Reis, Cell interactions in bone tissue engineering, J Cell Mol Med 14(1-2) (2010) 93-102.

[2] M. Mehta, K. Schmidt-Bleek, G.N. Duda, D.J. Mooney, Biomaterial delivery of morphogens to mimic the natural healing cascade in bone, Advanced drug delivery reviews 64(12) (2012) 1257-76.

[3] X.X. Lou, Induced Pluripotent Stem Cells as a new Strategy for Osteogenesis and Bone Regeneration, Stem Cell Rev Rep 11(4) (2015) 645-651.

[4] R.F. Loeser, S.R. Goldring, C.R. Scanzello, M.B. Goldring, Osteoarthritis: a disease of the joint as an organ, Arthritis Rheum 64(6) (2012) 1697-707.

[5] H.A. Wieland, M. Michaelis, B.J. Kirschbaum, K.A. Rudolphi, Osteoarthritis - an untreatable disease?, Nat Rev Drug Discov 4(4) (2005) 331-44.

[6] J. Martel-Pelletier, L.M. Wildi, J.P. Pelletier, Future therapeutics for osteoarthritis, Bone 51(2) (2012) 297-311.

[7] F.J. Blanco, C. Ruiz-Romero, New targets for disease modifying osteoarthritis drugs: chondrogenesis and Runx1, Ann Rheum Dis 72(5) (2013) 631-4.

[8] D.J. Hunter, Pharmacologic therapy for osteoarthritis--the era of disease modification, Nat Rev Rheumatol 7(1) (2011) 13-22.

[9] M. Lotz, F.J. Blanco, J. von Kempis, J. Dudler, R. Maier, P.M. Villiger, Y. Geng, Cytokine regulation of chondrocyte functions, J Rheumatol Suppl 43 (1995) 104-8.

[10] J.P. Pelletier, J. Martel-Pelletier, S.B. Abramson, Osteoarthritis, an inflammatory disease: potential implication for the selection of new therapeutic targets, Arthritis Rheum 44(6) (2001) 1237-47.

[11] J. Campisi, Aging, cellular senescence, and cancer, Annu Rev Physiol 75 (2013) 685-705.

[12] J. Campisi, Cancer, aging and cellular senescence, In Vivo 14(1) (2000) 183-8.

[13] J.M. van Deursen, The role of senescent cells in ageing, Nature 509(7501) (2014) 439-46.

[14] J.P. Coppe, P.Y. Desprez, A. Krtolica, J. Campisi, The senescence-associated secretory phenotype: the dark side of tumor suppression, Annu Rev Pathol 5 (2010) 99-118.

[15] K. McCulloch, G.J. Litherland, T.S. Rai, Cellular senescence in osteoarthritis pathology, Aging Cell (2017).
[16] J.A. Martin, T. Brown, A. Heiner, J.A. Buckwalter, Post-traumatic osteoarthritis: the role of accelerated chondrocyte senescence, Biorheology 41(3-4) (2004) 479-91.

Chapter 2. Engineering bone tissues from human iPSC-derived osteoblast and osteoclast lineages in 3D scaffolds

2.1 Introduction

Bone grafting is required to facilitate repair and regeneration of bone defects resulting from severe fracture in elderly osteoporosis patients, trauma, tumor ablation, or congenital abnormalities. Autologous grafts are regarded as the current gold standard, but due to their significant limitations bone tissue engineering has been explored as a promising alternative to autologous grafts [1, 2]. Most of the current strategies in bone tissue engineering involve the cultivation of osteoblasts (OB) derived from human bone marrow mesenchymal stem cells (MSCs) on 3D alloplastic materials (primarily calcium phosphate, CaP) prior to re-implantation [3] **(Fig 2.1)**. However, this approach fails to emulate physiological bone regeneration involving a well-orchestrated series of cytokines and regulatory molecules secreted from immune cells, including monocytes, macrophages, and osteoclasts (OC) **(Fig 2.1)**. An orchestrated performance of these molecules is required to mimic functional and structural intricacies of native bone, to integrate with the host environment, and to establish mechanical stability of the bone substitutes [4, 5]. Thus, recreating the complex interplay between bone and immune cells in engineered substitutes may be necessary to create a functional tissue, rather than just to induce bone formation. We hypothesized that OBs and OCs—and their respective bone-building and -resorbing activities—must be balanced on bone-like synthetic scaffolds to create such bone substitutes.

Human induced pluripotent stem cells (hiPSC) constitute an exciting prospective cell source for engineering bone, as they can generate patient- or disease-specific mesenchymal and monocyte/macrophage precursors that in turn differentiate into OBs and OCs, respectively [6] **(Fig 2.2)**. hiPSCs have been differentiated into OBs on 2D plastic and 3D CaP scaffolds [7-11] and produced dense bone matrix on 3D decellurized bone scaffolds in a perfusion bioreactor [12]. OCs have been generated from hiPSCs on 2D plastic and on mineralized substrates by embryonic body (EB) formation [13] and by co-culturing with stromal cells [14]. Nevertheless, to our knowledge, these derived OB and OC precursors have not been co-cultured to capture the functional coupling of bone resorption and formation that is typical of living bone.

Taking cues from natural bone tissue, the goal of this study was to engineer functional bone like-tissue constructs by co-culturing hiPSC-MSC and hiPSC-macrophages. Our previous work defined optimal scaffold compositions and tissue quality of bone engineered from human embryonic stem cells (hESC) [15, 16]. In the present work, we first differentiated hiPSC-derived MSCs and macrophages into osteogenic and osteoclastogenic lineages, respectively, and established a 3D model of human bone by co-culturing these cells within HA-based scaffolds. We then explored bone formation and resorption *in vitro* and in a subcutaneous implantation model. We also studied molecular changes to identify the coupling signals and inflammatory molecules responsible for coordinating OB and OC activities.

2.2 Materials and Methods

EB formation from hiPSC

The MJ hiPSC used in this study were derived from a healthy individual and have been previously described [17]. For embryoid body (EB) formation, hiPSC were detached from plates and transferred to six-well ultra-low-attachment plates. To differentiate three germ layers *in vitro*, EBs were maintained in EB culture medium for 15–20 days with half of the medium changed every other day. EB medium consisted of DMEM-F12 (Invitrogen), 20% (v/v) Knockout Serum Replacement (Invitrogen), 1 mM L-glutamine, 0.1 mM β-mercaptoethanol (β-ME), and 1X nonessential amino acids (NEAA) [17].

Differentiation (adipogenic, chondrogenic, and osteogenic) and characterization of MSCs from hiPSCs

To generate mesenchymal progenitors, the EBs were transferred onto tissue culture plates coated with gelatin (0.1% w/v) and cultured for 10 additional days until the outgrowth from the EBs occurred in MSC growth medium consisting of DMEM (Invitrogen) supplemented with 10% FBS (Hyclone), 1% Glutamax (Invitrogen), 100 U/ml penicillin-streptomycin (Invitrogen), and 8 ng/mL basic fibroblast growth factor (bFGF) (PeproTech). Migrating cells isolated from EBs were subcultured at an initial cell density of 2 x 10^4 cells/cm^2 and subsequently expanded as MSCs under the same conditions (3 - 5 passages used for all experiments).

For adipogenic differentiation, we cultured the hiPSC-derived MSCs at 1 x 10^4 cells/cm^2 for three weeks in adipogenic media consisting of DMEM, 10% FBS, 100 U/ml

penicillin-streptomycin, 1 μM dexamethasone, 100 μM indomethacin, 500 μM 3-isobutyl-1-methtlxanthine (IBMX), and 10 μg/ml Insulin (all from Sigma). To evaluate adipogenesis, lipid droplets were stained with 30 mg/ml oil red O (Sigma-Aldrich) in 60% isopropanol after fixation of cells with 10% formaldehyde.

Chondrogenic differentiation of hiPSC-MSCs was evaluated in 3D micromass cultures. Cells (5 x 10^4) were seeded in the 96-well MicroWell™ round bottom plate (Thermo Fisher Scientific) and the 3D micromass was formed in the bottom by centrifuging at 2000 rpm for 5 min. The micromass was maintained at 37°C with 5% CO_2 in the chondrogenic media consisting of DMEM, 10% FBS, 100 U/ml penicillin-streptomycin, 1% ITS premix (BD Bioscience), 100 mM sodium pyruvate (Life Technologies), 40 mg/ml L-proline (Sigma), 50 mM ascorbic acid-2-phosphate, and 10 ng/mL of transforming growth factor-β1 (TGF-β1) (PeproTech). To evaluate chondrogenesis, the micromass was harvested after 4 weeks, fixed in 4% paraformaldehyde overnight, dehydrated in increasing concentrations of ethanol, embedded with paraffin, and sectioned at 5 μm. The amount of proteoglycans was evaluated by aqueous Safranin-O (0.1%) using standard procedures.

For osteogenic differentiation, 1 x 10^4 hiPSC-derived MSCs were cultured for 3 weeks in osteogenic media composed of DMEM, 10% FBS, 10% FBS, 100 U/ml penicillin-streptomycin, 100 nM dexamethasone, 10 mM β-glycerophosphate, and 0.1 mg/mL ascorbic acid-2-phosphate (all from Sigma). To assess osteogenic potential (calcium deposition), cells were fixed with 10% formaldehyde, rinsed with distilled water, and stained with Alizarin red [Sigma; 0.5% (v/v) in distilled water (pH 4.2)] for 10 min. For ALP staining, cells were rinsed with Tyrode's balanced salt solution, fixed with

citrate-buffered acetone, and incubated in a mixture of fast violet B salt (Sigma) and naphthol AS-MX phosphate (3-(Phosphonooxy)-N-(2,4-xylyl)naphthalene-2-carboxamide) solution (Sigma).

Differentiation and characterization of osteoclastogenic monocytes/macrophages from hiPSCs

Directed differentiation of hiPSC to monocytes/macrophages was carried out as previously described [18, 19]. Briefly, for EB formation, hiPSCs were detached from plate and feeder cells by treatment with 0.2% dispase for 4 min and were collected by scraping. The hiPSCs were transferred into 6-well, ultra-low-attachment plates (Costar) in EB culture medium and were cultured for 4 d at 37°C. For monocyte differentiation, 4–10 large EBs were transferred into gelatin-coated six-well plates containing monocyte differentiation media comprised of DMEM, 10% FBS, 50 ng/mL human macrophage colony-stimulating factor (hM-CSF) (PeproTech), 25 ng/mL human IL-3 (PeproTech), 1 mM L-glutamine, 1× NEAA, and 0.1 mM β-ME. Continuous monocyte production started within 15-20 d and monocytes were harvested every 4–5 d for 2 months [17].

For macrophage differentiation, monocytes harvested from EB factories were resuspended in macrophage differentiation medium comprised of RPMI, 10% FBS, 100 ng/mL hM-CSF, glutamine, and 100 U/ml penicillin-streptomycin and plated at a density of 3 - 5 × 10^4 cells in 24 well plates or Corning^R osteo assay surface 96-well plates, changing the media once in two days. For osteoclast differentiation, after 3 days of seeding, we added 100 ng/ml recombinant human soluble RANK ligand in macrophage differentiation medium for 3 weeks. Osteoclastogenic potential was assessed by TRAP

and CATK-positive osteoclastic cells. Resorbed calcium phosphate was visualized by Von Kossa staining after the removal of all cells on osteo assay surface 96-well plates. Briefly, the plates were stained with 5% silver nitrate solution under ultraviolet light for 15 min, washed three times with distilled water, and incubated with 5% sodium thiosulfate for 5 min at room temperature under regular light to quench unreacted silver. Then images were acquired by using a light microscope. In addition, iPSC-osteoclasts were stained for cathepsin K using mouse anti-cathepsin K (Millipore) and for F-actin using Alexa fluor 568 phalloidin (Life technologies).

Polymer scaffold preparation

The HA composite scaffolds composed of a 1:1 ratio of poly(lactide-*co*-glycolide) (PLGA) (Sigma, Mw ≈ 30 kDa) and poly(L-lactic acid) (PLLA) (Sigma, Mw ≈ 55 kDa) were fabricated by salt-leaching method, as described previously [15]. Briefly, PLGA and PLLA (1:1) were dissolved in chloroform to yield a solution of 5% (w/v) polymer with or without HA particles (Sigma, 1% or 5% w/v). Sponges (1 x 1 x 0.5 cm^3) were sterilized overnight in 75% (v/v) ethyl alcohol overnight, washed three times with PBS, and coated with fibronectin (10 ng/ml) for 3 h before cell seeding.

Flow cytometry

hiPSC-MSCs, -monocytes, and -macrophages were harvested and resuspended to 3 x 10^5 cells in 50 µl of PBS containing 0.1% BSA. Cells were separately labeled with phycoerythrin (PE)-conjugated mouse anti-human antibody CD44 (Millipore), CD68 and CD73 (Pharmingen), FITC-conjugated mouse anti-human antibody CD105, CD45 (Pharmingen), and CD115 (Millipore), and APC-conjugated mouse anti-human antibody

CD14 and CD68 (Pharmingen) on ice for 30 min. An isotype-matched mAb was used as a control (Becton Dickinson). Data were analyzed with the BD Accuri^{TM} C6 flow cytometer and FlowJo X 10.0 software (Becton Dickinson).

RNA extraction and real-time RT-PCR

Total RNA was extracted from cells, micromass, and HA composite scaffolds using Trizol reagent (Life Technologies) and cDNA was synthesized by using Superscript(R) II reverse transcriptase following the manufacturer's protocol (Invitrogen, Carlsbad, CA). Real-time PCRs were performed using StepOnePlus(R) Real Time PCR System (Applied Biosystems, Carlsbad, CA) with SYBR Green PCR Master Mix (Life Technologies). The relative expression of each target was calculated using the ΔΔCT method and β-actin were used as endogenous references. All expression levels of samples were normalized to controls. The PCR primers used for RT-PCR are listed in **Table 1**. Expression of all markers was normalised to the expression of the housekeeping gene β-actin.

Osteocalcin and TRAP 5b ELISA assay

The osteocalcin ELISA assay was performed with the MicroVue Osteocalcin EIA Kits (Cat 8002; Quidel) following the manufacturer's instructions. The TRAP ELISA assay was performed with the BoneTRAP (TRACP 5b human) ELISA (Cat SB-TR201R; ids) following the manufacturer's instructions. For assaying the osteocalcin and TRAP released from HA composite scaffolds, a serum-free medium was used 48 h before protein harvest. Optical density was measured at 405nm using the microplate reader (Biotek). Samples were analyzed in triplicate for secreted soluble osteocalcin and TRAP

using quadratic curve fit.

In vivo subcutaneous transplantation

hiPSC-derived MSCs were expanded (passage 4), seeded (1.5 x 10^6) onto the polymer sponges (1 x 1 x 0.5 cm^3), and cultured under MSC growth medium for 1 day. After treatment with an osteogenic-supplement dexamethasone and β-glycerophosphate and 10 nM 1α,25 dihydroxyvitamin D3 (Sigma) for 7 days, hiPSC-MSC/scaffolds were seeded with hiPSC-macrophages (passage 0; 1.5 x 10^6) and incubated for 5 days without osteogenic-supplements but containing 50 ng/ml M-CSF followed by co-culture in the presence of 100 ng/ml RANKL and 100 ng/ml M-CSF for another 5 days. The cell-seeded scaffolds were implanted subcutaneously into the dorsal region of 6-week-old athymic female nude mice (Charles River Laboratories; n = 18) and the skin was closed with a nylon suture. Constructs were harvested after 8 weeks and processed for histology. All procedures were performed under a pre-established protocol (The Johns Hopkins University Animal Care and Use Committee approved the animal procedures, protocol number MO14M126).

Histological analysis of explanted scaffolds

The tissue constructs were fixed in 10% formalin, embedded in optimum cutting temperature (OCT) compound (Tissue-Tek, Sakura Finetek), and cryosectioned (8 μm thick). The cryosections were immediately stained with hematoxylin and eosin, Masson's Trichrome, Alizarin Red S, Von Kossa, or TRAP or stored at -80°C until use. Images of Alizarin Red S and Von Kossa staining were quantified using ImageJ (NIH). Briefly, a

minimal intensity threshold was used to eliminate the background and then the stained Alizarin Red S and Von Kossa were measured as image % area coverage.

For immunohistochemistry, the sections were blocked with 20% normal goat serum in 2% BSA for 30 min, and incubated with rabbit polyclonal antibodies against osteocalcin (Millipore) (1:100 dilution), type I collagen (Abcam) (1:100 dilution), and cathepsin K (Biovision) (15 μg/ml dilution) at 4°C overnight. The sections were then incubated with Alexa Fluor 594 goat anti-rabbit secondary antibody H+L (Life Technologies) (1:300 dilution) or FITC-conjugated affinipure goat anti-rabbit secondary antibody H+L (Jackson Immunoresearch) (1:50 dilution) for 1 h and counterstained with DAPI (Chemicon) for 10 min. Human-specific nuclei staining was also performed with mouse IgG1 human lamin A+C (Abcam) (1:100 dilution) and goat anti-mouse Alexa fluor 488 (Life technology) (1:400 dilution). All images were collected with a Zeiss LSM Metal Confocal microscope. The intensity of osteocalcin and type II collagen was quantified as the integrated density subtracted from the mean fluorescence of background using the ImageJ software (NIH).

Statistical analysis

All analyses were performed in triplicate samples for $n = 3$ at least. Real time RT-PCR was also performed on triplicate samples ($n = 3$) with triplicate readings. Data are expressed as average +/- standard deviation and the statistical significance (P value) was determined by One-way analysis of variance (ANOVA) with the Turkey post hoc test using GraphPad Prism 5.

2.3 Results

Differentiation of osteoblasts and osteoclasts from hiPSCs

hiPSCs cultured in suspension as EBs for 1 week differentiated into mesenchymal precursor cells after 10 days on gelatin-coated tissue culture plates. Cells that isolated from outgrowth of EBs and then expanded in monolayer culture with MSC growth medium exhibited typical fibroblastic cell morphology **(Fig 2.3A)**, expression of MSC surface markers CD44, CD73, and CD105 **(Fig 2.3B)**, and the potential to differentiate into three different cell linages: osteoblast **(Fig 2.3C)**, chondrocyte **(Fig 2.3D)**, and adipocyte **(Fig 2.3E)**. Under osteogenic conditions, hiPSC-MSCs displayed bone-specific alkaline phosphatase (ALP), calcium deposition, and up-regulation of runt-related transcription factor 2 (*RUNX2*), type I and X collagen (*COLI* and *COLX*), and osteocalcin (*OCN*) genes during 14 days of monolayer culture **(Fig 2.3C)**. hiPSC-MSCs grown for 28 days in 3D micromass culture or monolayer culture under chondrogenic or adipogenic conditions, respectively, produced proteoglycans and accumulated lipid with up-regulation of *SOX-9* and *Aggrecan* **(Fig 2.3D)** as well as gene expression of fatty acid binding protein (*FABP*), lipoprotein lipase (*LPL*), and CCAAT-enhancer-binding proteins (*C/EBP*α) **(Fig 2.3E)**.

To induce OC from hiPSCs, we used a stepwise mono-culture approach based on our previous derivation strategy [18] involving EB formation **(Fig 2.4A, i)**, direct differentiation to monocytes **(Fig 2.4A, ii** and **iii)** and macrophages **(Fig 2.4A, iv)**, and differentiation into OCs **(Fig 2.4C)**. With this approach, hiPSCs cultured in suspension as EB for 10 days produced round, monocyte-like cells that arose from flattened EBs after

17 days with monocyte differentiation medium. Monocyte surface marker CD14 was expressed in more than 80% of collected cells floating in the culture medium **(Fig 2.4B)**. Monocytes were then differentiated into macrophages after plating onto adherent tissue culture plates for 5 days with macrophage differentiation medium supplemented with macrophage colony-stimulating factor (M-CSF) and IL-3. These cells had similar morphologies to spread-out macrophages **(Fig 2.4C, iv)** and expressed macrophage markers CD14, CD68, and CD115 **(Fig 2.4B)**.

Next, hiPSC-derived macrophages were cultured in the presence of RANKL and M-CSF, which are essential cytokines for osteoclast differentiation and survival. Fourteen days after RANKL stimulation, multinucleated (>3 nuclei) and tartrate-resistant acid phosphatase (TRAP)–positive OCs were observed, as well as resorptive pits left by OCs **(Fig 2.4C)**. In hiPSC-derived OCs, cathepsin K colocalized with F-actin—a cysteine protease secreted by OCs during bone resorption and a characteristic feature of those cells to appose the bony surface for matrix digestion—, indicating functional OCs.

Engineered 3D model of bone using both hiPSC-derived MSCs and macrophages

We developed a two-step culture approach to provide hiPSC-MSCs with a scaffold on which to differentiate into OBs and deposit bone like-matrix; then, OCs could be activated and survived. The goal was to co-culture hiPSC-MSCs and -macrophages committed to OB and OC lineages, respectively, on a HA-based 3D porous polyester composite scaffold. We reasoned that such a co-culture would mimic the *in vivo* bone environment and allow for natural crosstalk between bone cells.

Osteogenic supplements dexamethasone and β-glycerophosphate inhibit

monocyte differentiation into OC formation and their related function [20, 21]. Thus, we first focused on identifying an optimal culture regimen to ensure development of OC by inducing the differentiation of hiPSC-MSCs in medium with osteogenic supplements dexamethasone, β-glycerophosphate, and 1α,25-dihydroxyvitamin D_3 followed by co-culturing with hiPSC-macrophages either with (+) or without (-) osteogenic supplements in a monolayer. Co-culture without osteogenic supplements exhibited large multinucleated OCs with diameters of 50-100 μm embedded in OBs **(Fig 2.5A)** in contrast to co-culture with osteogenic supplements. In the absence of osteogenic supplements, there were significant increases in the expression of OC-related genes nuclear factor-activated T cells c1 (*NFATC1*), calcitonin receptor (*CTR*), and cathepsin K (*CATK*), as well as *RANKL*, which is expressed by OBs, compared to co-culture in osteogenic supplements **(Fig 2.5B)**. OB-related gene expression of *OCN* was higher for both hiPSC-derived cultures under the osteogenic supplements, which showed a typical high value due to the addition of osteogenic supplements. As a reference, the expression levels of all OC-related markers were not detected in the hiPSC-MSC mono-culture with and without osteogenic supplements. Thus, OCs could be differentiated from hiPSC-macrophages in osteogenic supplement–free medium when co-culturing with hiPSC-derived OBs.

The established monolayer co-culture method was then adapted for 3D tissue-engineered model of bone to evaluate whether crosstalk between these cells improves bone formation over existing mono-culture approaches **(Fig 2.5C)**. We first seeded hiPSC-MSCs onto the scaffolds with varying amounts of HA (HA-0, -1, and -5: poly(lactic-*co*-glycolic acid)/poly(L-lactic acid) (PLGA/PLLA) scaffold with 0%, 1%,

and 5% w/v HA, respectively). The cells were allowed to attach on the surface of the scaffolds and adapt to the new environment under MSC growth medium supplemented with basic fibroblast growth factor (b-FGF) for 2 days. Subsequently, the hiPSC-MSC-seeded scaffolds were differentiated into OBs by cultivation with osteogenic supplements for 7 days. The scaffold was then seeded with hiPSC-macrophages and incubated for an additional 5 days, without osteogenic supplements, but with M-CSF followed by RANKL and M-CSF for another 5 days. These cell-seeded scaffolds were either grown *in vitro* to develop bone tissue for analysis or implanted subcutaneously into athymic nude mice (an ectopic bone regeneration model).

Adding hiPSC-macrophages to hiPSC-MSCs accelerates *in vitro* bone tissue formation

In the engineered 3D constructs with only hiPSC-MSCs, after 28 days there was a noticeable increase in expression of OB-related genes, including *RUNX2*, *COLI*, *ALP*, *OCN* in HA-5 compared with no HA **(Fig 2.6A)**. When hiPSC-MSCs were co-cultured with hiPSC-macrophages in HA-5, there was a shift in osteogenic gene expression: increases in expression of osteopontin *(OPN)* and release of OCN as later stage of osteogenic markers [22] **(Fig 2.6A, B)**, with a concomitant decrease in early osteogenic markers *COLI* and *ALP* as well as *RUNX2* transcriptional expression. Co-cultured cells on HA-5 composite scaffolds produced more maturation of bone-specific matrix and mineralization than HA-1 and HA-0 scaffolds **(Fig 2.6C)**.

In HA-5 3D composite scaffolds with co-culture, hiPSC-macrophages appeared well-differentiated into OCs, as demonstrated by higher expression of *NFATC1*, *CATK*,

CTR, and *TRAP 5b* **(Fig 2.7A)** and TRAP 5b enzyme activity than HA-0 and -1 composite scaffolds **(Fig 2.7B)**. TRAP-positive OCs were observed at the construct edges or scaffold surfaces in the HA-containing co-culture scaffolds **(Fig 2.7C**, red arrowhead). As a reference, the expression levels of all OC-specific markers and TRAP activity were not detected in the hiPSC-MSC mono-culture under the same conditions, indicating that OC differentiation did not occur. Overall, the accelerated tissue development in the HA-based co-culture constructs suggests the important role of a dynamic interplay between OCs (TRAP activity) and OBs (OCN presence) in bone maturation.

hiPSC-MSC/-macrophage co-culture induces mature bone-like tissue formation *in vivo*

To determine whether hiPSC-MSCs co-cultured with hiPSC-macrophages within the 3D scaffold could maintain stable osteoblast and osteoclast lineage commitments and constitute functional bone tissues *in vivo*, we implanted constructs subcutaneously in athymic nude mice. Eight weeks after implantation, explanted scaffolds (lacking HA) from mono-cultured hiPSC-MSCs were filled with fibrous connective tissue, but did not have bone matrix deposition. However, hiPSC-MSCs on HA-5 composite scaffolds produced copious osseous tissue and high levels of OCN, COLI, and calcium deposition, resulting in faster bone formation than HA-0 and -1 composite scaffolds **(Fig 2.8A)**. In agreement with our *in vitro* finding, the co-culture constructs formed more mature bone with lamellar structure (H&E), organized collagen fibers (Masson's trichrome), more OCN and COLI production, and osteocytes embedded in mineralized extracellular matrix (Alizarin Red S and Von Kossa) in HA-5 composite scaffolds compared with the hiPSC-MSC mono-culture **(Fig 2.8A)**. Semi-quantitative analysis of these markers of bone

formation further confirmed that hiPSC-MSC/-macrophage on HA-5 composite scaffolds formed large areas of mineralized bone in the form of calcium and phosphate deposits with concomitant increases in OCN and COLI production, compared with mono-cultured hiPSC-MSCs **(Fig 2.8B)**. No evidence of teratoma around the site of implant was observed in any of the scaffolds at 8 weeks. We also confirmed the human origin of engineered bone tissues for all scaffolds by staining for human lamin A+C **(Fig 2.9)**.

We then analyzed functional behavior of OCs in the engineered bone constructs from hiPSC-MSC/-macrophage co-cultures *in vivo*. Histological examination revealed that TRAP-positive and CATK-expressing OCs in co-culture were more homogeneous and abundant, in a HA-dose dependent manner, compared with mono-cultured hiPSC-MSCs **(Fig 2.10)**. Mono-cultured hiPSC-MSCs showed similar, but much lower, production of the TRAP resorbing enzyme at the construct edges or surfaces of scaffolds than co-cultured hiPSC-MSC/-macrophage. These data point toward active bone resorption by osteoclastogenic hiPSC-macrophages in HA-containing scaffolds, as well as bone formation and functional maturation by hiPSC-derived OBs.

Coordinated hiPSC-derived OB and OC activity leads to engineered bone-like tissues

We next examined the molecular details of the pathways that accelerated bone-like tissue formation in our HA scaffolds. OPG/RANKL are key molecular coordinators expressed by OBs that regulate bone resorptive activity of OCs and are responsible for the homeostatic mechanism of bone remodeling [23]. RANKL stimulates OC precursors to commit to the OC phenotype by binding to its receptor RANK, which is present on

precursor and mature OCs. OPG is a suppressor of osteoclastic bone degradation by competing with RANK for binding of RANKL. In the engineered constructs from hiPSC-MSCs treated *in vitro* with osteogenic supplements for 28 days, the expression of *OPG* remained unchanged in varying HA concentrations while *RANKL* expression increased two fold in HA-5 composite scaffolds **(Fig 2.11A)**. However, the constructs with hiPSC-MSCs/-macrophages co-cultured showed a significant increase in both *OPG* and *RANKL* expression in HA-5 composite scaffolds. These data suggest that the high dose of HA prevents unintended, excessive hiPSC-macrophage osteoclastogenesis by increasing OPG production, which blocks the actions of RANKL in the co-culture. As a consequence, the ratio of *OPG/RANKL*, which determines the extent of OC activity [24], was close to 1 in HA-5 with hiPSC-MSC/-macrophage co-culture, further supporting balanced bone formation and resorption processes.

We also assessed several inflammatory molecules, expressed by OCs and their precursors, that bound directly to OB precursors to enhance the differentiation and function of OBs [25]. Co-culture systems with a higher percentage of HA resulted in a dose-dependent up-regulation of *IL-6* and *IL-1β* expression with no significant change in *TNFα* in all scaffolds **(Fig 2.11B)**. However, the expression of *IL-6*, *IL-1β*, and *TNFα* did not change markedly in all scaffolds when only hiPSC-MSCs were cultured under osteogenic conditions. Taken together, our findings suggest that co-cultured cells on the HA-based constructs induce coupling signals coordinating OB and OC activity, resulting in enhanced bone-like tissue formation.

2.4 Discussion

The field of tissue engineering is increasingly focused on harnessing hiPSCs and their derivatives with the combined use of biomaterials to build or regrow patient-specific tissues, such as bone. hiPSCs developed from a patient's own somatic cells have an indefinite potential to differentiate into all cell types residing in the human bone—osteoblast, osteocyte, and immune cells, such as monocytes, macrophages, and osteoclasts [6, 13]. However, current bone tissue engineering approaches, which primarily rely on the cultivation of MSCs as bone-forming osteoblast precursors, do not produce functional bone substitutes in a way akin to the physiological bone regeneration process. In the body, bone cells (mainly osteoblasts and osteoclasts) coordinate and balance their respective anabolic and catabolic processes to maintain functional equilibrium during the extracellular matrix remodeling process [26]. Thus, an attempt to recreate the crosstalk between these two cell types, using hiPSCs and biomaterial platforms, could produce functional and sophisticated bone substitutes.

Recent studies have similarly evaluated using hiPSCs for bone regeneration [7, 10, 11, 27-29]. However, our data highlighted the need for bone extracellular matrix remodeling that is modulating through immune cells being required for maturation of bone by including hiPSC-derived OCs in addition to OBs. We hypothesized that the formation of new bone *in vivo* requires a balance between the anabolic activity of osteoblasts and the catabolic function of osteoclasts. We report a novel 3D human bone model that was engineered by co-culturing hiPSC-derived MSCs and macrophages on HA-coated polymer scaffolds—cells and materials that together mimic both function and

structure of native human bone [10]. In our *in vitro* study, the composite scaffolds with higher percentage of HA not only induce the osteoclastic differentiation of hiPSC-Macrophage (by *NFATC1*, *CATK*, *CTR*, and *TRAP5b*) but also stronger osteogenic activity of hiPSC-MSCs compared to low HA or PLLA/PLGA alone. Notably, co-cultured cells with HA-based composites showed the expression level of *OCN* and *OPN* increased while early osteogenic markers including *COL1* and *ALP* decreased compared with mono-cultured hiPSC-MSC, indicating differentiation into mature OBs. Decreased *RUNX2* observed in co-cultured hiPSC-MSC/-macrophage on high-HA composites could be due to the temporal changes in its mRNA expression during osteogenesis [30].

Our ectopic bone formation model demonstrated that unlike the composite scaffolds containing low HA or without HA, where fibrous connective tissues are found throughout the constructs, in high-concentration HA scaffolds co-cultured hiPSC-MSC/-macrophage formed mature bone with lamellar collagen fibers and increased nonmineralized (by OCN and COLI) and mineralized bone matrix deposition. The underlying mechanisms appear to involve the balanced OPG/RANKL ratio that mediate the coordinated activity between actions of bone-building osteoblasts and bone-resorbing osteoclasts critical for bone remodeling [23]. Like our previous study [15], this could be attributed that special biochemical and biophysical cues created by the addition of HA particles preferentially direct the differentiation of hiPSC-MSCs/-macrophages into OBs and OCs, thereby allowing for functional engraftment of hiPSC-derived cells into engineered bone tissues.

Osteoblasts control the formation and activity of osteoclasts and, therefore, the resorption of bone through coupling mechanisms such as RANK, RANKL, and OPG [31, 32]. Conversely, as progenitors for OCs, macrophages and their monocyte precursors

play a pivotal, non-immunological regulatory role in bone formation, regeneration, and homeostasis *in vivo* [25, 33]. Indeed, bone-specific macrophages named osteal macrophages have been identified recently in human bone and secrete inflammatory molecules to facilitate bone formation and remodeling [34, 35]. There are also clinical reports that the inhibition of OC-mediated bone resorption by bisphosphonate administration in patients with osteoporosis developed osteonecrosis of the jaw [36], implying an important role of immune cells in supporting the bone repair and regeneration process. It is clear from our *in vitro* and *in vivo* studies that macrophages and differentiated OCs in combination with OBs are necessary for engineering mature bone-like tissues.

We also verified that bone-specific signaling pathways were reproduced in our engineered scaffold co-cultures. IL-6, for instance, is a potent cytokine secreted by osteoclasts and their precursors, which facilitates calvarial bone formation in mice [37], and IL-1β induces MSC differentiation into osteoblasts [38] and is required for tissue ingrowth and bone formation in rabbits [39]. TNFα plays an essential role in commitment to the osteoclastic lineage and activation of mature OCs by precisely tuning IL-6, RANKL, M-CSF, and OPG [40]. Here, we found that the induction of IL-6, IL-1β, and TNFα—expressed by hiPSC–derived OCs and their precursor macrophages in our HA-based constructs—worked together to stimulate OB differentiation and bone formation, indicating the necessity of crosstalk between these bone cell types (Fig. 5C). Furthermore, promotion of RANKL production by OBs induced differentiation of hiPSC-macrophages into OCs. Interestingly, OPG synthesis was stimulated by cellular interaction with the HA microenvironment, and the presence of OPG counteracted the action of RANKL on OCs.

Thus, the balance of bone formation versus resorption was improved by pairing co-cultured cells with HA-based composites. These findings suggest that local cues provided by the HA niche can guide intercellular signaling between hiPSC-MSCs and -macrophages to more accurately mimic bone physiology. Similar to wound healing [41], it is clear that cytokines and regulatory molecules secreted by immune cells (macrophages and OCs) can tightly regulate extracellular matrix remodeling required during development and maturation of bone.

2.5 Conclusions

3D bone tissue model engineered from hiPSCs not only elicited controlled differentiation of two bone cell precursors, but also demonstrated preliminarily functional regeneration of human bone-like tissue *in vivo*. Further investigation in orthotopic implantation models will be required to validate the functionality, especially for vascularization, which leads to better bone formation [42], and to confirm safety of bone grafts engineered from hiPSCs in the long run. From a translational standpoint, our 3D tissue-engineered bone using patient-specific iPSCs could capture the functional interplay between osteoclastic and osteoblastic activities and thus, it could be used in understanding of bone cell phenotypes in the pathology of bone disease and in the testing of drugs regulating bone homeostasis.

2.6 Figures

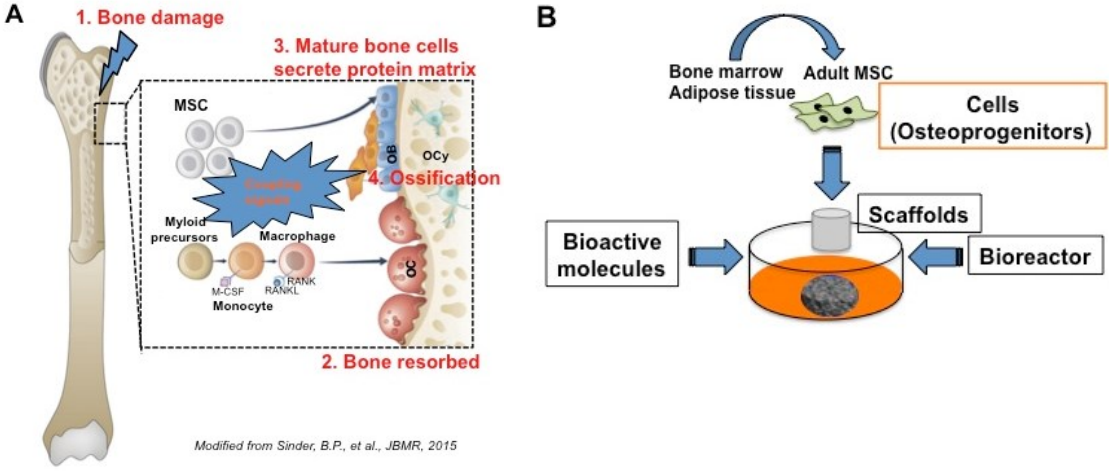

Figure 2.1 Regeneration in human bone and bone tissue engineering. (A) Human bone regeneration is comprised of a complex series of bone formation along with remodeling of bone through heterotypic interactions between monocytes/macrophage and bone cells (osteoblast and osteoclast). (B) Current bone tissue engineering approach uses synergistic combinations of osteoprogenitors, scaffolds, and factors to produce bone substitutes.

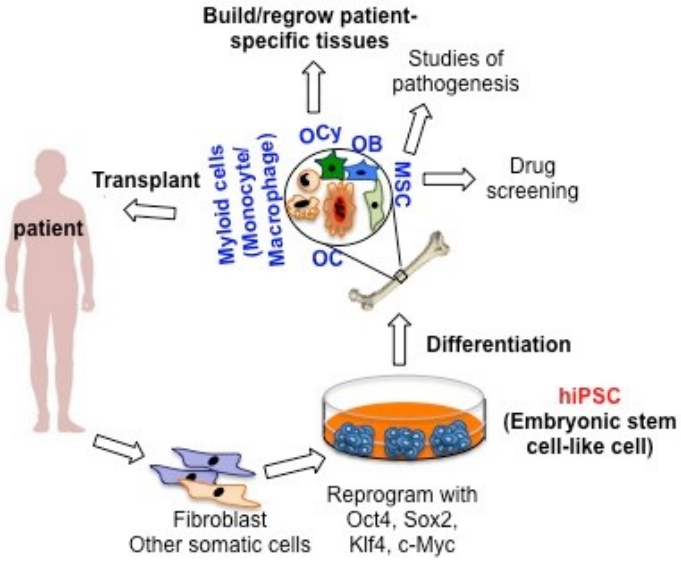

Figure 2.2 Human induced pluripotent stem cells (hiPSCs) for bone tissue engineering. hiPSCs are prospective cell sources for engineering bone because they have an unlimited potential to generate all cell types residing in human bone such as OB and MSCs as OB precursors and OC and monocytes/macrophages as OC precursors.

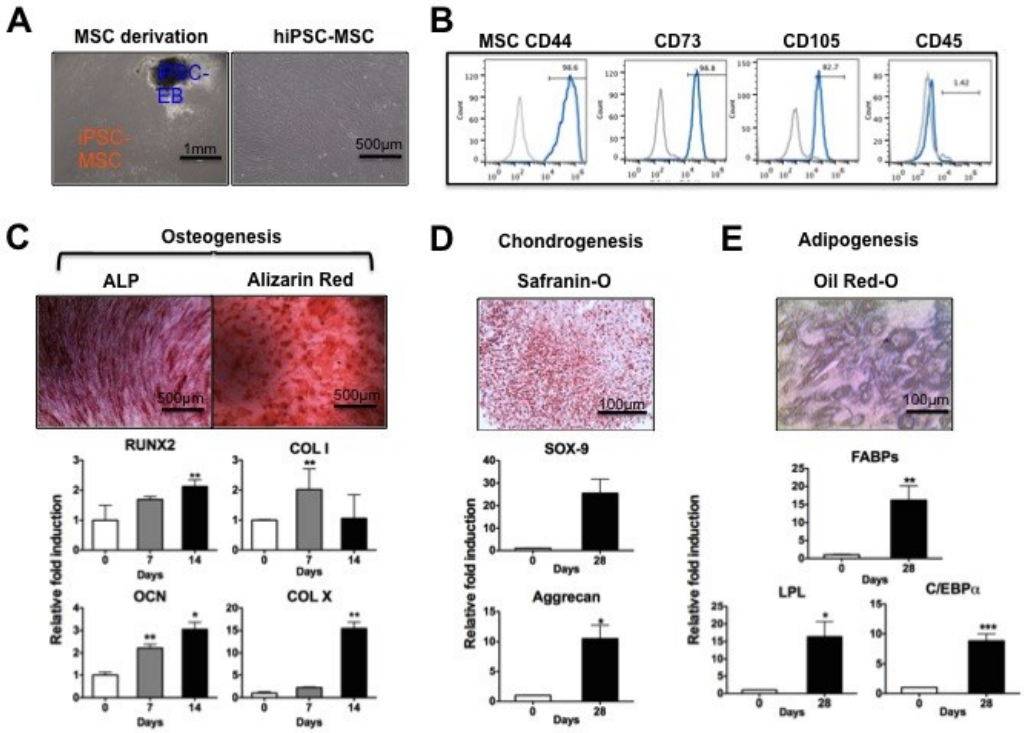

Figure 2.3 Isolation and characterization of hiPSC derived-MSC. (A) Light microscopy of hiPSC-MSCs migrating out of the embryoid body (EBs) for a week (Left) were harvested and expanded in monolayer culture with MSC growth medium (Right). (B) Flow cytometry analysis of hiPSC-MSCs indicates that these cells express MSC surface markers (at passage 3). Histograms show the percentage of cells stained with antibodies to specific markers (Blue) and isotype controls (Grey). *In vitro* differentiation potential of hiPSC-MSCs towards: (C) an osteogenic lineage (ALP and Alizarin red staining and gene expression of *RUNX2, COL I, COL X,* and *OCN* after 7 and 14 days in monolayer cultures); (D) a chondrogenic lineage (proteoglycan production confirmed by Safranin-O staining and gene expression of *SOX-9* and *Aggrecan*); and (E) an adipogenic lineage (Oil Red-O staining and gene expression of *FABPs, LPL*, and *C/EBPα*). Data in (C-E) are averages ± SD (n=3). $^{*}p < 0.05$, $^{**}p < 0.01$, and $^{***}p < 0.001$ versus day 0.

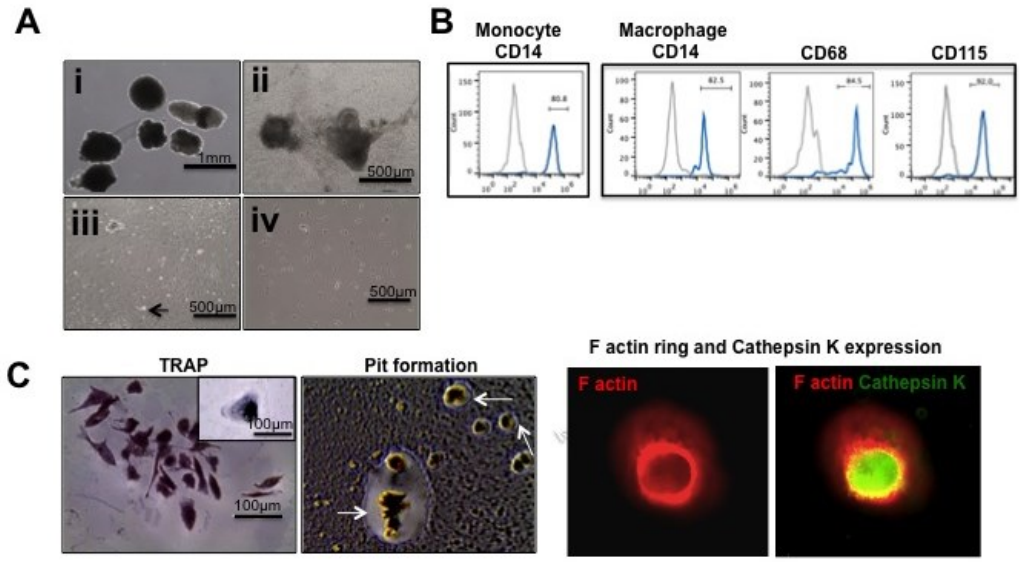

Figure 2.4 Isolation and characterization of hiPSC derived-macrophage and their potential of osteoclastogenesis. (A) A stepwise derivation strategy for differentiation of macrophage from hiPSCs. (i) Ten-day-old embryoid body (EBs) in suspension culture, (ii) flattened EBs that were ready to produce monocytes after 17 d with monocyte differentiation medium, (iii) EB factories producing monocytes (Floating round monocyte-like in the culture medium, arrow), and (iv) monocytes differentiated into macrophages after plating onto adherent tissue culture plates for 5 days with macrophage differentiation medium supplemented with M-CSF and IL-3. (B) Flow cytometry analysis of hiPSC-monocytes and macrophages. Histograms show the percentage of cells stained with antibodies to specific markers (Blue) and isotype controls (Grey). (C) Differentiation of osteoclast from hiPSCs shown by TRAP-positive osteoclastic cells (left), resorption pits created by functional hiPSC-derived OCs (arrow; Middle), and colocalization of cathepsin K (green) with F-actin ring (red; Right).

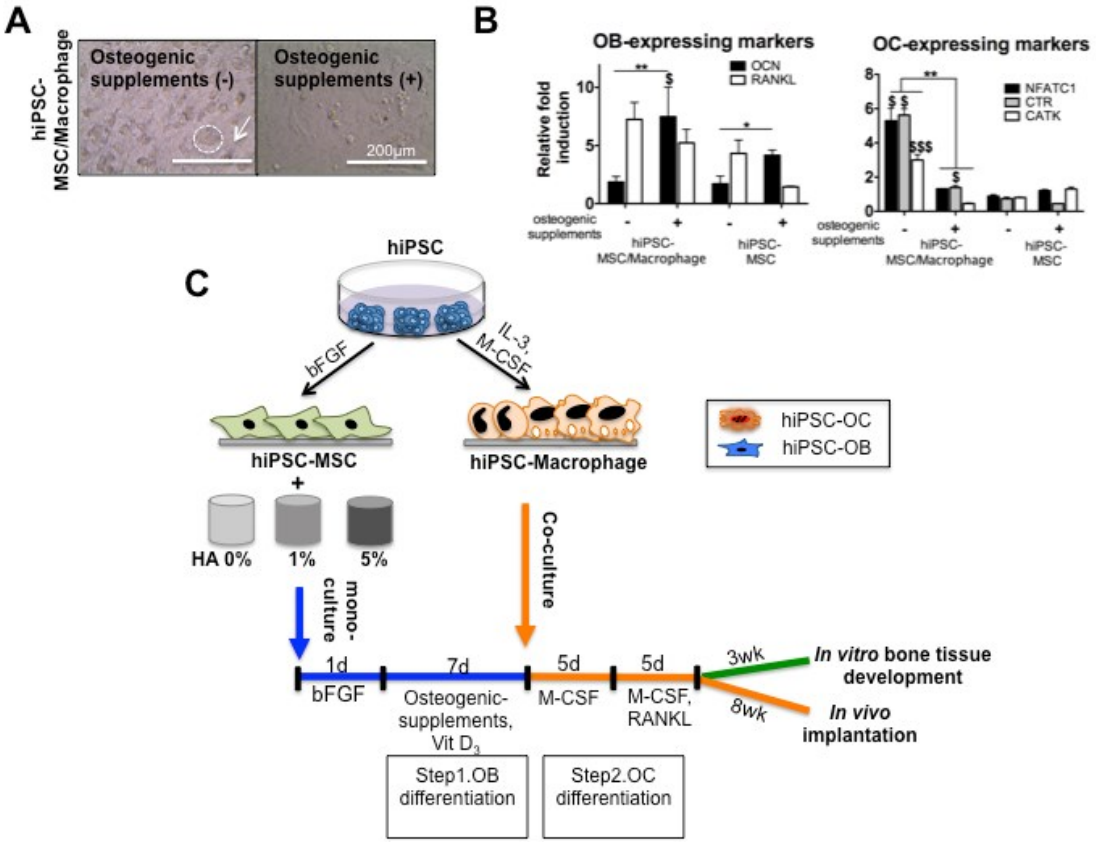

Figure 2.5 Engineered 3D model of bone using hiPSC-derived MSC and macrophage combination. (A) hiPSC-MSCs and -macrophages were co-cultured for 14 days with (+) or without (-) osteogenic supplements. Light microscopy images show multinucleated OCs (circles) embedded in an osteoblastic cell layer (arrow). Scale bars, 200 μm. (B) Gene expression for OC-expressing markers, *NFATC1, CTR*, and *CATK* (Right) and OB-expressing markers *OCN* and *RANKL* (Left) on day 14 of co-culturing hiPSC-MSCs and -macrophages in a monolayer with or without osteogenic supplements. Data are averages ± SD (n=3). $^{*}p < 0.05$, $^{**}p < 0.01$, for osteogenic supplements (-) vs. (+); $^{\$}p < 0.05$, $^{\$\$\$}p < 0.001$, for hiPSC-MSC/macrophage co-culture vs. hiPSC-MSC mono-culture. (C) Schema for protocol and timeline. hiPSC-MSCs were seeded and allowed to attach to the HA-based composite scaffolds in MSC growth medium for 1 day. Medium containing osteogenic supplements was used to commit these cells to the OB lineage for 7 days, after which it was seeded with hiPSC-macrophages and incubated without osteogenic supplements, containing M-CSF and RANKL, to differentiate into both OB and OC lineages for 10 days. hiPSC-derived multicellular bone constructs were either grown *in vitro* or implanted subcutaneously into athymic nude mice for 8 weeks.

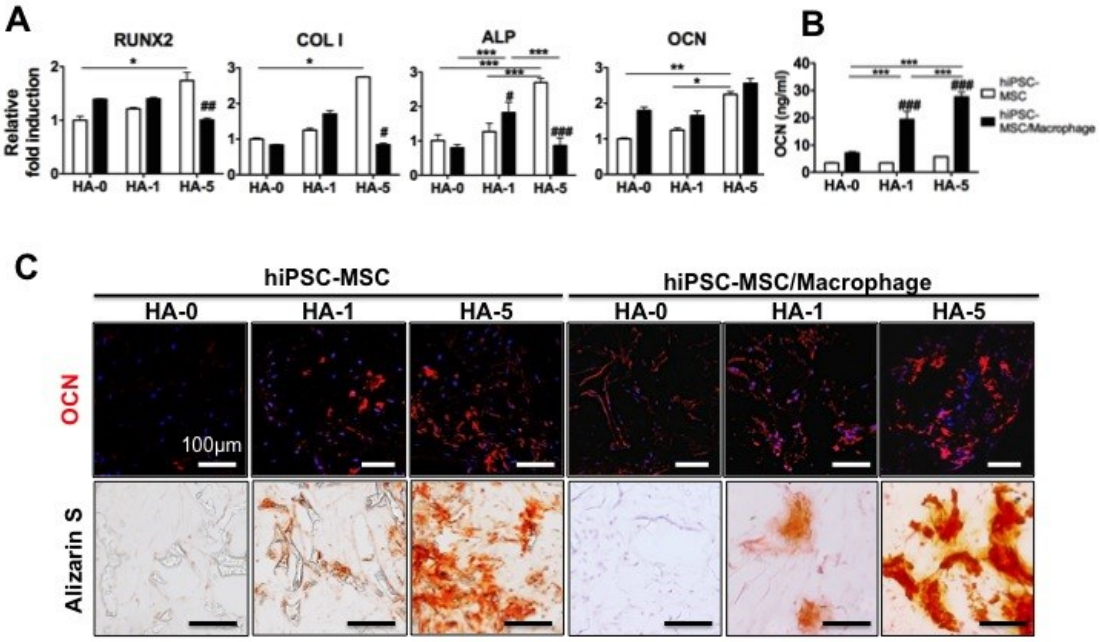

Figure 2.6 hiPSC-macrophage addition to hiPSC-MSC culture accelerates *in vitro* bone tissue formation. Bone tissue development from hiPSC-MSCs was compared with hiPSC-MSCs/-macrophages on PLGA/PLLA scaffolds or HA composite PLGA/PLLA scaffolds for 3 weeks. (A) Quantitative real-time PCR of gene expression for osteogenic markers *RUNX2, COLI, ALP*, and *OCN*. (B) OCN released into culture medium, indicative of bone maturation. Data in (A and B) are averages ± SD (n=3). $^{*}p < 0.05$, $^{**}p < 0.01$, $^{***}p < 0.001$, as indicated; $^{\#}p < 0.05$, $^{\#\#}p < 0.01$, and $^{\#\#\#}p < 0.001$ vs. hiPSC-MSC in the same dose of HA. (C) Immunofluorescent staining for OCN and Alizarin S red staining of hiPSC-MSC and hiPSC-MSC/macrophage in the various concentrations of HA-based scaffolds. HA-0: PLGA/PLLA scaffold, HA-1: PLGA/PLLA scaffold with 1% w/v HA; HA-5: PLGA/PLLA scaffold with 5% w/v HA. Scale bars, 200 μm

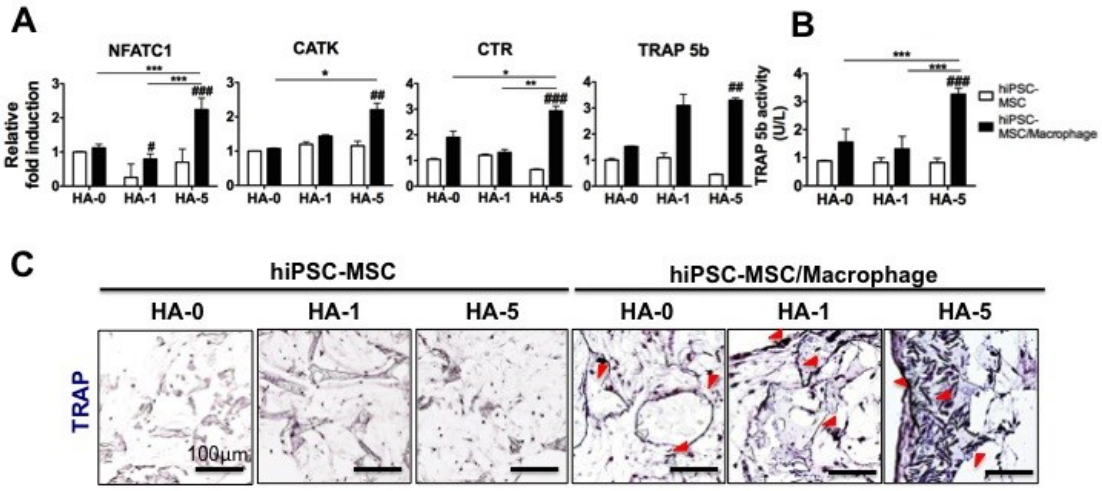

Figure 2.7 hiPSC-macrophages differentiated into OCs in HA-based co-culture bone constructs *in vitro*. Osteoclastogenic potential of hiPSC-macrophages was characterized *in vitro* in hiPSC-MSC/-macrophage and hiPSC-MSC on PLGA/PLLA scaffolds or HA composite PLGA/PLLA scaffolds for 3 weeks. (A) Quantitative real-time PCR of gene expression for OC markers *NFATC1*, *CATK, CTR, and TRAP5b*. (B) TRAP5b released into culture medium, indicative of OC cell number. Data in (A and B) are averages ± SD (n=3). $^{*}p < 0.05$, $^{**}p < 0.01$, $^{***}p < 0.001$, as indicated; $^{\#}p < 0.05$, $^{\#\#}p < 0.01$, and $^{\#\#\#}p < 0.001$ vs. hiPSC-MSC in the same HA dose. (C) Histological analysis of TRAP-positive OCs (red arrowhead) in hiPSC-MSC and hiPSC-MSC/macrophage in various HA-based scaffolds. HA-0: PLGA/PLLA scaffold, HA-1: PLGA/PLLA scaffold with 1% w/v HA; HA-5: PLGA/PLLA scaffold with 5% w/v HA. Scale bars, 100 μm

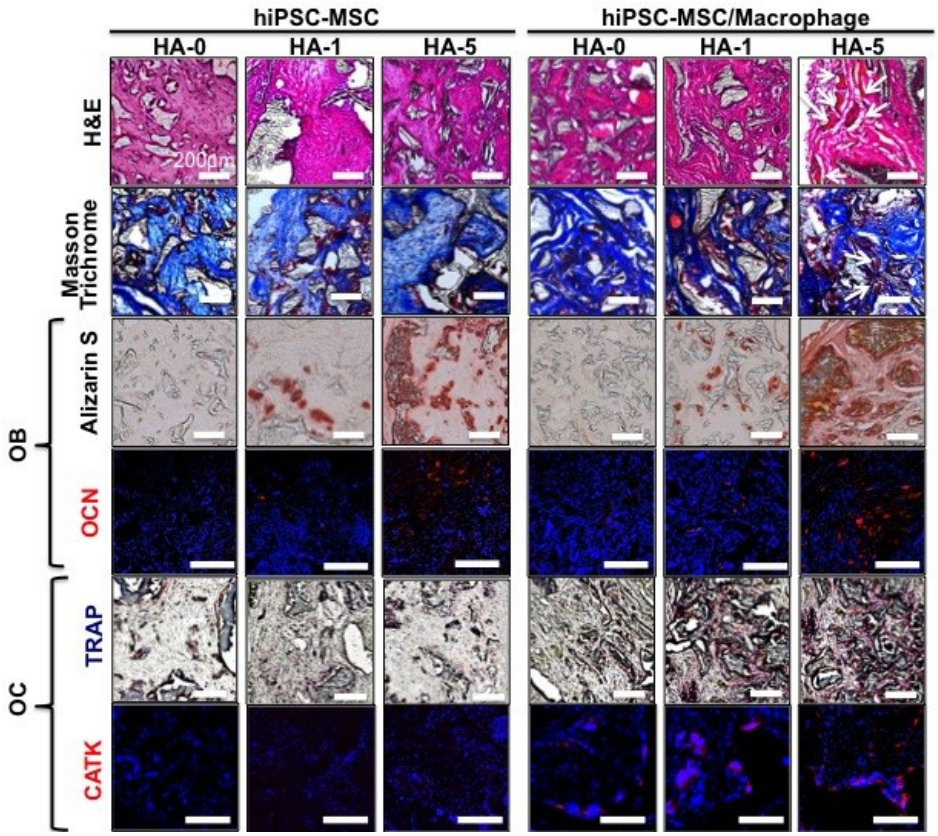

Figure 2.8 hiPSC-MSC/-macrophage co-culture induces mature bone-like tissue formation *in vivo* in mice. hiPSC-MSCs and hiPSC-MSC/-macrophages on PLGA/PLLA scaffolds or HA-composite PLGA/PLLA scaffolds were implanted subcutaneously for 8 weeks in the athymic nude mice. Histology revealed deposition of osseous tissue (H&E) and collagen (Masson's Trichrome, blue), calcium accumulation (Alizarin red), and OCN expression. Bone resorptive activity of OCs was confirmed by TRAP and CATK staining. HA-0: PLGA/PLLA scaffold, HA-1: PLGA/PLLA scaffold with 1% w/v HA; HA-5: PLGA/PLLA scaffold with 5% w/v HA. Scale bars, 200 μm

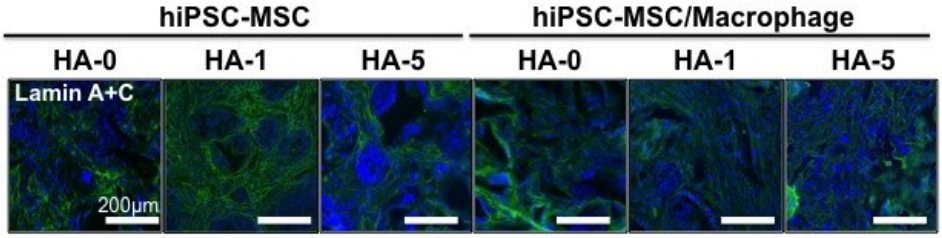

Figure 2.9 Anti-human nuclei staining of Lamin A+C confirming human origin of 3D engineered bone tissue. Human origin of the cells was confirmed by anti-human nuclei staining of Lamin A+C both in the engineered bone tissue for all hiPSC-MSC (Left) and hiPSC-MSC/-Macrophage groups (Right) investigated (Lamin A+C: green and DAPI: blue). HA-0: PLGA/PLLA scaffold, HA-1: PLGA/PLLA scaffold with 1% w/v HA; HA-5: PLGA/PLLA scaffold with 5% w/v HA. Scale bars, 200 μm

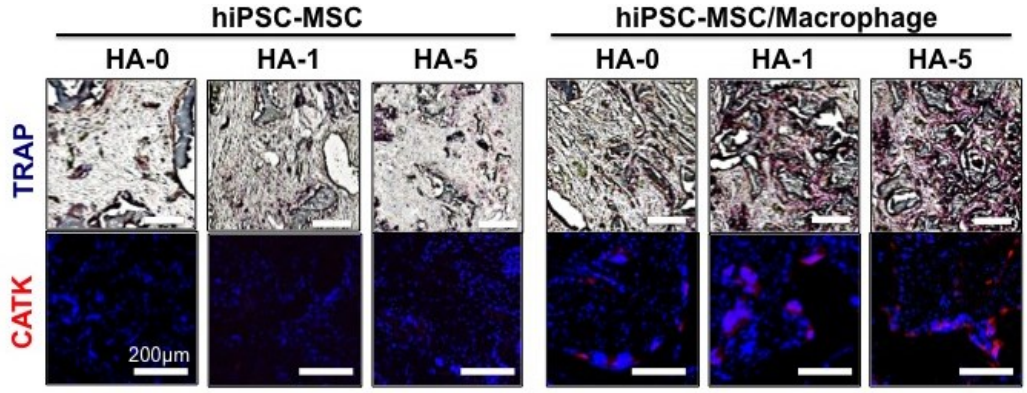

Figure 2.10 Phenotypic and differentiation stability of hiPSC-macrophages to OCs in HA-based co-culture bone constructs *in vivo*. Bone resorptive activity of OCs differentiated from hiPSC-macrophages was confirmed by TRAP and CATK staining of the implanted scaffolds after 8 weeks. HA-0: PLGA/PLLA scaffold, HA-1: PLGA/PLLA scaffold with 1% w/v HA; HA-5: PLGA/PLLA scaffold with 5% w/v HA. Scale bars, 200 μm

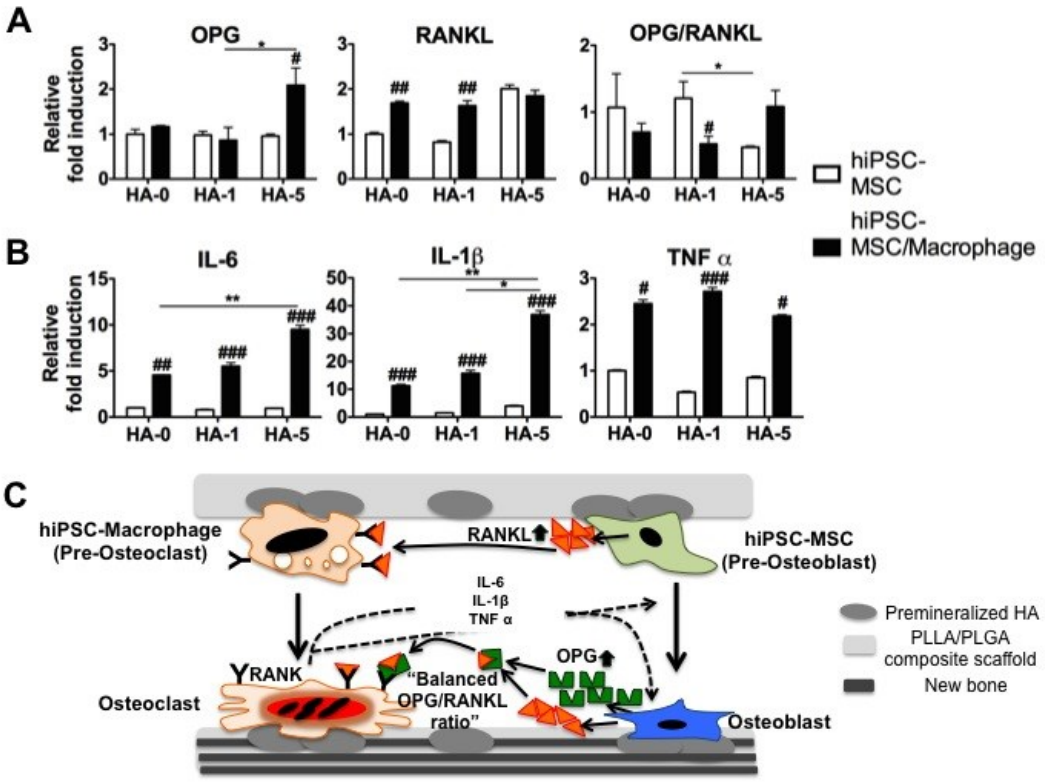

Figure 2.11 Well-orchestrated coupling of hiPSC-derived OBs and OCs leads to bone-like engineered tissues. Bone tissue was created from hiPSC-MSC and hiPSC-MSC/-macrophage on PLGA/PLLA scaffolds or HA composite PLGA/PLLA scaffolds for 3 weeks. (A) Expression of coupled factors *OPG* and *RANKL*, and their ratio. (B) Expression of cytokines *IL-6, IL-1β,* and *TNFα*. Quantitative real-time PCR data in (A and B) are averages ± SD (n=3). $^{*}p < 0.05$, $^{**}p < 0.01$, as indicated; $^{\#}p < 0.05$, $^{\#\#}p < 0.01$, and $^{\#\#\#}p < 0.001$ vs. hiPSC-MSC in the same HA dose. (C) Schematic for possible coupling mechanisms among hiPSC-derived OBs, OCs, and their progenitors under interaction with HA microenvironment for bone tissue development. HA-0: PLGA/PLLA scaffold, HA-1: PLGA/PLLA scaffold with 1% w/v HA; HA-5: PLGA/PLLA scaffold with 5% w/v HA.

2.7 References

[1] W.L. Grayson, B.A. Bunnell, E. Martin, T. Frazier, B.P. Hung, J.M. Gimble, Stromal cells and stem cells in clinical bone regeneration, Nat Rev Endocrinol 11(3) (2015) 140-50.

[2] O.H. Jeon, J. Elisseeff, Orthopedic tissue regeneration: cells, scaffolds, and small molecules, Drug Deliv Transl Res 6(2) (2016) 105-20.

[3] I. Drosse, E. Volkmer, R. Capanna, P. De Biase, W. Mutschler, M. Schieker, Tissue engineering for bone defect healing: an update on a multi-component approach, Injury 39 Suppl 2 (2008) S9-20.

[4] R.P. Pirraco, A.P. Marques, R.L. Reis, Cell interactions in bone tissue engineering, J Cell Mol Med 14(1-2) (2010) 93-102.

[5] M. Mehta, K. Schmidt-Bleek, G.N. Duda, D.J. Mooney, Biomaterial delivery of morphogens to mimic the natural healing cascade in bone, Advanced drug delivery reviews 64(12) (2012) 1257-76.

[6] X.X. Lou, Induced Pluripotent Stem Cells as a new Strategy for Osteogenesis and Bone Regeneration, Stem Cell Rev Rep 11(4) (2015) 645-651.

[7] M. Tang, W. Chen, J. Liu, M.D. Weir, L. Cheng, H.H. Xu, Human induced pluripotent stem cell-derived mesenchymal stem cell seeding on calcium phosphate scaffold for bone regeneration, Tissue engineering. Part A 20(7-8) (2014) 1295-305.

[8] J. Liu, W. Chen, Z. Zhao, H.H. Xu, Reprogramming of mesenchymal stem cells derived from iPSCs seeded on biofunctionalized calcium phosphate scaffold for bone engineering, Biomaterials 34(32) (2013) 7862-72.

[9] M.D. Phillips, S.A. Kuznetsov, N. Cherman, K. Park, K.G. Chen, B.N. McClendon, R.S. Hamilton, R.D.G. McKay, J.G. Chenoweth, B.S. Mallon, P.G. Robey, Directed Differentiation of Human Induced Pluripotent Stem Cells Toward Bone and Cartilage: In Vitro Versus In Vivo Assays, Stem Cell Transl Med 3(7) (2014) 867-878.

[10] P. Wang, L. Zhao, J. Liu, M.D. Weir, X. Zhou, H.H. Xu, Bone tissue engineering via nanostructured calcium phosphate biomaterials and stem cells, Bone Res 2 (2014) 14017.

[11] J. Ji, X. Tong, X. Huang, J. Zhang, H. Qin, Q. Hu, Patient-Derived Human Induced Pluripotent Stem Cells From Gingival Fibroblasts Composited With Defined

Nanohydroxyapatite/Chitosan/Gelatin Porous Scaffolds as Potential Bone Graft Substitutes, Stem Cells Transl Med (2015).

[12] G.M. de Peppo, I. Marcos-Campos, D.J. Kahler, D. Alsalman, L. Shang, G. Vunjak-Novakovic, D. Marolt, Engineering bone tissue substitutes from human induced pluripotent stem cells, Proceedings of the National Academy of Sciences of the United States of America 110(21) (2013) 8680-5.

[13] A.E. Grigoriadis, M. Kennedy, A. Bozec, F. Brunton, G. Stenbeck, I.H. Park, E.F. Wagner, G.M. Keller, Directed differentiation of hematopoietic precursors and functional osteoclasts from human ES and iPS cells, Blood 115(14) (2010) 2769-76.

[14] K.D. Choi, M.A. Vodyanik, Slukvin, II, Generation of mature human myelomonocytic cells through expansion and differentiation of pluripotent stem cell-derived lin-CD34+CD43+CD45+ progenitors, The Journal of clinical investigation 119(9) (2009) 2818-29.

[15] N.S. Hwang, S. Varghese, H.J. Lee, Z. Zhang, J. Elisseeff, Biomaterials directed in vivo osteogenic differentiation of mesenchymal cells derived from human embryonic stem cells, Tissue engineering. Part A 19(15-16) (2013) 1723-32.

[16] N.S. Hwang, S. Varghese, H.J. Lee, Z. Zhang, Z. Ye, J. Bae, L. Cheng, J. Elisseeff, In vivo commitment and functional tissue regeneration using human embryonic stem cell-derived mesenchymal cells, Proceedings of the National Academy of Sciences of the United States of America 105(52) (2008) 20641-6.

[17] L.M. Panicker, D. Miller, O. Awad, V. Bose, Y. Lun, T.S. Park, E.T. Zambidis, J.A. Sgambato, R.A. Feldman, Gaucher iPSC-Derived Macrophages Produce Elevated Levels of Inflammatory Mediators and Serve as a New Platform for Therapeutic Development, Stem Cells 32(9) (2014) 2338-2349.

[18] L.M. Panicker, D. Miller, T.S. Park, B. Patel, J.L. Azevedo, O. Awad, M.A. Masood, T.D. Veenstra, E. Goldin, B.K. Stubblefield, N. Tayebi, S.K. Polumuri, S.N. Vogel, E. Sidransky, E.T. Zambidis, R.A. Feldman, Induced pluripotent stem cell model recapitulates pathologic hallmarks of Gaucher disease, Proceedings of the National Academy of Sciences of the United States of America 109(44) (2012) 18054-9.

[19] K.R. Karlsson, S. Cowley, F.O. Martinez, M. Shaw, S.L. Minger, W. James, Homogeneous monocytes and macrophages from human embryonic stem cells following coculture-free differentiation in M-CSF and IL-3, Exp Hematol 36(9) (2008) 1167-75.
[20] S.E. Haynesworth, M.A. Baber, A.I. Caplan, Cytokine expression by human marrow-derived mesenchymal progenitor cells in vitro: effects of dexamethasone and IL-1 alpha, Journal of cellular physiology 166(3) (1996) 585-92.
[21] S. Takeyama, Y. Yoshimura, Y. Deyama, Y. Sugawara, H. Fukuda, A. Matsumoto, Phosphate decreases osteoclastogenesis in coculture of osteoblast and bone marrow, Biochemical and biophysical research communications 282(3) (2001) 798-802.
[22] W. Huang, S. Yang, J. Shao, Y.P. Li, Signaling and transcriptional regulation in osteoblast commitment and differentiation, Front Biosci 12 (2007) 3068-92.
[23] S.S. Kohli, V.S. Kohli, Role of RANKL-RANK/osteoprotegerin molecular complex in bone remodeling and its immunopathologic implications, Indian journal of endocrinology and metabolism 15(3) (2011) 175-81.
[24] A. Rogers, R. Eastell, Circulating osteoprotegerin and receptor activator for nuclear factor kappaB ligand: clinical utility in metabolic bone disease assessment, J Clin Endocrinol Metab 90(11) (2005) 6323-31.
[25] L. Dong, C. Wang, Harnessing the power of macrophages/monocytes for enhanced bone tissue engineering, Trends in biotechnology 31(6) (2013) 342-6.
[26] N.A. Sims, T.J. Martin, Coupling the activities of bone formation and resorption: a multitude of signals within the basic multicellular unit, Bonekey Rep 3 (2014) 481.
[27] H. Kang, Y.R. Shih, Y. Hwang, C. Wen, V. Rao, T. Seo, S. Varghese, Mineralized gelatin methacrylate-based matrices induce osteogenic differentiation of human induced pluripotent stem cells, Acta Biomater 10(12) (2014) 4961-70.
[28] W. TheinHan, J. Liu, M. Tang, W. Chen, L. Cheng, H.H. Xu, Induced pluripotent stem cell-derived mesenchymal stem cell seeding on biofunctionalized calcium phosphate cements, Bone Res 4 (2013) 371-384.
[29] B. Levi, J.S. Hyun, D.T. Montoro, D.D. Lo, C.K. Chan, S. Hu, N. Sun, M. Lee, M. Grova, A.J. Connolly, J.C. Wu, G.C. Gurtner, I.L. Weissman, D.C. Wan, M.T. Longaker, In vivo directed differentiation of pluripotent stem cells for skeletal regeneration,

Proceedings of the National Academy of Sciences of the United States of America 109(50) (2012) 20379-84.
[30] T. Komori, Regulation of bone development and extracellular matrix protein genes by RUNX2, Cell Tissue Res 339(1) (2010) 189-95.
[31] A. Teti, Mechanisms of osteoclast-dependent bone formation, Bonekey Rep 2 (2013) 449.
[32] S.J. Morrison, D.T. Scadden, The bone marrow niche for haematopoietic stem cells, Nature 505(7483) (2014) 327-34.
[33] L. Pederson, M. Ruan, J.J. Westendorf, S. Khosla, M.J. Oursler, Regulation of bone formation by osteoclasts involves Wnt/BMP signaling and the chemokine sphingosine-1-phosphate, Proceedings of the National Academy of Sciences of the United States of America 105(52) (2008) 20764-9.
[34] M.K. Chang, L.J. Raggatt, K.A. Alexander, J.S. Kuliwaba, N.L. Fazzalari, K. Schroder, E.R. Maylin, V.M. Ripoll, D.A. Hume, A.R. Pettit, Osteal tissue macrophages are intercalated throughout human and mouse bone lining tissues and regulate osteoblast function in vitro and in vivo, J Immunol 181(2) (2008) 1232-44.
[35] A.R. Pettit, M.K. Chang, D.A. Hume, L.J. Raggatt, Osteal macrophages: a new twist on coupling during bone dynamics, Bone 43(6) (2008) 976-82.
[36] A. Cheng, A. Mavrokokki, G. Carter, B. Stein, N.L. Fazzalari, D.F. Wilson, A.N. Goss, The dental implications of bisphosphonates and bone disease, Aust Dent J 50(4 Suppl 2) (2005) S4-13.
[37] M. Darowish, R. Rahman, P. Li, S.V. Bukata, J. Gelinas, W. Huang, L.M. Flick, E.M. Schwarz, R.J. O'Keefe, Reduction of particle-induced osteolysis by interleukin-6 involves anti-inflammatory effect and inhibition of early osteoclast precursor differentiation, Bone 45(4) (2009) 661-8.
[38] K. Sonomoto, K. Yamaoka, K. Oshita, S. Fukuyo, X.M. Zhang, K. Nakano, Y. Okada, Y. Tanaka, Interleukin-1 beta induces differentiation of human mesenchymal stem cells into osteoblasts via the Wnt-5a/receptor tyrosine kinase-like orphan receptor 2 pathway, Arthritis Rheum-Us 64(10) (2012) 3355-3363.

[39] T. Ma, K. Miyanishi, M.C.D. Trindade, M. Genovese, D. Regula, R.L. Smith, S.B. Goodman, Interleukin 1 receptor antagonist inhibits localized bone formation in vivo, J Rheumatol 30(12) (2003) 2547-2552.

[40] G. Valles, E. Gil-Garay, L. Munuera, N. Vilaboa, Modulation of the cross-talk between macrophages and osteoblasts by titanium-based particles, Biomaterials 29(15) (2008) 2326-35.

[41] T.R. Cox, J.T. Erler, Remodeling and homeostasis of the extracellular matrix: implications for fibrotic diseases and cancer, Dis Model Mech 4(2) (2011) 165-78.

[42] O. Tsigkou, I. Pomerantseva, J.A. Spencer, P.A. Redondo, A.R. Hart, E. O'Doherty, Y. Lin, C.C. Friedrich, L. Daheron, C.P. Lin, C.A. Sundback, J.P. Vacanti, C. Neville, Engineered vascularized bone grafts, Proceedings of the National Academy of Sciences of the United States of America 107(8) (2010) 3311-6.

Chapter 3. A potent sugar-based disease modifying osteoarthritis drug with chondroprotective and chondrogenic effects

3.1 Introduction

Osteoarthritis (OA) is the most common cause of joint pain and physical disability in the elderly. The characteristics of OA include an irreversible loss of articular cartilage, subchondral bone thickening, osteophyte formation, and local joint inflammation[1] **(Fig 3.1)**. Current pharmacologic OA treatments are the use of analgesics, non-steroidal anti-inflammatory drugs (NSAIDs), and viscosupplementation (e.g. hyaluronic acid) with intra-articular injections **(Fig 3.2)**. These treatments focus on short-term symptomatic pain relief and care of joint function. With advances in the understanding of the OA pathogenesis, a variety of disease-modifying OA drugs (DMOADs) have been developed to block or reverse OA progressions, which target specific OA pathophysiological networks[2]. In spite of these successes, there still remains an unmet need for a desirable pharmacologic OA therapy.

Recent pharmacological discoveries have been catalyzed by the recognition of OA as a whole joint disease [3]. The pathological changes of OA result from an imbalance in the dynamic equilibrium between the breakdown and repair of all the joint tissues including bone, synovium, and cartilages [4]. At the molecular level, they are mediated by a large

number of anabolic and catabolic factors in autocrine and paracrine manners [5]. These factors also participate in cross-talks and feedbacks between the joint tissues in order to regulate their expression. Due to this complex interrelationship, a single pharmacologic approach of DMOADs would provide limited therapeutic efficacy on OA. In fact, the most effective DMOADs in development have an action on OA through a combination of several therapeutic targets. For example, strontium ranelate exhibited OA structure-modifying activity via modulation of bone turnover and anabolic effects on chondrocytes. Calcitonin has been shown to have beneficial metabolic effects on both bone and cartilage, promoting the growth of cartilage tissues. Bone morphogenetic protein 7 (BMP-7) showed strong anabolic and anti-catabolic activities on cartilage matrix, inhibiting OA progression[6]. Therefore, a comprehensive approach to target multiple elements would be desirable in the development of new DMOADs[7].

Recently, as a new class of DMOADs, small molecules that stimulate MSCs residing in articular cartilages into chondrocytes have shown great promise as novel therapeutics for cartilage repair[8-10]. However, inflammatory cytokines present in an OA joint can disrupt chondrogenic differentiation capabilities of the MSCs and reduce therapeutic efficacy of the DMOADs[11]. These inflammatory mediators continuously can create positive feedback loop of the inflammatory pathways and further disturb the regeneration capability[12]. Modulating the inflammation in an OA joint thus would be necessary to create optimal conditions for the drug action along with advantageous anti-catabolic effects[13]. In this work, we investigated the use of a sugar-based compound, a tributanoylated N-acetyl-D-galactosamine (GalNAc-a) as a potential OA drug. Treatment of GalNAc-a enhanced chondrogenic differentiation of human MSCs and reduced

inflammation of human OA chondrocytes by modulating the Wnt/□-catenin signaling. Consequently, it improved cartilage tissue production on three-dimensional (3D) *in vitro* cultures. We further investigated the therapeutic efficacy of GalNAc-a an *in vivo* OA rat model. Intra-articularly injected GalNAc-a improved cartilage repair in the damaged joints. Additionally, its incorporation into a sustained-release drug delivery system could avoid multiple GalNAc-a injections, facilitating clinical translation. These results show that GalNAc-a has dual benefits for both endogenous MSCs and diseased OA chondrocytes, demonstrating its potential as a disease modifying OA drug.'

3.2 Materials and Method

Cell isolation and culture

Human articular cartilage samples explanted from OA patients undergoing total knee arthroplasty were received from the National Disease Resource Institution (Philadelphia, PA, USA) according to an IRB-approved protocol. The cartilage tissue was cut into 1 mm3 pieces, washed 3 times with phosphate-buffered saline (PBS) supplemented with 1% (v/v) penicilline streptomycin (Pen/Strep) solution, and digested on an orbital shaker for 16 h at 37 ◦C with 0.17% (w/v) type II collagenase (Worthington Biochemical, Lakewood, NJ, USA) in high-glucose Dulbecco's modified Eagle's medium (DMEM; In-vitrogenTM, Life Technologies) with 10% fetal bovine serum (FBS, Thermo Fisher Scientific). After the digestion, the filtrate was passed through a 70 μm

strainer and cells were rinsed 3 times with the DMEM supplemented with 1% Pen/Strep and 10 % FBS.

Human MSCs (hMSCs) were obtained from the Arnold Caplan's lab, Case Western Reserve University, hMSCs were maintained in MSC medium with FBS from a lot defined by the Caplan Lab as supporting MSC growth. The human MSCs were maintained in growth medium composed of low-glucose DMEM supplemented with 1% l-glutamine, 1% Pen/Strep, 10% defined FBS, and 1ng/mL basic fibroblast growth factor (bFGF; PeproTech). Passage 3–5 cells were used for all experiments.

Mesenchymal stem cell differentiation

For chondrogenic differentiation (monolayer, pellet, and 3D hydrogel cultures), hMSC were induced in chondrogenic medium consisting of high-glucose DMEM, 1% Pen/Strep, 1% ITS premix (BD Bioscience, San Jose, CA, USA), 100 mM sodium pyruvate (Life Technologies), 40 mg/ml L-proline (Sigma-Aldrich), 50 mM ascorbic acid-2-phosphate, and 10ng/mL of transforming growth factor-β1 (TGFβ1). For osteogenic differentiation in monolayer cell culture studies, hMSCs were plated and cultured in the growth medium until they were confluent. Differentiation toward an osteogenic phenotype was then achieved through culture in osteogenic medium comprised of high-glucose DMEM supplemented with 10% FBS, 1% Pen/Strep, 100 nM dexamethasone, 10 mM □-glycerophosphate, and 0.1 mg/mL ascorbic acid-2-phosphate.

Cell viability test with Alamar Blue assay

For measuring cell viability, hMSCs or hOA chondrocytes were plated in 96 well plates at a density of 10,000 cells/well. The cells were allowed to adhere for 1 days and

then medium was changed to chondrogenic or osteogenic medium containing 100 uM of GalNAc-a and cultured for an additional 3 days. The medium was aspirated from each well and the wells were washed 3 times with PBS. 100 ul of Alamar blue working solution (10% (v/v) Alamar blue in medium) was added to each well and the cells were further incubated for 4 h in an incubator at 37 °C. The cell viability was then determined by measuring the fluorescence intensity at 570 nm. The result was shown as a percentage over the control (no GalNAc-a treatment).

3D Pellet culture of hMSC

For hMSC pellets cultures, 400,000 cells were seeded in the 96 well MicroWell™ round bottom plate (Thermo Fisher Scientific) and the pellets were formed in the bottom by centrifuging at 150g for 10 min. The pellets were maintained at 37 °C with 5% CO_2 in 200 ul of the chondrogenic medium and were harvested after 21 days for analysis. The media were changed 3 times a week until the end of the experiment.

3D hydrogel cell cultures

For the 3D hydrogel culture, hMSC or human osteoarthritic chondrocytes (2 million cells) were suspended in 100 uL of the poly(ethylene glycol)-diacrylate (PEGDA; SunBio, Seoul, Korea) precursor solution and the cell suspension transferred into sterile cylindrical molds. The PEGDA precursor solution was prepared by dissolving 100 mg of PEGDA in 1 mL sterile PBS and 5 uL of the photoinitiator (Irgacure 2959) in 70 % ethanol to create a final concentration of 0.05% (w/v) in the solution. Polymer cross-linking was initiated by exposing UV light at 3 mW/cm2 with a wavelength of 365 nm for 5 min. The hydrogels encapsulating cells were transferred into 24-well plates and

cultured in a 1 mL of either chondrogenic or osteogenic medium with or without 100 uM of GalNAC-a. For human chondrocyte experiments, the medium was supplemented with 10 ng/ mL of IL-1□ to maintain OA pathophysiological condition. The media were changed 3 times a week until the end of the experiment.

Biochemical analysis for GAG contents

The hydrogel constructs or pellets (n = 3 per group) were lyophilized for 2 days and then digested overnight in 125 mg/ml papainase (Worthington Biochemical Corp.) for 16 h at 60°C. The sulfated glycosaminoglycan (sGAG) content was determined by 1,9-dimethylmethylene blue (DMMB) dye assay with measuring the absorbance at 525 nm and using chondroitin sulfate as a standard. The DNA content was determined by using Hoescht Dye 33342 DNA assay and calf thymus DNA as a standard.[1] The GAG content levels were expressed as micrograms of GAG per microgram of DNA for each construct.

Alkaline phosphatase (ALP), Alizarin red and oil red O staining

For calcium deposition staining, cells were fixed with 10% formaldehyde for 15 min at room temperature and rinsed 3 times with an excess of distilled water. The cells were then stained with alizarin red (Sigma; 0.5% (v/v) in distill water (pH 4.2)) for 10 min at room temperature. For oil red O staining, after fixation of cells with 10% formaldehyde, lipid droplets were stained with 30 mg/ml oil red O (Sigma-Aldrich) in 60% isopropanol. For alkaline phosphatase (ALP) staining, cells were rinsed with Tyrode's balanced salt solution and fixed for 30 seconds with citrate-buffered acetone.

The cells were washed 3 times with distilled water and then incubated in a mixture of fast violet B salt and naphthol AS-MX phosphate solution in the dark for 45 min.

RNA Isolation and Real-Time PCR

Total RNA was extracted from cells, hydrogels, and pellets using Trizol reagent (Life Technologies, Grand Island, NY) and cDNA was synthesized by using Superscript(R) II reverse transcriptase following the manufacturer's protocol (Invitrogen, Carlsbad, CA). Real-time PCRs were performed using StepOnePlus(R) Real Time PCR System (Applied Biosystems, Carlsbad, CA) with SYBRW Green PCR Master Mix (Life Technologies). The relative expression of each target was calculated using the ΔΔCT method and □-actin and GAPDH were used as endogenous references. All expression levels of samples were normalized to controls. The PCR primers are listed as followings: **Table 1**.

Western blot analysis

To assay the β-catenin protein, cells were harvested, washed twice with ice-cold PBS, and lysed with NE-PER™ nuclear and cytoplasmic extraction reagents (Thermo Scientific, USA) containing protease inhibitor mixture (Sigma, USA) according to the manufacturer's instructions. Concentration of collected cytoplasmic and nuclear proteins was determined using the BCA assay (Pierce, USA). Protein were separated by 10% SDS-PAGE and then transferred onto polyvinylidene difluoride (PVDF) membranes. The membranes were blocked for two hours with 5% nonfat powdered milk in Tris-buffered saline containing 0.1% tween-20 (TBST) and incubated overnight at 4°C with primary antibody specific for β-catenin (1:1000, Cell signaling, USA), β-actin (1:300, Sigma,

USA), and β-tubulin (1:1000, Cell signaling, USA). After washing away unbound primary antibodies, the membranes were incubated with horseradish peroxidase-conjugated secondary antibodies (1:5000, Bio-Rad, USA) and proteins were detected by chemiluminescence (Thermo scientific, USA). β-actin and β-tubulin were used as the internal control for the cytoplasmic and nuclear proteins, individually.

Histology and immunohistochemistry of pellets and hydrogel

The pellets and hydrogel constructs were fixed in 4% paraformaldehyde overnight, dehydrated in increasing concentrations of ethanol, and embedded with paraffin. Five micrometer-thick sections were cut from the paraffin block and collected onto the glass slides. The sections were stained for proteoglycans with aqueous Safranin-O (0.1%) for 5 mins, and then the specimens were mounted. For immunohistochemical staining, endogenous peroxidase of the sections was quenched using 2.5% (v/v) hydrogen peroxide in methanol and then incubated at 37°C with 0.25% (w/v) hyaluronidase for 1 h. AEC Broad Spectrum Histostain-SP Kit (Invitrogen, USA) was used following the manufacturer's instructions. Primary antibodies for type I, type II, and type X collagen (Abcam, USA) using a 1:100, 1:300, and 1:50 dilution factor in 4% BSA dissolved in PBS.

Immunocytochemistry

Monolayer cultures of human MSCs and chondrocytes were fixed in 4% paraformaldehyde, permeabilized with PBS containing 0.25% Triton X-100 for 10 mins, and then blocked with 4% bovine serum albumin (BSA) containing 0.25% Triton X-100 for 30 mins at room temperature. The cells were incubated primary antibodies of β-

catenin (1:100, Cell signaling, USA) overnight at 4°C. The cells were rinsed 3 times with PBS and incubated was goat anti-rabbit IgG (H & L) conjugated with Alexa Fluor 594 (1:1000, Life technologies, USA). After washing, the nuclei were counterstained with DAPI for 5 mins. The expression of β-catenin in MSCs and chondrocytes were imaged by fluorescence microscopy (Carl Zeiss, USA).

Preparation of PLGA-GalNAc-a microspheres and in vitro release

The GalNAc-a encapsulated PLGA microspheres (PLGA-GalNAc-a) were prepared by the solvent evaporation method. 150 mg of PLGA (poly (lactic-co-glycolic acid), acid terminated, lactide:glycolide 75:25, Mw 4,000-15,000, Sigma-Aldrich) polymer and 20 mg of GalNAc-a was in 2 ml of methylene chloride. The solution was slowly added into 50 mL of a 1% PVA (poly(vinyl alcohol), Mw ~25,000, Polyscience, Inc.) solution and stirred at 1000 rpm for 5 min. The mixture was then poured into 100ml of 0.5% PVA and stirring at ~ 700 rpm for 2 h at room temperature. The PLGA-GalNAc-a microsphere were washed 5 times with distilled water and recovered by centrifugation. After re-suspension, the microspheres were freeze-dried and stored in - 20 °C before experiment. Particle size distribution of the microspheres was determined using a Zetasizer Nano ZS (Malvern, USA) and their morphologies were characterized by using scanning electron microscopy with an electron voltage of 5 kV. To determine *in vitro* release of GalNAc-a from the microspheres, 15 mg of PLGA-GalNAc-a (loading 1.5 mg of GalNAc-a) microspheres were suspended in 1 mL of PBS and incubated in a shaker bath at 37 °C. The microspheres were settled down by centrifugation and the amount of GalNAc-a released was calculated from the UV absorption measurements of the supernatant. The microspheres were re-suspended in 1 mL of PBS and incubated in a

shaker bath at 37 ℃ for next measurements. After 32 days, the release profile showed a plateau region, indicating around 10% loading efficacy.

Surgically induced OA rat model

Six-week old male Sprague-Dawley rats (Charles River, Germantown, MD) weighing approximately 240g were used in the work. Rats were anesthetized with 3–5% isoflurane, and the skin over the medial aspect of the right femoro-tibial joint was shaved. The knee joint was exposed by a 1 cm longitudinal incision of skin and then joint capsule opened with a #10 scalpel. The medial meniscus was fully transected and reflected the meniscus toward the femur. The joint capsule overlying muscle and then skin were closed with 4 Vicryl suture. All procedures were performed according to the Institutional Animal Care and Use Committee at Johns Hopkins University School of Medicine.

After the OA surgery, the rats of the multi-Gal group were given IA injections with 500 μg of GalNAc-a in 100 ul of vehicle (5 % DMSO in PBS) on days 7, 14 and 21. The rats of the single-Gal group were given IA injections with 100 μM of GalNAc-a in 100 ul of the vehicle once on days 7. The rats of the PLGA-GalNac-a group were given IA injections with 15 mg of PLGA-GalNAc-a (loading 1.5 mg of GalNAc-a) in the PBS once on days 7. On day 28, the rats were sacrificed and the cartilage was collected for histological assessment of the medial tibial plateau joint through blinded graded observations by 2 observers, according to the Osteoarthritis Research Society International (OARSI) Scoring System.

Statistical analysis

Data are expressed as mean standard deviation and the statistical significance (p value) was determined by an unpaired t test or one-way analysis of variance (ANOVA). The statistical significance was determined at $p < 0.05$.

3.3 Results

Enhanced chondrogenic differentiation of human MSC upon GalNAc-a treatment

The sugar analog compound, GalNAc-a **(Fig 3.3A)** was synthesized and characterized as previously reported[14]. The promoting chondrogenic effect of GalNAc-a on human MSCs (hMSCs) was initially evaluated in monolayer culture over 48 h under chondrogenic condition. Real time-PCR (RT-PCR) with mRNA isolated from the cells confirmed the increased expression of genes associated with chondrogenic markers including Sox9 and aggrecan **(Fig 3.3B)**. We then investigated the involvement of Wnt genes and proteins because the Wnt/□-catenin signaling pathway influences chondrogenic differentiation of MSC[15]. The protein expression of □-catenin, the signal transducer to regulate the transcription of Wnt target genes, was determined by western blot analysis **(Fig 3.3D)**. The □-catenin levels decreased in both nuclear and cytoplasmic compartments when treated by GalNAc-a. This finding was further confirmed by immunofluorescence of □-catenin **(Fig 3.3E)**. RT-PCR analysis showed that treatment of GalNAc-a down-regulated the mRNA levels of □-catenin and Wnt target gene, axin2 **(Fig 3.3C)**.

Next, we evaluated the chondrogenesis promoting effect of GalNAc-a on 3D pellet cultures of hMSCs. Upon treatment of GalNAc-a for 3 weeks, RT-PCR analysis from the differentiated MSC pellets confirmed up-regulated expression of genes

associated with chondrogenic differentiation, including Sox9, type II collagen, and aggrecan **(Fig 3.4A)**. Biochemical analysis of the pellets demonstrated that the amount of glycosaminoglycans (sGAG) per DNA content significantly increased while DNA levels had no significant difference **(Fig 3.4B, C)**. The increased proteoglycan deposition further confirmed via histological staining using Safranin-O **(Fig 3.4D)**. In addition, immunohistochemical staining of pellets revealed up-regulation of type II collagen but down-regulation of hypertrophic chondrocyte specific marker, type X collagen and the osteogenic marker, type I collagen, indicating retention of the cartilage phenotype.

We also sought to evaluate the effects of GalNAc-a on the chondrogenic differentiation of hMSCs in a 3D hydrogel culture that mimics the cartilage environment and supports chondrogenesis[16]. RT-PCR results indicated significant up-regulation of the gene expression for chondrogenic markers, Sox9, aggrecan, and type II collagen **(Fig 3.5A)**. The GalNAc-a exposure increased GAG content in the 3D hydrogel constructs **(Fig 3.5B, C)**. and increased extracellular matrix (ECM) accumulation was confirmed via Safranin-O staining for proteoglycans and immunohistochemistry for type II collagen **(Fig 3.5D, E)**.

Adverse effect of GalNAc-a on osteogenesis of hMSC

Wnt/β-catenin signaling also has a critical role in bone development and homeostasis[17]. In particular, disruption of Wnt//□-catenin impairs osteogenesis of MSC *in vitro*[18, 19]. To further examine the role of GalNAc-a on possible Wnt/□-catenin signaling, the effect of GalNAc-a on osteogenic differentiation was investigated in hMSC monolayer culture. After 5 days osteogenic induction of hMSC, early

osteogenic marker, alkaline phosphatase (ALP) activity was attenuated upon treatment of GalNAc-a, confirmed by ALP staining **(Fig 3.6A)**. This inhibitory effect of GalNAc-a was also reflected in the down-regulated gene expression of □-catenin, the osteogenic transcriptional factor, Runx2, and Wnt transcription cofactor, LEF-1 **(Fig 3.6B)**.

After 10 days osteogenic induction, alizarin red staining for calcium deposition also exhibited a decreased mineralization in the GalNAc-a group **(Fig 3.6C)**. RT-PCR results further confirmed that the gene expression for type X collagen and bone matrix markers, osteocalcin (OCN) and osteopontin (OPN) was significantly reduced **(Fig 3.6D).** However, at this point, gene expression of Runx2 showed basal level **(Fig 3.7A)**. At 15 days of osteogenic induction, the calcium deposition and gene expression of Runx2, OCN, and OPN showed no significant difference between control and GalNAc-a treatment groups **(Fig 3.7B, C)**. Interestingly, hMSC treated with GalNAc-a exhibited lipid droplet accumulations, which were visualized by oil red O staining **(Fig 3.6E)**. The intracellular lipid accumulation is commonly observed in adipocyte cells and adipogenic lineage of MSC[20]. RT-PCR further confirmed up-regulation of several adipogenic-related markers, fatty-acid-binding proteins (FABPs), lipoprotein lipase (LPL), and CCAAT/enhancer-binding protein alpha (CEBPA) **(Fig 3.6F)**.

Similar to what was shown in the monolayer culture, the adverse effect of GalNAc-a on osteogenesis of hMSC was also observed in a 3D hydrogel system. hMSCs encapsulated in the hydrogels were cultured in osteogenic medium containing GalNAc-a for 3 weeks. The histological analysis of the constructs showed that GalNAc-a treatment reduced calcium accumulation with alizarin red staining **(Fig 3.6G)**. RT-PCR results

confirmed significant down-regulation of the gene expression for osteogenic markers, Runx2, OCN, and type I collagen **(Fig 3.6H)**.

Anti-inflammatory effect of GalNAc-a on human OA chondrocytes

Next, we investigated the anti-inflammatory effects of GalNAc-a on human diseased articular chondrocytes. Primary human articular chondrocytes isolated from OA patients undergoing total knee arthroplasty were grown in the presence of IL-1□ to maintain OA pathophysiological condition [21]. We examined mRNA expression of genes transcriptionally regulated by NF□B, specifically, NF□B1 and I□B□ for the auto-regulatory behavior of NF□B, and IL-1□ for pro-inflammatory cytokine expression. Treatment of GalNAc-a on the human OA chondrocytes for 48 h in monolayer culture significantly reduced gene expression of the inflammatory targets which are involved in OA **(Fig 3.7A)**.

This anti-inflammatory effect of GalNAc-a via modulating NF□B activity was also observed in our previous report [22]. Because pro-inflammatory cytokine-induced cartilage degradation in OA associates with the Wnt/□-catenin signaling pathway [23, 24], we next evaluated the involvement of Wnt genes and proteins. Western blotting analysis and immunofluorescence demonstrated that protein expression level of □-catenin was decreased in both nuclear and cytoplasmic compartments by GalNAc-a treatment **(Fig 3.7C, D)**. RT-PCR showed that treatment of GalNAc-a down-regulated the mRNA levels of □-catenin, LEF-1, TCF-1, axin2, and c-jun **(Fig 3.7B)**.

We further evaluated the inhibitory effects of GalNAc-a on the human OA chondrocytes in a 3D hydrogel culture system as it more closely mimics the *in vivo*

articular cartilage environments, and maintains chondrocyte phenotype better than monolayer cultures [16]. The human OA chondrocytes in the hydrogel were treated with GalNAc-a for 21 days in the presence of IL-1□. RT-PCR results confirmed down-regulation of NF□□1, I□B□, IL-1□, and cartilage matrix-degrading enzyme, MMP13 **(Fig 3.8A)**. The anti-inflammatory effect accompanied by inhibition of Wnt/□-catenin signaling has been shown to have anti-catabolic effects on cartilage[25]. We further confirmed up-regulated gene expression for aggrecan and type II collagen, indicting its anabolic effect **(Fig 3.8B)**. Additionally, the GalNAc-a exposure increased GAG content and ECM accumulation in the 3D hydrogel constructs, confirmed by biochchemical analysis **(Fig 3.8C, D)** and immunohisto- and Safranin-O staining **(Fig 3.8E, F)**.

Cartilage repair of OA induced rats by intra-articular injection of GalNAc-a

Given that GalNAc-a showed both chondrogenic and chondroprotective effects on endogenous MSC and OA chondrocytes respectively, we investigated the efficacy of GalNAc-a *in vivo* via the medial meniscal transection (MMT) model of OA in the rat [26]. After MMT was performed, GalNAc-a (500 □g in 100 □l of vehicle) was injected through the knee joint weekly (days 7, 14, and 21). There were no obvious post-surgical complications and systemic effects of GalNAc-a treatment (weight loss or significant swelling). At 5 weeks after the surgery induction of OA, the rats were sacrificed and histological assessments according to Safranin-O staining were carried out on the medial tibial plateau where the majority of the lesions were located on **(Fig 3.9A)**. Grading of the histological assessments based on OARSI score exhibited the score of the multi-GalNAc-a treated rats showed a 74% reduction as compared to that of the vehicle-treated rats (OA surgery), indicating its efficacy on cartilage repair.

The local intra-articular (IA) injection of therapeutics is feasible for OA treatment but rapid clearance of the IA injected drugs in the joint would limit their prolonged residence time from the target tissues [27]. Therefore, we evaluated sustained-release drug delivery of GalNAc-a by using PLGA (poly(lactic-co-glycolic acid)) microspheres that can maintain optimal systemic concentration of drugs for months in the joint [28]. We fabricated PLGA-GalNAc-a microspheres (size of diameter: 3.8 ± 0.4 um) and showed sustained *in vitro* release profiles of GalNAc-a from PLGA-GalNAc-a microspheres for over a month **(Fig 3.9B, C)** The PLGA-GalNAc-a was intra-articularly injected one week after surgical induction of OA. Controls consisted of a single GalNAc-a injection- and PLGA microsphere only-treated rats. The OARSI score showed improved cartilage repair in the PLGA-GalNAc-a treatment group, which is comparable to the multiple GalNAc-a treatment group **(Fig 3.9D)**.

3.4 Discussion

OA is a chronic joint disease with accompanying cartilage degradation leading to persistent pain and limited mobility. This progressive and irreversible cartilage destruction is a hallmark in the development of OA. It results from imbalances between the production and breakdown of the joint tissues, associated with a number of anabolic and catabolic factors [29]. In a joint tissue, MSCs and chondrocytes play a key role in the articular cartilage regeneration. Chondrocytes located in articular cartilage produce both the extracellular matrix components and the enzymes to degrade aging ECM, maintaining homeostasis of the cartilage. In the OA state, the homeostatic balance is disturbed by dominant catabolic regulators, resulting in cartilage tissue degradation. Due to the low

mitotic activity of the chondrocytes and avascularity of cartilage tissue, the articular cartilage lacks innate ability to self-healing after the onset of OA [30].

MSCs are multipotent stem cells with the capability to self-renew and differentiate into multiple cell lineages, including chondrocytes, osteoblasts, and adipocytes. Recently, MSC-like cells have been identified in adult cartilage and they are also known to contribute to the maintenance of the cartilage homeostasis [31]. MSCs have received considerable attention for their potential use in cell-based therapies for OA treatment [32]. For example, microfracturing on subchondral bone utilizes and stimulates resident MSCs in bone marrow to repair cartilage damage. Additionally, local delivery of *ex vivo* cultured MSCs have shown promising outcomes in OA, likely as a result of the paracrine or immunomodulatory effects of the MSCs.

Regulating cell fate, state, and function of MSCs by small molecules provides a new tool for stem cell-based therapies [33]. Recent efforts involving small molecule stimulation of latent articular cartilage MSCs to form chondrogenic nodules has shown great potential as a novel therapeutic strategy to repair diseased cartilage. In this work, we investigated GalNAc-a as a potential small molecule inducer of chondrogenic differentiation of human MSCs. Gene expression studies confirmed the enhanced chondrogenic effect of GalNAc-a **(Fig 3.3B)**. It has been known that the Wnt/□-catenin signaling pathway is involved in the regulation of MSC differentiation into cartilage. The Wnt/□-catenin pathway is one of the fundamental mechanisms for cell fate, proliferation, and differentiation in embryonic development and tissue homeostasis [34]. So, we further investigated the involvement of Wnt genes and proteins upon GalNAc-a exposure and confirmed a decrease in the protein and gene expression level of □-catenin **(Fig 3.3)**. Day

et al. found that inactivation of □-catenin during the developmental process caused an enhanced chondrocytes differentiation. Similarly, others have shown that inhibiting Wnt signaling in MSCs resulted in promoting chondrogenesis [35, 36]. In line with previous findings, our results suggest that GalNAc-a promoted chondrogenesis of hMSC by interfering with the Wnt/□-catenin signaling activity. The cartilage tissue production associated with the stimulating chondrogenic effect was further examined on 3D hydrogel and pellet culture systems [37]. We observed recapitulation of the chondrogenic effect in the 3D cell culture environment, which confirmed the anabolic of GalNAc-a. Additionally, immunohistochemical staining of pellets treated with GalNAc-a exhibited down-regulation of hypertrophic chondrocyte specific proteins **(Fig 3.4D)**, indicating retention of cartilage phenotype [38].

The molecular mechanisms underlying chondrocyte hypertrophy is linked with activation of the Wnt signaling [38]. This motivated us to further investigate an effect of GalNAc-a on hMSC under osteogenic condition. It was reported that disruption of the Wnt signaling pathways improves chondrogenesis of MSC while impairing the osteogenic differentiating capacity of MSC [37]. Both gene expression and histological studies confirmed the observation of the adverse effect of GalNAc-a on the osteogenic differentiation of the hMSC. Interestingly, adipocyte features were observed after 15 days of osteogenic induction supplemented with GalNAc-a. The inverse relationship between osteogenic and adipogenic differentiation has been reported both *in vitro* and *in vivo*. Multiple signaling pathways are committed to the preferential induction of one lineage at the expense of the other. Particularly, inhibition of Wnt signaling promotes adipogenesis while suppressing osteogenesis [39]. Given other data that suggest the action of GalNAc-

a on the Wnt pathway, it is suggested that our observation to the adipocytic phenotype presumably occurred at the expense of the reduced osteogenic differentiation by disruption of Wnt signaling activity. This adverse effect on the osteogenic differentiation concomitantly supports the results of the promoting effect of GalNAc-a on chondrogenic commitment of MSCs by modulation of Wnt signaling.

The stimulation of endogenous MSCs into the chondrogenic lineage by small molecules has shown great promise as a novel cartilage-regeneration strategy. However, chronic inflammatory conditions in an OA joint may provide a sub-optimal environment for the small molecules to function. A large number of inflammatory cytokines present in an OA joint that disrupt regeneration capacity of the MSC could also limit the therapeutic potential of the small molecules. Modulating the inflammation could create favorable condition for the drug action on the endogenous MSCs. Moreover, inhibiting the inflammation has another benefit on cartilage homeostasis, which has been a primary therapeutic approach to the development of DMOADs. The inflammatory process secretes a variety of pro-inflammatory cytokines and inflammatory mediators, creating the catabolic state in autocrine and paracrine manner in the OA joint [12]. Therefore, anti-inflammatory drugs directed at the cytokines or inflammatory pathways could restore the cartilage homeostasis, delaying and reversing the progression of OA.

Chondrocytes in the OA joint are one of the primary sources of inflammatory cytokines and mediators [40]. In the present study, we demonstrated that GalNAc-a exposure to the human osteoarthritic chondrocytes under OA pathophysiological conditions exhibited significant down-regulated gene expression of the inflammatory targets involved in OA **(Fig 3.7A)**. Recently, is has been found that Wnt/□-catenin

signaling in osteoarthritic chondrocytes is more activated than normal chondrocytes and linked with inflammatory cytokine-induced cartilage degradation in OA [41]. In line with the findings, Landman *et al*. reported that inhibition of Wnt/□-catenin signaling in cytokine-stimulated chondrocytes reduced cartilage degradation. Similarly, our results confirmed the involvement of Wnt related genes and proteins with the anti-inflammatory effect **(Fig 3.7)**. In addition, the anti-catabolic effect of GalNAc-a increased chondrogenic-specific gene expression and the proteoglycan and ECM production in the 3D culture, indicating its chondroprotective effect on the OA chondrocytes **(Fig 3.8)**. GalNAc-a's aforementioned ability to inhibit the inflammation combined with its ability to promote chondrogenesis associated with the modulation of Wnt activity, makes it a strong potential candidate as a DMOAD to be efficacious under pathophysiological conditions. Further target identification and mechanistic studies of GalNAc-a action on the molecular signaling pathways are under way.

In consideration of the fact that GalNAc-a exhibited the enhanced chondrogenic and chondroprotective effects on cartilage, we evaluated the potential of OA disease modifying interventions in surgically induced OA rat model. The histological assessments showed that the multiple weekly GalNAc-a treated rats showed improved cartilage repair of the damaged joints **(Fig 3.9)**. Despite IA injection of therapeutics would be suitable for local drug delivery without the risk of systemic side effects, rapid clearance of IA injected drugs through the draining lymphatic system of the synovial fluid limits residence time of the drugs within knee (1-5 hours) [27]. In light of these restrictions, GalNAc-a was encapsulated in PLGA (poly(lactic-co-glycolic acid)) microspheres for prolonged drug release [42]. PLGA microspheres have been widely

used as drug delivery carrier because of their excellent biocompatibility and biodegradability. It has been reported that PLGA microspheres can maintain optimal systemic concentration of drugs for months in the joint. Our results showed sustained release profiles of GalNAc-a from PLGA-GalNAc-a microspheres for over a month *in vitro*. While the systemic exposure of the IA injected GalNAc-a in a joint will be further investigated, we confirmed that a single IA injection of the PLGA-GalNAc-a microspheres one week after OA induction improved cartilage repair, which is comparable to the results observed in the multiple treatments of GalNAc-a **(Fig 3.9D)**. Altogether, the *in vitro* and *in vivo* results support anabolic capacity of GalNAc-a on cartilage matrix to prevent OA progression. Further *in vivo* studies are under way to assess an optimized dosing and the therapeutic potential of GalNAc-a at the late stages of OA.

3.5 Conclusions

We found a sugar based compound, GalNAc-a that has enhancing chondrogenic and chondroprotective capacity. The dual benefits of GalNAc-a on MSC and chondrocytes could improve cartilage tissue production *in vitro* and cartilage repair in damaged joints *in vivo*. Furthermore, its incorporation into the microsphere drug delivery system showed efficient therapeutic outcomes without multiple injections. These findings suggest that the potential for the use of GalNAc-a as a new disease modifying OA drug.

3.6 Figures

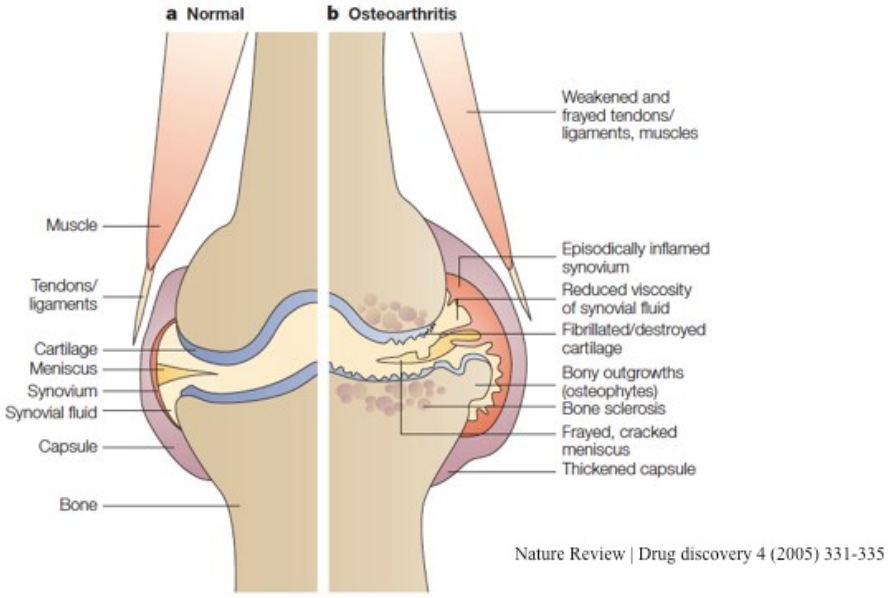

Figure 3.1 Osteoarthritis (OA) is the degenerative joint disease with trauma and aging. The characteristics of OA include an irreversible loss of articular cartilage, subchondral bone thickening, osteophyte formation (bony projections that form along joint margins), and local synovial inflammation.

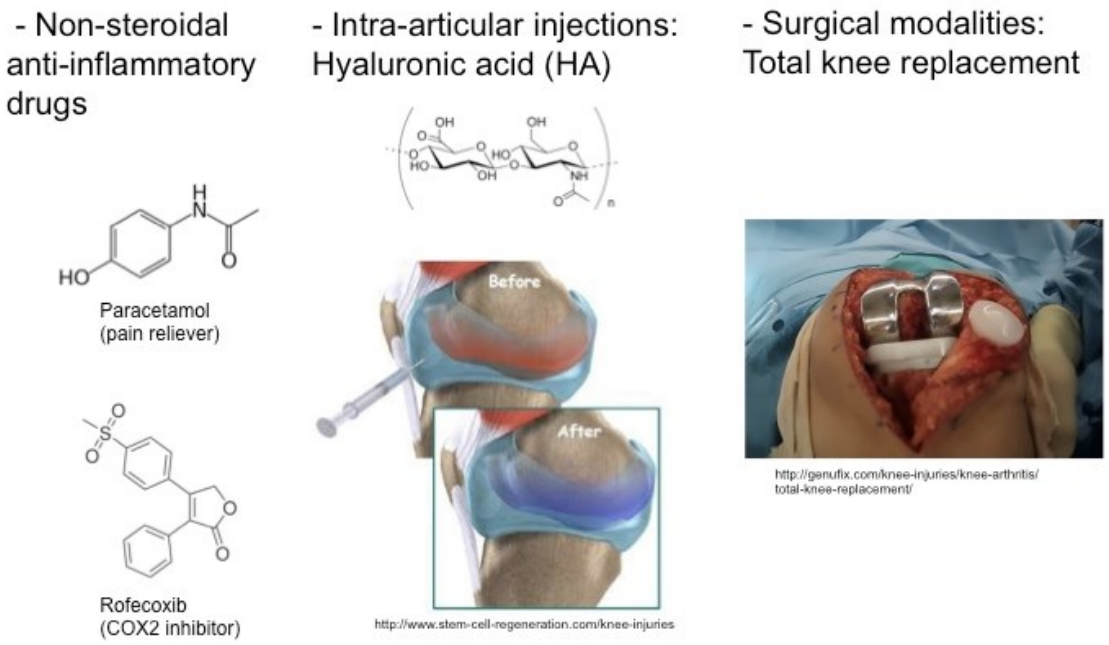

Figure 3.2 Limitation of current OA treatments. Current OA treatments are limited to symptomatic control including non-steroidal anti-inflammatory drugs, intra-articular injections of hyaluronic acid, or total knee replacement. These treatments focus on short-term symptomatic pain relief and care of joint function.

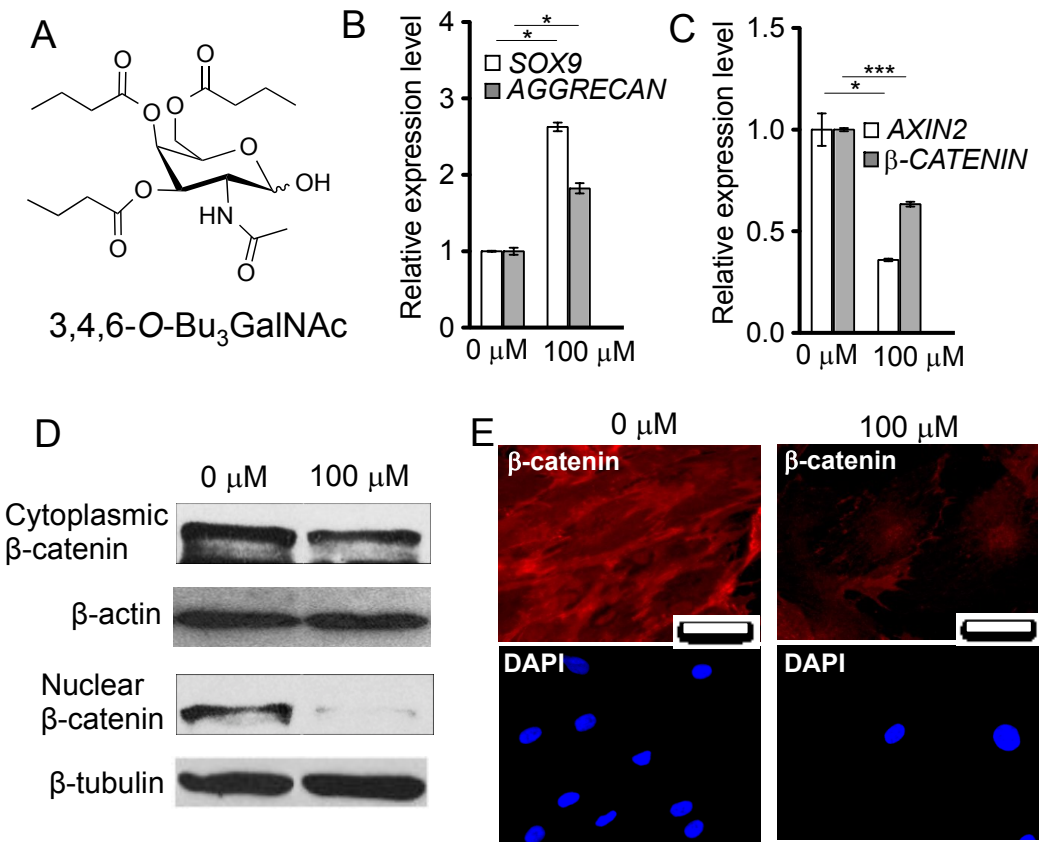

Figure 3.3 3,4,6-*O*-Bu$_3$GalNAc promoted chondrogenesis of hMSCs. Cells were treated with or without GalNAc-a (100 μM) in chondrogenic medium for two days. **A.** Chemical structure of 3,4,6-*O*-Bu$_3$GalNAc. **B.** Gene expression level of chondrogenic markers *SOX9* and *AGGRECAN*. **C.** Expression levels of Wnt-related genes *AXIN2* and *β-catenin*. Data in (B and C) are averages of three individual samples relative to *β-ACTIN* mRNA. (**P*<0.05, ****P*<0.001). **D.** Protein expression of β-catenin in cytoplasmic and nuclear compartments was confirmed by Western blotting. β-Actin and □-tubulin were used as respective loading controls. **E.** Immunofluoresence staining for cytoplasmic β-catenin. Nuclei were stained with DAPI (scale bars: 50 □m).

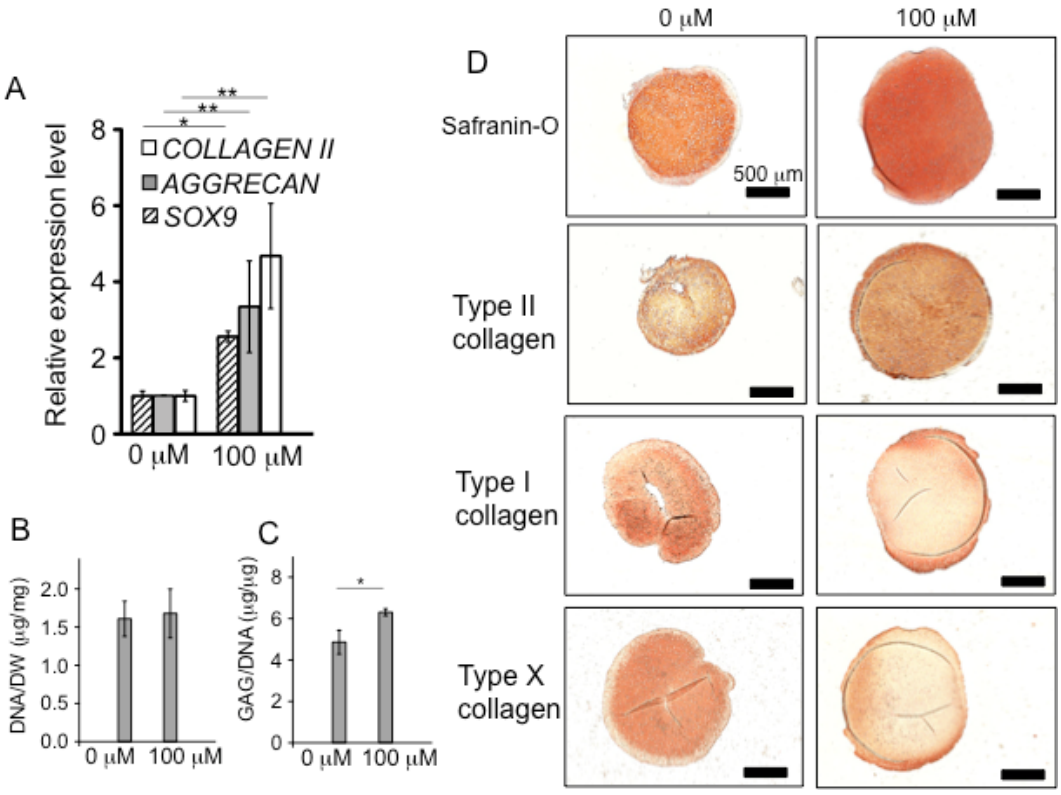

Figure 3.4 Treatment of 3,4,6-*O*-Bu$_3$GalNAc increased chondrogenic markers of 3D pellets of hMSCs and cartilage ECM production. Pellets were treated with or without 3,4,6-*O*-Bu$_3$GalNAc (100 μM) in the chondrogenic medium for 21 days. **A.** Gene expression level of chondrogenic markers, *SOX9, AGGRECAN*, and *TYPE II COLLAGEN* (*COLLAGEN II*). Data are averages of three individual samples relative to *β-ACTIN* mRNA (* $P<0.05$, ** $P<0.01$). **B.** DNA contents normalized to dry weight. **C.** sGAG contents normalized to the DNA content. Data in (B and C) are averages of three individual samples. **D.** Safranin-O and immunohistochemical staining of pellets (type I, type II, and type X collagen). Scale bar: 500 □m.

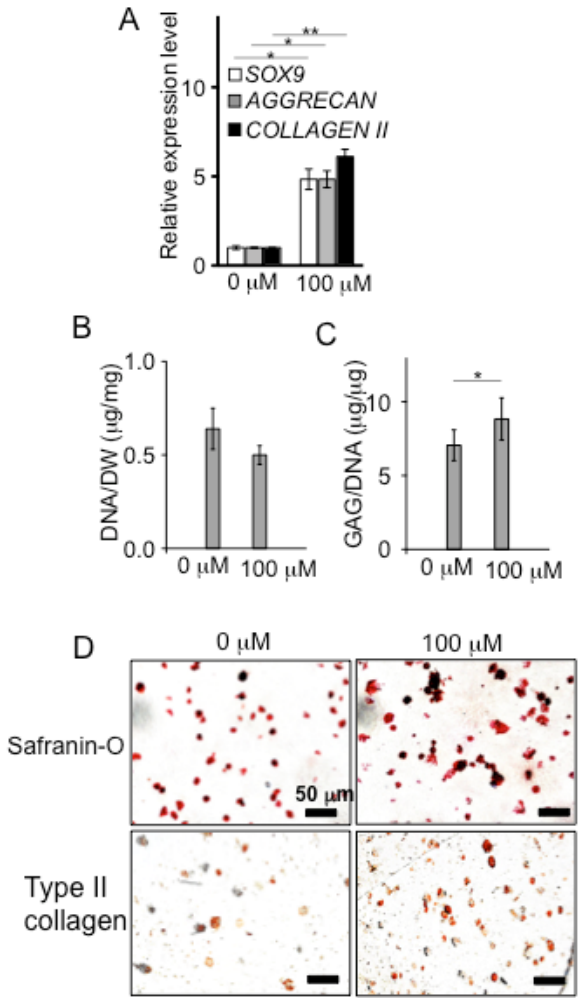

Figure 3.5 3,4,6-*O*-Bu$_3$GalNAc treatment increases chondrogenic expression and cartilage ECM deposition by hMSCs encapsulated in 3D hydrogels. The hydrogels were incubated with or without 3,4,6-O-Bu$_3$GalNAc (100 μM) in chondrogenic medium for 21 days. **A.** Gene expression levels of chondrogenic markers *SOX9*, *AGGRECAN*, and *TYPE II COLLAGEN* (*COLLAGEN II*). Data are averages normalized to *GAPDH* (n = 3, * P<0.05, ** P<0.01). **B.** Biochemical analysis of DNA content, normalized to dry weight. **C.** GAG content, normalized to the DNA content. Data in (B and C) are averages of three individual samples. **D.** Safranin-O and immunohistochemical staining (type II collagen) of cross-section of the hydrogel (Scale bar: 500 □m).

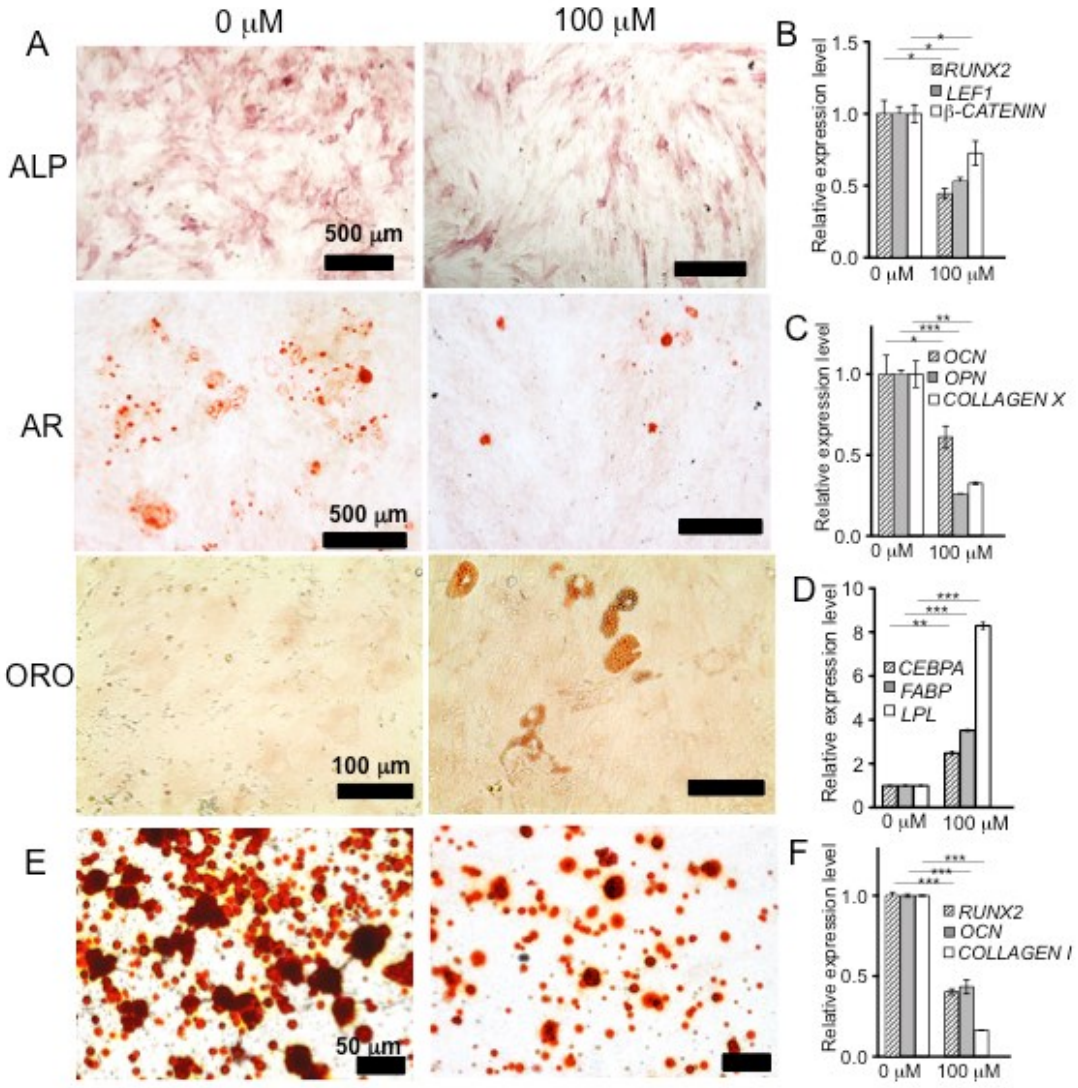

Figure 3.6 3,4,6-*O*-Bu$_3$GalNAc reduces osteogenic capacity of hMSCs. Cells on monolayer and 3D hydrogel cultures were incubated with or without 3,4,6-*O*-Bu$_3$GalNAc in the osteogenic medium. A. Alkaline phosphatase (ALP) activity (scale bar: 500 □m), Alizarin red (AR, scale bar: 500 □m), and Oil red O (ORO, scale bar: 100 □m). **B.** RT-PCR analysis of gene expression after 5 days osteogenic induction of hMSCs. **C.** RT-PCR analysis of osteogenic markers at 10 days of the osteogenic induction. **D.** RT-PCR analysis of adipogenic markers at 15 days of the osteogenic induction. For RT-PCR analysis, *β-ACTIN* mRNA was used as a control and three individual samples were collected and averaged (* P<0.05, ** P<0.01, *** P<0.001). **E.** Alizarin red staining (scale bar: 50 □m) of cross section of hydrogel. F. RT-PCR analysis of osteogenic markers after 21 days osteogenic induction of hMSCs encapsulated in the hydrogels (Endogenous mRNA control: *GAPDH*, n = 3, *** P<0.001).

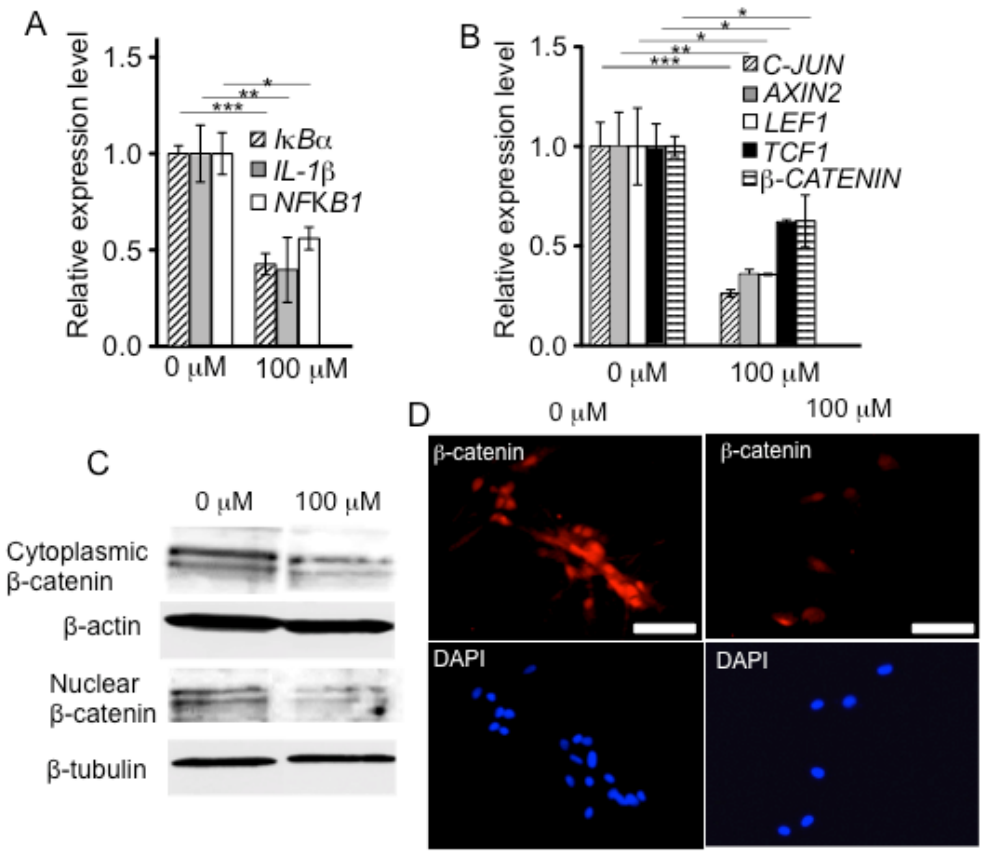

Figure 3.7 3,4,6-*O*-Bu$_3$GalNAc exerts an anti-inflammatory effect on human OA chondrocytes. Primary human OA chondrocytes were cultured in chondrogenic medium supplemented with IL-1β for 24 h and then further incubated with or without 3,4,6-*O*-Bu$_3$GalNAc (100 μM) in the presence of IL-1β for another 24 h. **A.** Gene expression of inflammatory markers and **B.** Wnt signaling genes. Data are averages normalized to *β-ACTIN* ($n = 3$, * $P<0.05$, ** $P<0.01$, *** $P<0.001$). **C.** β-catenin protein bars: 50 □m).

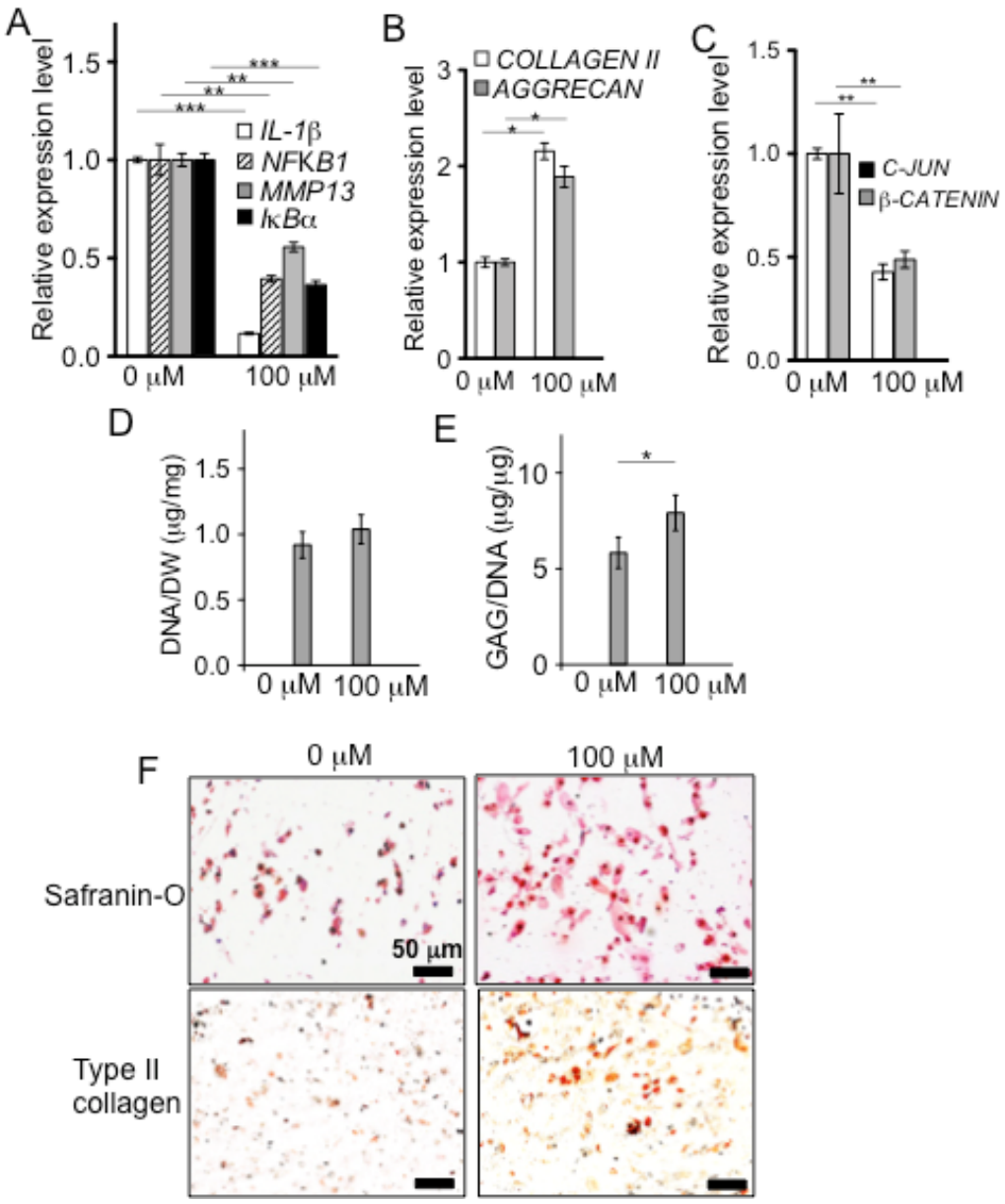

Figure 3.8 3,4,6-*O*-Bu$_3$GalNAc increased chondrogenic markers and cartilage ECM production in 3D hydrogel culture. The hydrogels were incubated with or without 3,4,6-*O*-Bu$_3$GalNAc (100 μM) in the presence of IL-1β for 21 days. **A.** RT-PCR analysis of inflammatory markers, **B.** chondrogenic markers, and **C.** Wnt related markers (endogenous mRNA control: *GAPDH*, n = 3, * P<0.05, ** P<0.01, *** P<0.001). **D.** Biochemical analysis of DNA contents and **E.** sGAG, normalized to the DNA content (n = 3). **F.** Safranin-O and immunohistochemical staining (type II collagen) of cross-section of the hydrogel (Scale bar: 50 μm).

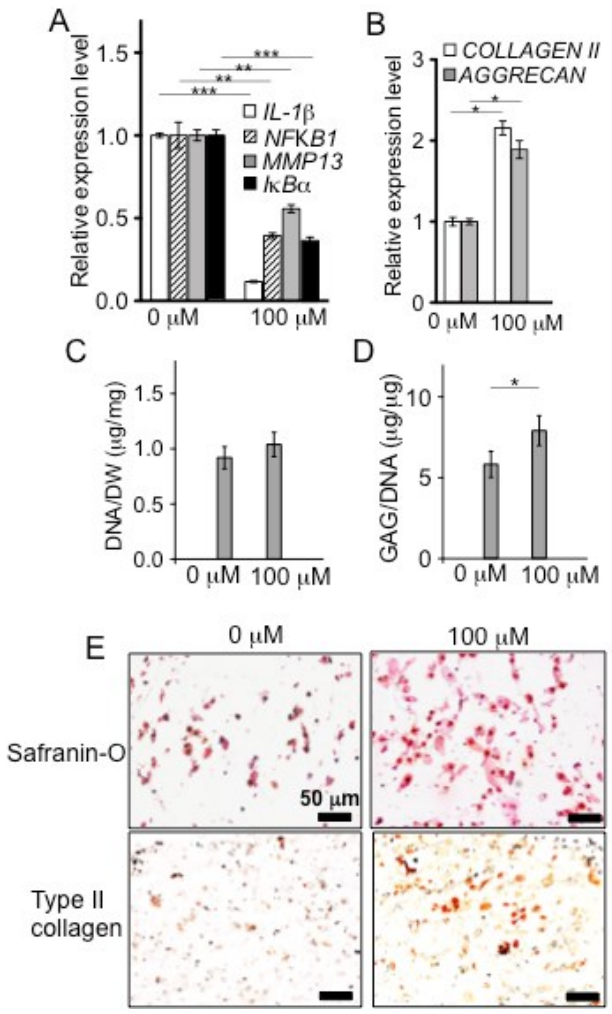

Figure 3.9 3,4,6-*O*-Bu$_3$GalNAc increased chondrogenic markers and cartilage ECM production in 3D hydrogel culture. The hydrogels were incubated with or without 3,4,6-*O*-Bu$_3$GalNAc (100 μM) in the presence of IL-1β for 21 days. **A.** RT-PCR analysis of inflammatory markers and **B.** chondrogenic markers (endogenous mRNA control: *GAPDH*, n = 3, * P<0.05, ** P<0.01, *** P<0.001). **C.** Biochemical analysis of DNA contents and **D.** sGAG, normalized to the DNA content (n = 3). E**.** Safranin-O and immunohistochemical staining (type II collagen) of cross-section of the hydrogel (Scale bar: 50 □m).

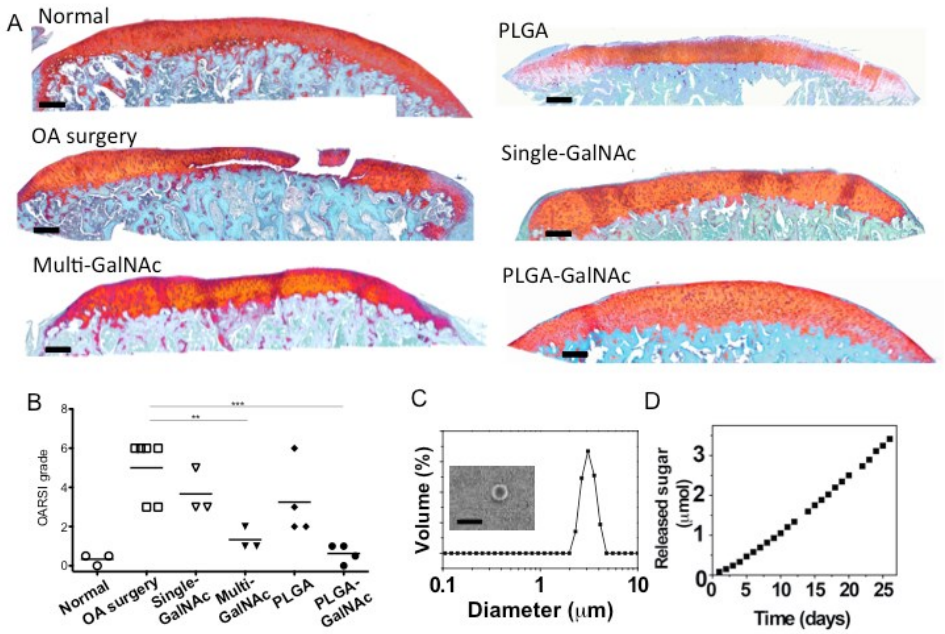

Figure 3.10 Cartilage repair of OA induced rats by intra-articular injection of 3,4,6-*O*-Bu$_3$GalNAc. A. Representative safranin-O stained histological images of the tibial plateau to evaluate the pathological changes 4 weeks after medial meniscal transection (scale bar: 200 □m). The Multi-GalNAc group was given IA injections of 3,4,6-*O*-Bu$_3$GalNAc on days 7, 14, and 21 after the OA surgery. The Single-3,4,6-*O*-Bu$_3$GalNAc, PLGA, and PLGA-3,4,6-*O*-Bu$_3$GalNAc groups were given IA injections on days 7 after the surgery. **B.** Comparison of the tibial plateau joint based on the OARSI scoring system (n = 3~6, ** P<0.01, *** P<0.001). **C.** The size distribution of PLGA-3,4,6-*O*-Bu$_3$GalNAc and scanning electron microscopic image of fabricated PLGA-3,4,6-*O*-Bu$_3$GalNAc microspheres (scale bar: 5 □m). **D.** The cumulative *in vitro* release profile showed sustained release of 3,4,6-*O*-Bu$_3$GalNAc (sugar) from PLGA-3,4,6-*O*-Bu$_3$GalNAc microspheres for over a month.

3.7 References

[1] H.A. Wieland, M. Michaelis, B.J. Kirschbaum, K.A. Rudolphi, Osteoarthritis - an untreatable disease?, Nat Rev Drug Discov 4(4) (2005) 331-44.

[2] F.J. Blanco, C. Ruiz-Romero, New targets for disease modifying osteoarthritis drugs: chondrogenesis and Runx1, Ann Rheum Dis 72(5) (2013) 631-4.

[3] R.F. Loeser, S.R. Goldring, C.R. Scanzello, M.B. Goldring, Osteoarthritis: a disease of the joint as an organ, Arthritis Rheum 64(6) (2012) 1697-707.

[4] J. Martel-Pelletier, L.M. Wildi, J.P. Pelletier, Future therapeutics for osteoarthritis, Bone 51(2) (2012) 297-311.

[5] D.J. Hunter, Pharmacologic therapy for osteoarthritis--the era of disease modification, Nat Rev Rheumatol 7(1) (2011) 13-22.

[6] D.J. Hunter, M.C. Pike, B.L. Jonas, E. Kissin, J. Krop, T. McAlindon, Phase 1 safety and tolerability study of BMP-7 in symptomatic knee osteoarthritis, BMC Musculoskelet Disord 11 (2010) 232.

[7] A. Mobasheri, The future of osteoarthritis therapeutics: targeted pharmacological therapy, Curr Rheumatol Rep 15(10) (2013) 364.

[8] K. Johnson, S. Zhu, M.S. Tremblay, J.N. Payette, J. Wang, L.C. Bouchez, S. Meeusen, A. Althage, C.Y. Cho, X. Wu, P.G. Schultz, A stem cell-based approach to cartilage repair, Science 336(6082) (2012) 717-21.

[9] F. Yano, H. Hojo, S. Ohba, A. Fukai, Y. Hosaka, T. Ikeda, T. Saito, M. Hirata, H. Chikuda, T. Takato, H. Kawaguchi, U.I. Chung, A novel disease-modifying osteoarthritis drug candidate targeting Runx1, Ann Rheum Dis 72(5) (2013) 748-53.

[10] H. Joos, A. Wildner, C. Hogrefe, H. Reichel, R.E. Brenner, Interleukin-1 beta and tumor necrosis factor alpha inhibit migration activity of chondrogenic progenitor cells from non-fibrillated osteoarthritic cartilage, Arthritis Res Ther 15(5) (2013) R119.

[11] P.H. Ousema, F.T. Moutos, B.T. Estes, A.I. Caplan, D.P. Lennon, F. Guilak, J.B. Weinberg, The inhibition by interleukin 1 of MSC chondrogenesis and the development of biomechanical properties in biomimetic 3D woven PCL scaffolds, Biomaterials 33(35) (2012) 8967-74.

[12] M. Kapoor, J. Martel-Pelletier, D. Lajeunesse, J.P. Pelletier, H. Fahmi, Role of proinflammatory cytokines in the pathophysiology of osteoarthritis, Nat Rev Rheumatol 7(1) (2011) 33-42.

[13] A. Mobasheri, The future of osteoarthritis therapeutics: emerging biological therapy, Curr Rheumatol Rep 15(12) (2013) 385.

[14] N. Elmouelhi, U. Aich, V.D. Paruchuri, M.A. Meledeo, C.T. Campbell, J.J. Wang, R. Srinivas, H.S. Khanna, K.J. Yarema, Hexosamine template. A platform for modulating gene expression and for sugar-based drug discovery, J Med Chem 52(8) (2009) 2515-30.

[15] A. Augello, C. De Bari, The regulation of differentiation in mesenchymal stem cells, Hum Gene Ther 21(10) (2010) 1226-38.

[16] G.D. Nicodemus, S.J. Bryant, Cell encapsulation in biodegradable hydrogels for tissue engineering applications, Tissue Eng Part B Rev 14(2) (2008) 149-65.

[17] A.W. James, Review of Signaling Pathways Governing MSC Osteogenic and Adipogenic Differentiation, Scientifica (Cairo) 2013 (2013) 684736.

[18] S.L. Holmen, C.R. Zylstra, A. Mukherjee, R.E. Sigler, M.C. Faugere, M.L. Bouxsein, L. Deng, T.L. Clemens, B.O. Williams, Essential role of beta-catenin in postnatal bone acquisition, J Biol Chem 280(22) (2005) 21162-8.

[19] D.A. Glass, 2nd, P. Bialek, J.D. Ahn, M. Starbuck, M.S. Patel, H. Clevers, M.M. Taketo, F. Long, A.P. McMahon, R.A. Lang, G. Karsenty, Canonical Wnt signaling in differentiated osteoblasts controls osteoclast differentiation, Dev Cell 8(5) (2005) 751-64.

[20] M.F. Pittenger, A.M. Mackay, S.C. Beck, R.K. Jaiswal, R. Douglas, J.D. Mosca, M.A. Moorman, D.W. Simonetti, S. Craig, D.R. Marshak, Multilineage potential of adult human mesenchymal stem cells, Science 284(5411) (1999) 143-7.

[21] M. Lotz, F.J. Blanco, J. von Kempis, J. Dudler, R. Maier, P.M. Villiger, Y. Geng, Cytokine regulation of chondrocyte functions, J Rheumatol Suppl 43 (1995) 104-8.

[22] J.M. Coburn, L. Wo, N. Bernstein, R. Bhattacharya, U. Aich, C.O. Bingham, 3rd, K.J. Yarema, J.H. Elisseeff, Short-chain fatty acid-modified hexosamine for tissue-engineering osteoarthritic cartilage, Tissue Eng Part A 19(17-18) (2013) 2035-44.

[23] M. Corr, Wnt-beta-catenin signaling in the pathogenesis of osteoarthritis, Nat Clin Pract Rheumatol 4(10) (2008) 550-6.

[24] S.G. Hwang, S.S. Yu, S.W. Lee, J.S. Chun, Wnt-3a regulates chondrocyte differentiation via c-Jun/AP-1 pathway, FEBS Lett 579(21) (2005) 4837-42.

[25] E.B. Landman, R.L. Miclea, C.A. van Blitterswijk, M. Karperien, Small molecule inhibitors of WNT/beta-catenin signaling block IL-1beta- and TNFalpha-induced cartilage degradation, Arthritis Res Ther 15(4) (2013) R93.

[26] M. Gibson, H. Li, J. Coburn, L. Moroni, Z. Nahas, C. Bingham, 3rd, K. Yarema, J. Elisseeff, Intra-articular delivery of glucosamine for treatment of experimental osteoarthritis created by a medial meniscectomy in a rat model, J Orthop Res 32(2) (2014) 302-9.

[27] S.G. Owen, H.W. Francis, M.S. Roberts, Disappearance kinetics of solutes from synovial fluid after intra-articular injection, Br J Clin Pharmacol 38(4) (1994) 349-55.

[28] M.L. Kang, G.I. Im, Drug delivery systems for intra-articular treatment of osteoarthritis, Expert Opin Drug Deliv 11(2) (2014) 269-82.

[29] P. Qvist, A.C. Bay-Jensen, C. Christiansen, E.B. Dam, P. Pastoureau, M.A. Karsdal, The disease modifying osteoarthritis drug (DMOAD): Is it in the horizon?, Pharmacol Res 58(1) (2008) 1-7.

[30] D.J. Huey, J.C. Hu, K.A. Athanasiou, Unlike bone, cartilage regeneration remains elusive, Science 338(6109) (2012) 917-21.

[31] S. Koelling, J. Kruegel, M. Irmer, J.R. Path, B. Sadowski, X. Miro, N. Miosge, Migratory chondrogenic progenitor cells from repair tissue during the later stages of human osteoarthritis, Cell Stem Cell 4(4) (2009) 324-35.

[32] S.C. Mastbergen, D.B. Saris, F.P. Lafeber, Functional articular cartilage repair: here, near, or is the best approach not yet clear?, Nat Rev Rheumatol 9(5) (2013) 277-90.

[33] L.L. Lairson, C.A. Lyssiotis, S. Zhu, P.G. Schultz, Small molecule-based approaches to adult stem cell therapies, Annu Rev Pharmacol Toxicol 53 (2013) 107-25.

[34] B.T. MacDonald, K. Tamai, X. He, Wnt/beta-catenin signaling: components, mechanisms, and diseases, Dev Cell 17(1) (2009) 9-26.

[35] G.I. Im, Z. Quan, The effects of Wnt inhibitors on the chondrogenesis of human mesenchymal stem cells, Tissue Eng Part A 16(7) (2010) 2405-13.

[36] S. Saraswati, D.L. Deskins, G.E. Holt, P.P. Young, Pyrvinium, a potent small molecule Wnt inhibitor, increases engraftment and inhibits lineage commitment of mesenchymal stem cells (MSCs), Wound Repair Regen 20(2) (2012) 185-93.

[37] B. Gustafson, B. Eliasson, U. Smith, Thiazolidinediones increase the wingless-type MMTV integration site family (WNT) inhibitor Dickkopf-1 in adipocytes: a link with osteogenesis, Diabetologia 53(3) (2010) 536-40.

[38] Y.F. Dong, Y. Soung do, E.M. Schwarz, R.J. O'Keefe, H. Drissi, Wnt induction of chondrocyte hypertrophy through the Runx2 transcription factor, J Cell Physiol 208(1) (2006) 77-86.

[39] C.N. Bennett, S.E. Ross, K.A. Longo, L. Bajnok, N. Hemati, K.W. Johnson, S.D. Harrison, O.A. MacDougald, Regulation of Wnt signaling during adipogenesis, J Biol Chem 277(34) (2002) 30998-1004.

[40] J.P. Pelletier, J. Martel-Pelletier, S.B. Abramson, Osteoarthritis, an inflammatory disease: potential implication for the selection of new therapeutic targets, Arthritis Rheum 44(6) (2001) 1237-47.

[41] Y. Nakamura, M. Nawata, S. Wakitani, Expression profiles and functional analyses of Wnt-related genes in human joint disorders, Am J Pathol 167(1) (2005) 97-105.

[42] M.S. Shive, J.M. Anderson, Biodegradation and biocompatibility of PLA and PLGA microspheres, Adv Drug Deliv Rev 28(1) (1997) 5-24.

Chapter 4. Targeting senescent cells in osteoarthritis for cartilage repair

4.1 Introduction

Osteoarthritis and Senescent cells

OA is generally considered a degenerative disease of joints with aging since the incidence of OA increases with increasing age but younger populations are at risk in the case of post-traumatic OA. The characteristics of OA include an irreversible loss of articular cartilage, subchondral bone thickening, osteophyte formation, and local joint inflammation[1]. Current pharmacologic OA treatment options are analgesics, non-steroidal anti-inflammatory drugs, and viscosupplementation (e.g. hyaluronic acid (HA)) with intra-articular (IA) injections[2]. These treatments focus on short-term symptomatic pain relief, however with advances in the understanding of the OA pathogenesis there is a focus now on disease-modifying OA drugs (DMOADs) designed to block or reverse OA progression by targeting specific OA catabolic pathways and pathophysiological signaling pathways[3]. Examples of other therapeutic strategies to treat OA include the biologic platelet-rich plasma, Lubricin, HA and biomimetic aggrecan IA injections[4].

Cellular senescence is defined as an irreversible proliferation arrest. It prevents the proliferation of damaged and dysfunctional cells, thereby protecting multicellular organisms against cancer development[5, 6]. However Senescent cells (SnCs) can also contribute to the tissue deterioration that underlies aging and many age-related pathologies and chronic diseases. SnCs accumulate in many vertebrate tissues with age,

where they promote age-related phenotypes and pathologies, presumably through the senescence-associated secretory phenotype (SASP)[7]. The SASP is the transcriptional upregulation and secretion of several extracellular proteases, pro-inflammatory cytokines, chemokines and growth factors[8, 9]. Removal of SnCs in the progeroid mouse model delays several pathologies and increases healthy life span in normal mice [10, 11]. In the case of cartilage, senescent chondrocytes are associated with both post-traumatic and age-related OA as they have been found in cartilage tissue isolated from patients with OA undergoing joint replacement surgery.

A number of the senescence associated molecular pathways have been defined. SnCs induced by stress share common stress-response signaling and senescence activation molecular pathways[12]. The first pathway is activated by DNA-damaging stressors, which stabilize the tumor suppressor protein 53 (p53) and upregulate the p53 transcriptional target p21[13]. Then p21 prevents cyclin-dependent kinase 2 (CDK2)-mediated inactivation of retinoblastoma (RB), which prevents the cells from entering the cell cycle phase S. A second pathway is the $p16^{INK4a}$–retinoblastoma protein (pRB) tumor suppressor pathway. Senescence signals induce the expression of p16INK4a, an inhibitor of CDK. Then CDK further prevents pRB phosphorylation and inactivation, which stops cells from proliferating. Despite the complementary relationship between these two pathways, senescent cells may have distinct responses depending on which pathway is responsible for their development, and this may evolve over time.

SnCs, through their SASP, can also provide beneficial signals for a number of biological processes including the development of embryonic structures[14], wound healing[15, 16] and even insulin secretion from pancreatic beta cells[17]. SnCs have been

found among chondrocytes, the major cellular component of articular cartilage, of older OA patients. These cells express matrix-degrading enzymes that include SASP factors. In vitro studies have shown that the senescence marker $p16^{INK4a}$ was expressed in human OA chondrocytes and triggered osteoarthritic cell/tissue changes such as increased gene and protein expressions for matrix metalloproteinases (MMPs), cartilage degradation, and cartilage calcification[18, 19]. SnCs have been also found after cellular trauma[20]. For example, when young chondrocytes were exposed to oxidative stress *in vitro* (mimicking the release of reactive oxygen species following joint trauma), they underwent cumulative and accelerated senescence. The secretion profile of SnCs and their presence in human OA cartilage strongly suggest that cellular senescence contributes to the age-related and traumatic changes in the chondrocytes and joint tissues with OA.

While the presence of SnC in age-related and traumatic OA has been observed, the removal of these cells as a treatment for OA has not yet been considered or realized. Provided herein are the methods and results of further investigation into how senescent cells can affect cellular processes related to OA. In this study, how senescent cells contribute to OA progression and an investigation into therapeutic benefit of clearing these cells by using GCV in p16-3MR transgenic mice and UBX0101 in wild type C57BL/6 mice.

4.2 Materials and Methods

Mice generation and drug treatment

We purchased young (10-week-old) male C57BL mice from Charles River (Germantown, MD, USA). p16-3MR transgenic mice (a C57BL/6J strain) were generated

as previously described[16] and were bred in the animal facility of the Johns Hopkins University School of Medicine. All studies described using INK-ATTAC mice (a C57BL/6J strain) were generated and performed as previously described[10]. The experimental protocol was approved and performed in accordance with the Institutional Animal Care and Use Committee at Johns Hopkins University and the Mayo Clinic Institutional Animal Care and Use Committee. All mice were housed under pathogen-free conditions, with 5 or less mice per cage. Mice had free access to food and water. The mice used for all experiments were randomly assigned to control or treatment groups, and those used in OA evaluation. For drug treatments, p16-3MR and normal C57BL mice were injected intra-articularly (IA) with 1 or 2 mM of GCV (Sigma-Aldrich, USA, #G2036) in 10 μl of saline or 0.2, 1, or 5 mM of UBX0101 in 10 μl of saline. INK-ATTAC mice were administrated intraperitoneally 2.0 μg AP20187 (B/B homodimerizer, Clontech, USA) per g body weight or vehicle from 12 months until the end of life.

Cell isolation and culture

Human articular cartilage samples explanted from OA patients undergoing total knee arthroplasty were received from the National Disease Resource Institution (Philadelphia, USA) according to an IRB-approved protocol. The cartilage tissue was cut into 1mm^3 pieces, washed 3 times with phosphate-buffered saline (PBS) supplemented with 100 U/mL penicillin and 100 μg/mL streptomycin (Pen/Strep; Invitrogen, USA, #15140-122), and digested on an orbital shaker for 16 h at 37 °C with 0.17% (w/v) type II collagenase (Worthington Biochemical, USA, #4176) in high-glucose Dulbecco's modified Eagle's medium (DMEM; Gibco, USA, #11965-092) with 10% fetal bovine serum (FBS; Hyclone, USA, #SH30070.03). After the digestion, the filtrate was passed

through a 70 μm strainer and cells were rinsed 3 times with DMEM supplemented with 1% Pen/Strep and 10% FBS. For 3D pellet culture of human OA chondrocyte[21], 400,000 cells were seeded in 96 well MicroWell™ round bottom plates (Thermo Fisher Scientific, USA). The pellets were formed in the bottom by centrifugation at 150xg for 10 min. The human OA chondrocytes pellets were maintained at 37 °C with 5% CO_2 in 200 μl of chondrocyte growth medium consisting of high-glucose DMEM, 1% Pen/Strep, 10 % FBS, 1% NEAA (Gibco, USA, #11140-050), 1 M HEPES (Gibco, USA, #15630-080), 100 mM Sodium pyruvate (Gibco, USA, #11360-070), 0.2 M L-Proline (Sigma, USA, #P5607), and 25 mg/ml ascorbic acid (Sigma, USA, #A5960). Pellets were harvested after 21 days for evaluation. The media were changed 3 times a week until the end of the experiment.

Surgically induced OA mouse model

Anterior cruciate ligaments transection (ACLT) and sham surgery were performed on 10-week old or 19-month old male p16-3MR and 10-week old C57BL mice. Animals were placed under general anesthesia with 3% isoflurane, and the hind limbs shaved and prepared for aseptic surgery. For the sham operation, the knee joint was exposed following a medial capsular incision, which cuts the patellar tendon and surgical skin incision was closed with suture. For the ACLT surgery, after opening the joint capsule, the ACL were transected with micro-scissors under a surgical microscope. After irrigation with saline to remove tissue debris, the skin incision was closed. All procedures were performed according to the Institutional Animal Care and Use Committee at Johns Hopkins University School of Medicine. On week 4, 8 or 12, the mice were sacrificed and the joint was collected for mRNA quantification and

histological assessment of the medial tibial plateau joint through blinded graded observations by 2 observers, according to the Osteoarthritis Research Society International (OARSI) Scoring System[22].

Bioluminescence

For in vivo luminescence imaging, p16-3MR mice were injected intra-articular with 10 µl (150 µg/ml) of Xenolight RediJect Coelentarazine h (Calipers, Waltham MA, USA). Twenty-five minutes later, the mice were anesthesized with isofluorane and luminescence was measured with a PerkinElmer IVIS SpectrumCT in vivo imaging System (Caliper Life Sciences, Hopkinton MA, USA; 5 minutes, medium binning).

Real time RT-PCR

To extract RNA, the operated and control hind limbs were dissected and immediately transferred to liquid nitrogen and then pulverized with mortar and pestle. Total RNA was extracted from the knee joints using Trizol reagent and reverse transcribed to cDNA using Super-Script II reverse transcriptase following the manufacturer's protocol (Invitrogen, CA, USA). Real-time PCRs for *cdkn2a, cdkn1a, il1β, mmp3, mmp13, col2a1, acan, sox9, runx2, opg, bglap, rankl and ctsk* were performed using the StepOnePlus Real Time PCR System with SYBR Green PCR Master Mix (Applied biosystems by Life technologies, USA, #4367659). All signals were normalized to *β-actin*. Relative gene expression was calculated by the ΔΔCt method where the ΔCt was calculated using the *β actin* reference gene. ΔΔCt was calculated relative to the unoperated control group in *in vivo* studies and relative to control samples in *in vitro* studies. See supplemental information for a list of primers (**Table. 2**).

Hotplate analysis

Mice were placed on the hotplate analgesia meter at 55 °C (Columbus Instruments, USA). The latency period for hindlimb response (for example, shaking, jumping or licking) was recorded as response time before and at different time points after surgery[23] At least three measurements are taken per mouse. The observer was blinded to the genotype and the treatment of the mice.

Weight bearing

Static incapacitance measurements were performed using Incapacitance Tester (Columbus Instruments, USA). Mice were first acclimated to the chamber at least 3 times before measurement. After acclimitization, mice were maneuvered inside the chamber to stand with one paw on each scale. Weight placed on each hind limb was measured over a 3-second interval for at least 3 separate measurements. Results are expressed as a percentage of weight placed on the operated limb versus contralateral control limb. The observer was blinded to the genotype and treatment of the mice.

Pharmacokinetic half-life determination

Local and blood pharmacokinetics was performed after a single intra-articular administration of 1 mM UBX0101 in saline to determine the half-life and were generated by Seventh Wave laboratories (MO, USA).

Biochemical analysis for GAG contents

The pellets (n = 3 per group) were lyophilized for 2 days and then digested overnight in 125 mg/ml papainase (Worthington, USA, #3126) for 16 h at 60 °C. The

sulfated glycosaminoglycan (sGAG) content was determined by 1,9-dimethylmethylene blue (DMMB) dye assay, measuring absorbance at 525 nm and using chondroitin sulfate as a standard. DNA content was determined by the Hoescht Dye 33342 DNA assay, using calf thymus DNA as a standard. GAG content levels were expressed as micrograms of GAG per microgram of DNA.

Histology

The pellets and mice joints were fixed in 4% paraformaldehyde overnight, dehydrated in increasing concentrations of ethanol, and embedded in paraffin. Five micrometer-thick sections were cut from the paraffin block and collected onto glass slides. The sections were stained for proteoglycans with aqueous Safranin-O (0.1%) for 5 mins and then the specimens were mounted.

Quantification of subchondral bone damage

Osteophyte thickness (a distance on the marginal zone of medial tibial plateau starting an original edge of the tibial articular cartilage) was measured with AxioVision SE64 software. Medial tibial bone sclerosis (the extent of subchondral bone sclerosis/reduction in bone marrow area) was scored by measuring subchondral trabecular bone to marrow ratio. On each safranin-O stained joint section, the decrease or increase in trabecular bone area was assigned a score from -5 to 5, where 0 represents no increase or decrease, -5 represents severe bone loss and 5 represents severe bone sclerosis.

Immunohistochemistry

For immunohistochemical staining, endogenous peroxidase of the sections was quenched using 2.5% (v/v) hydrogen peroxide in methanol, then incubated at 3° C with 0.25% (w/v) hyaluronidase for 1 h. The AEC Broad Spectrum Histostain-SP Kit (Invitrogen, USA, #959944) was used following the manufacturer's instructions. Primary antibodies for $p16^{INK4a}$ (1:500;Abcam, USA, #ab54210), MMP-13 (1:200; Abcam, USA, #ab39012), type I collagen (1:100; Abcam, USA, #ab34710), type II collagen (1:300; Abcam, USA, #ab34712), and type X collagen (1:50; Abcam, USA, #ab58632), osteocalcin (1:100; Millipore, USA, #AB10911), HMGB1 (1:500; Abcam, USA; #ab18256), Ki67 (1:100; Novusbio, USA, #NB110-89717) and PCNA (1:100; Thermo scientific, # MA511358) were used and dilution in 4% BSA dissolved in PBST.

Immunofluorescence

Monolayer cultures of human OA chondrocytes were fixed in 4% paraformaldehyde, permeabilized with PBS containing 0.25% Triton X-100 for 10 min, then blocked with 4% BSA containing 0.25% Triton X-100 for 30 min at room temperature. The cells were incubated with primary antibodies against HMGB1 (1:100; abcam, USA) overnight at 4°C. The cells were rinsed 3 times with PBS and incubated was goat anti-rabbit IgG (H& L) conjugated with Alexa Fluor 594 (1:1000; Life technologies, USA, #A-11012). After washing, the nuclei were counterstained with DAPI for 5 min. Nuclear HMGB1 was imaged by fluorescence microscopy (Carl Zeiss, USA). Cell proliferation was detected using Click-iT® EdU (5-ethynyl-2'-deoxyuridine) Alexa Fluor® 488 imaging kits (Promega, USA, #C10337). Total cells were counted following nuclear DAPI counter staining in 10 random fields per culture dish to determine the percentage of EdU+ cells.

SA-β-galactosidase staining

SA-β-gal staining was done using a kit (Biovision, USA, #K320-250) according to the manufacturer's instructions. SnCs were identified as blue-stained cells under light microscopy. Total cells were counted using a nuclear DAPI counterstain in 10 random fields per culture dish to determine the percentage of SA-β-gal positive cells.

Flow cytometry analysis for apoptosis detection

For Annexin V/PI analysis, live trypsinized and floating cells were collected, centrifuged, rinsed with PBS. Cells were stained with Annexin V apoptosis detection kit APC according to the manufacturer's instructions (eBioscience, USA, #88-8007). Data were analyzed with the BD Accuri^{TM} C6 flow cytometer and FlowJo X 10.0 software (Becton Dickinson, USA).

Western blot

To assay the cleaved caspase-3, and $p16^{INK4a}$ protein, chondrocytes were harvested, washed twice with ice-cold PBS, and lysed with RIPA buffer (Thermo Scientific, USA, #89900) containing protease (Sigma, USA, #P8340) and phosphatase inhibitor mixture (Sigma, USA, #P5726) according to the manufacturer's instructions. Total proteins concentration was determined using the BCA assay (Pierce, USA, #23227). Protein were separated by 10% SDS-PAGE and then transferred onto nitrocellulose membranes. The membranes were blocked for one hour with 5% BSA in Tris-buffered saline containing 0.1% tween-20 (TBST) and incubated overnight at 4°C with primary antibody specific for cleaved caspase-3 (1:1000, Cell signaling, USA, #9661), $p16^{INK4a}$ (1:500, Abcam, USA, #ab54210) and β-actin (1:300, Sigma, USA), After washing away

unbound primary antibodies, the membranes were incubated with horseradish peroxidase-conjugated anti-rabbit secondary antibodies (1:5000, Bio-Rad, USA) and anti-mouse secondary antibodies (1:5000, Cell signaling, USA, #7076) and proteins were detected by ECL.

Statistics

The data displayed normal variance. No statistical method was used to predetermine sample size except early death of mice due to fighting. The experiments were not randomized, except for the *in vivo* animal studies with mice as described above. Any samples and animals didn't exclude from the analysis. All *in vivo* data are expressed as mean and each data point represents an individual mouse. All *in vitro* data are expressed as are averages ± S.D. Statistical significance (p value) was determined by an unpaired, two-tailed Student t test with Welch's correction (we do not assume equal S.D. in each group) or one-way ANOVA (Tukey's multiple comparison test). All analyses were performed by Prism 6 from GraphPad software (San Diego, CA, USA). Statistical significance was determined to be $P < 0.05$.

4.3 Results and Discussion

To critically test the idea that SnCs contribute to OA pathogenesis, we first asked whether SnCs develop after articular joint injury in mice by following the expression of $p16^{INK4a}$ (also known as cyclin-dependent kinase inhibitor 2a, encoded by the *cdkn2a* locus), a frequently used biomarker for SnCs[6, 10, 13, 24]. We induced post-traumatic OA by ACLT in p16-3MR transgenic mice in which $p16^{INK4a}$-positive SnCs can be non-

invasively monitored[16],[25] **(Fig 4.3a).** Luminescence in the articular joint region of the p16-3MR mice increased after ACLT surgery (**Fig. 4.4a, b**), peaking two weeks post-injury and decreasing thereafter to a low level steady state that remained above background (**Fig. 4.3b**). The mRNA level of *cdkn2a* increased and decreased with kinetics similar to that of the luminescence (**Fig. 4.4c** and **Fig. 4.3c**). mRNA levels of *cdkn1a* and the SASP marker interleukin (*il*)*6*[12] also increased in vehicle-treated ACLT mice compared to sham-operated controls 28 days after ACLT, further corroborating the development of SnCs in the injured joint (**Fig. 4.3d**). OA disease and cartilage degeneration after ACLT was confirmed histologically and through pain assessment. ACLT injury reduced Safranin-O proteoglycan staining with cartilage thinning and surface irregularities and induced type 2 collagen degradation (**Fig. 4.3e**, **f**). Behavioral assessment of OA-induced pain showed that ACLT surgery caused mice to decrease weight bearing on the injured leg and increase the latency period for the injured hind limb to reach a pain threshold after placement onto a 55℃ platform (**Fig. 4.3g)**.

To localize SnCs in the articular joint, we performed immunostaining for $p16^{INK4a}$ protein and loss of nuclear high-mobility group box 1 (HMGB1) – an extracellular alarmin that precedes the secretion of SASP components in cells undergoing senescence[26, 27]. In vehicle-treated ACLT mice, $p16^{INK4a}$ protein was largely restricted to the superficial zone, where 66% of cells were $p16^{INK4a}$-positive and 65% of cells had little to no nuclear HMGB1 staining in the articular cartilage (**Fig. 4.4e, f**). In contrast, there were lower numbers of cells that stained for $p16^{INK4a}$ protein and HMGB1 was largely nuclear in sham-operated controls. In addition to the cartilage surface, an increase in $p16^{INK4a}$-expressing cells was also observed in the synovium; however, there was no

apparent increase of $p16^{INK4a}$ expression in the infrapatellar fat pads in vehicle-treated p16-3MR ACLT mice compared to those without ACLT surgery (**Fig. 4.5a)**. The role of the synovium in OA has long been postulated[28], and these results suggest it also contributes to the senescence burden in articular joints during OA progression. SnC localization in the superficial layer of cartilage has particular significance for tissue regeneration, as this is where purported cartilage progenitor cells are located[29]. Furthermore, the superficial and deep cartilage layers interact to maintain homeostasis and increase new tissue production when needed[30], further indicating a regulatory role of these superficial layer cell populations that express $p16^{INK4a}$.

Next, we sought to determine whether selective removal of SnCs that develop after ACLT reduced or reversed the progression of OA and OA-related symptoms. We took advantage of the p16-3MR transgene that also includes the truncated herpes simplex virus 1 (HSV-1) thymidine kinase (HSV-TK) that permits the selective killing of $p16^{INK4a}$-expressing cells by ganciclovir (GCV)[31]. To clear SnCs, we reduced the number of GCV injections into the joint (2 cycles of 5 consecutive injections in **Fig. 4.3)** to once every two days starting at day 14 after ACLT surgery (**Fig. 4.4a)**. GCV treatment reduced luminescence in the ACLT mice (**Fig. 4.4b)**, indicative of clearing $p16^{INK4a}$-positive SnCs. Clearance was confirmed by reduced injury-induced increases in the mRNA levels of *cdkn2a* and *cdkn1a* (**Fig. 4.4c, d**), along with increased immunostaining for nuclear HMGB1 and reduced $p16^{INK4a}$ protein in the cartilage (**Fig. 4.4e, f**). We also observed a reduction in $p16^{INK4a}$ expression in the synovium in GCV-treated p16-3MR mice (**Fig. 4.5a).** Clearance of SnCs inhibited articular cartilage erosion such that proteoglycan staining was largely rescued and resembled that of normal tissue (**Fig. 4.4e,**

g). Pain associated with the ACLT injury also decreased when SnCs were removed (**Fig. 4.4h**), as was expression of the inflammatory markers matrix metalloproteinase (*mmp*)*13* and *il1β* (**Fig. 4.4d**) that are typical of OA disease and tissue degradation[32]. SnC removal increased expression of proteins and *col2a1* and *acan* mRNA (which encode the cartilage extracellular matrix molecules type II collagen and aggrecan). The expression of *sox9*, which among other activities regulates chondrogenesis, remained unchanged. However, pathological changes in the subchondral bone and expression of bone resorption-related genes[33] increased after ACLT surgery and OA development but were not rescued by GCV treatment (**Fig. 4.5b–d**), suggesting that GCV may not reach the bone when injected intra-articular and systemic administration may be required[25]. To confirm that GCV itself did not influence the local cartilage environment but only killed SnCs in p16-3MR mice, we injected GCV into ACLT-treated joints of non-transgenic C57BL mice where it was found to have no influence on OA disease progression or pain **(Fig. 4.3)**. Together these data suggest that SnCs develop after trauma in the articular cartilage and synovium of the knee joint, and their removal, even after OA and symptoms developed, reduces disease impact and creates a pro-chondrogenic environment.

To selectively clear SnCs using a pharmacologic approach, we tested a senolytic (UBX0101) that was recently identified for selective elimination of SnCs[25, 34]. First, we optimized the concentration of UBX0101 using p16-3MR mice using an injection regimen similar to that used to administer GCV. The development of SnCs was followed by luminescence to compare drug efficacy in clearing SnCs with that of GCV. An IA injection with as little as 0.2 mM UBX0101 14 days after ACLT effectively cleared the

SnCs induced by the surgery. The luciferase signal decreased after UBX0101 treatment (**Fig. 4.6a**) and SnC clearance was confirmed by reduced expression of *cdkn2a, cdkn1a, mmp13* and *il1β* (up to 50%) in UBX0101-treated ACLT mice (**Fig. 4.6b**). OA-related disease outcomes of pain and articular cartilage erosion were similarly reduced with both compounds (**Fig. 4.6c–e**). Proteoglycan loss, thinning and calcification of articular cartilage were attenuated in ACLT mice treated with 1 mM UBX0101. Moreover, injection of 0.2 to 5 mM UBX0101 also produced a pro-chondrogenic environment characterized by increased *col2a1* and *acan* gene expression, indicating new cartilage growth. The expression of *sox9* and *runx2*, which regulates chondrocyte hypertrophy and bone development[35], remained unchanged (**Fig. 4.6b).** Similar to the GCV response in the p16-3MR mice, abnormal subchondral bone remodeling and osteophyte formation in ACLT mice were not rescued by UBX0101 treatment.

The lifetime of UBX0101 in the articular joint is short, with concentrations falling below the IC50 after 1.5 hours. Systemic exposure is minimal (3.3% of IA dose reaches the circulation) and the IC50 is never reached (**Fig. 4.7**). This short half of UBX0101 in the joint cavity was effective in blocking cartilage erosion in our ACLT mouse model because UBX0101 eliminates SnCs rather than blocking their secretion. Once the cells have been eliminated, drug exposure is no longer necessary. Considering therapeutic translation, we next aimed to reduce the number of IA injections while still achieving successful SnC removal. We thus determined the number of UBX0101 injections (once every two days) required to reduce OA progression when injected 14 days after ACLT surgery (**Fig. 4.8**). Both five and six injections of 1 mM UBX0101 decreased expression

of *cdkn2a, mmp13* and *il1β*, increased the expression of *col2a1* and *acan*, and reduced OA-induced pain compared to vehicle-treated ACLT mice.

We next confirmed the efficacy of IA UBX0101 injections for treating ACLT-induced OA in C57BL mice. Based on the short drug lifetime in the articular space and the dosing experiments, six IA injections (1 mM, once every two days starting at day 14 after ACLT over 2 weeks) were performed (**Fig. 4.9a**). Similar to the effects of GCV in p16-3MR mice, UBX0101 treatment selectively killed SnCs that were induced by ACLT surgery in the articular cartilage. This SnC clearance was confirmed by (i) a reduced number of cells without nuclear HMGB1 and increased numbers of nuclear HMGB1 + non-SnCs (**Fig. 4.9b, c**); ii) an increased number of $p16^{INK4a}$, Ki-67 and proliferating cell nuclear antigen (PCNA) expressing non-SnCs **(Fig. 4.9b, c** and **4.10a)**; (iii) fewer mmp13-positive chondrocytes (**Fig. 4.9b, c**); and iv) reduced levels of *cdkn2a, cdkn1a, il6* and *mmp13* mRNAs 28 days post-injury (**Fig. 4.9d**). We also observed fewer Ki-67-expressing cells in the synovium of the vehicle-treated C57BL mice, consistent with the presence of SnCs, which was abrogated by UBX0101 treatment (**Fig. 4.10b**). This correlates with a reduction in expression of $p16^{INK4a}$ in the synovium of the GCV-treated p16-3MR mice.

The long-term durability of a single UBX0101 treatment course, and its ability to attenuate articular cartilage degeneration and ameliorate OA symptoms, was evaluated over 84 days (**Fig. 4.9c**–**f**, **4.11** and **4.12**). Pain reduction was maintained between 28 and 56 days after surgery and pro-chondrogenic gene and protein expression of *col2a1* and *acan* remained upregulated compared to the untreated control. Subchondral bone alterations induced by ACLT surgery did not change over the 84-day study. However,

OA-induced pain and disease (cartilage degradation and subchondral bone sclerosis) returned at 84 days after ACLT or 4 weeks after the last drug injection (**Fig. 4.12**), suggesting that SnCs may return by week 12 after ACLT. In the mouse ACLT, the ligament cannot be repaired so continued damage may occur in the joint in addition to age-related accumulation of SnCs that develop over time. Thus, repeated treatment may be required to remove SnCs that accumulate due to injury and aging to prevent disease development and achieve long term disease modification.

To test the potential of treating later stage disease, we injected UBX0101 42 days after ACLT (**Fig. 4.13a**). After the standard IA injections over two weeks, UBX0101 treatment increased the number of non-SnCs with nuclear HMGB1 (**Fig. 4.13b),** reduced OA-induced pain (**Fig. 4.13c)**, and reduced the levels of *cdkn2a, cdkn1a,* and *mmp13* mRNAs (**Fig. 13d**). Further, chondrogenic gene expression (*col2a1* and *acan* mRNAs) and proteoglycan staining in the articular cartilage increased even with the late UBX0101 treatment (**Fig. 4.13d, e**). ACLT mice treated with UBX0101 had a reduction in subchondral bone sclerosis but similar osteophyte formation relative to vehicle treated controls (**Fig. 4.13f).** Together these results indicate the UBX0101 can clear SnCs from articular cartilage to reduce OA symptoms and modify the disease by creating a pro-regenerative environment even in later stage disease.

Similar to humans, aging contributes to the development of spontaneous and injury-induced OA in mice[36, 37]. We therefore explored the consequences of selective removal of naturally occurring, age-related SnCs on arthritis development using the INK-ATTAC transgenic model that was previously reported[10, 11]. Starting at 12 months of age, AP20187, the molecule that induces apoptosis in $p16^{INK4a}$-expressing cells[10], was

injected intraperitoneal in female mice twice a week until animals became moribund. In the articular joints of these mice, elimination of naturally occurring $p16^{INK4a}$-positive SnCs markedly reduced aged-related cartilage degeneration compared to vehicle alone in the INK-ATTAC transgenic mouse as demonstrated by significantly increased Safranin-O staining for proteoglycans, cartilage thickness, and normalized Osteoarthritis Research Society International (OARSI) scores (**Fig. 4.14a–c** and **4.15a)**.

The synergistic impact of age and trauma may further exacerbate disease. To address this we performed the ACLT surgery on mice aged 19 months and evaluated the effect of selective SnC removal on OA disease. Contrary to young animals, luminescence in the articular joint region of vehicle-treated aged p16-3MR mice increased continually over 28 days after ACLT surgery (**Fig. 4.14d**). This SnC development in ACLT mice was corroborated by significant increases in *cdkn2a, cdkn1a* and the SASP factor *il1β* and increased ki-67 positive non-SnCs compared to no surgery controls (**Fig. 4.14e** and **4.15b)**. Moreover, distribution of the SnCs after ACLT was significantly different from the young mice. In particular, 40% of $p16^{INK4a}$-positive SnCs were localized throughout the articular cartilage of vehicle treated-ACLT mice instead of only the superficial layer (**Fig. 4.14e** and **4.15b)**.

More severe OA developed after ACLT surgery in the aged 3MR mice compared to young mice as demonstrated by histology and OARSI scoring of vehicle treated animals (**Fig. 4.14f, g)**. In fact, the baseline morphology of the aged animals without surgery showed thinning cartilage with reduced Safranin-O staining and higher OARSI scores. Removal of SnCs from the aged 3MR animals using the standard regimen of UBX0101 reduced OA-induced pain similar to the young animals (**Fig. 4.14h)**.

Furthermore, gene expression for *cdkn2a, cdkn1a, il6 and mmp13* was reduced with SnC clearance. Moreover, *cdkn2a, cdkn1a* and *mmp13* gene expression levels in mice with ACLT treated with UBX0101 were lower than animals that did not receive any surgery, suggesting higher baseline levels of SnCs in the aged mice (**Fig. 4.14f**). Contrary to the young animals though, there was no increase in pro-chondrogenic gene expression (*col2a1* and *acan* mRNA) in the older animals after treatment at 28 days (**Fig. 4.14f)**. Histologically, there was a small increase in Safranin-O staining of the articular cartilage in ACLT mice but the decrease in OARSI scoring was not statistically significant with the small number of animals in this study. ACLT- and age-induced changes in bone did not significantly change with UBX0101 treatment (**Fig. 4.15c, d)**. However, SnCs found in the synovium were cleared with UBX0101 treatment and those in the subchondral bone marrow were slightly reduced **(Fig. 4.15e)**. These findings suggest that UBX0101 can clear SnCs from aged articular cartilage but the age-related decline in proliferative and synthetic capacity of articular chondrocytes may reduce subsequent tissue regeneration[38]. However, based on the drastic articular joint improvement in the significantly older animals with naturally occurring OA, it is likely that additional treatments, and potentially systemic treatment, may be required to reduce disease and rebuild tissue.

The relevance of SnCs and their clearance in clinical OA was evaluated in explant and *in vitro* cultures from patients undergoing total knee arthroplasty. To validate the presence of SnCs in human disease tissues, we performed senescence associated-β-galactosidase (SA-β-gal) staining and HMGB1 immunhistochemistry on human arthritic and healthy cartilage explants. SA-β-gal-positive SnCs were observed throughout the

depth of osteoarthritic cartilage and little to no nuclear HMGB1 staining in OA tissues compared to healthy controls (**Fig. 4.16**). However, staining was variable in cartilage tissue isolated from different regions of the joint within an individual patient, suggesting variability across the articular surface. To avoid bias from this variability in SnCs across the articular joint, we isolated cells from the tissue for further testing.

Exposure to the UBX0101 senolytic effectively cleared SnCs isolated from human OA cartilage in monolayer. Preliminary screening showed that 43 μM UBX0101 killed senescent chondrocytes isolated from human OA tissue, as determined by the SA-β-gal assay (**Fig. 4.17**). To further understand the effects of UBX0101, human OA chondrocytes were exposed to UBX0101 for 2 days (43 μM) (**Fig. 4.17a)**; this regimen killed 20% of the SnCs and no more than 5% of non-SnCs, as determined by staining for SA-β-gal activity, nuclear HMGB1, and Annexin V—PI live-dead cell staining (**Fig. 4.17b, c**). Increased levels of activated caspase-3 suggest that UBX0101 kills SnCs through the apoptotic pathway in treated human OA chondrocytes (but not healthy chondrocytes, **Fig. 4.17d** and **4.18d**). After human OA chondrocytes were exposed to UBX0101 for 2 days, followed by drug-free culture for 8 days, the cultures showed a decline in the expression of the senescence-related genes *cdkn2a* (without statistical significance), *mmp3*, and *il6*. Protein levels of OA-related molecules – *mmp13*, and *il1β* also decreased (**Fig. 4.17e**). Furthermore, selective removal of SnCs from the OA chondrocyte cultures by UBX0101 increased proliferation of the remaining chondrocytes up to 15%, as determined by labeling of individual cells with 5-ethynyl-20-deoxyuridine (EdU) (**Fig. 4.17f**). These data suggest that transient UBX0101 treatment may cause a reversible cessation of cell growth (quiescence) in normal cells, which resume

proliferation after removal of UBX0101.

We next evaluated UBX0101 treatment of human OA chondrocytes in a three-dimensional (3D) pellet system that supports maintenance of the chondrocyte phenotype and chondrogenesis. After 21-days of culture human OA chondrocyte pellet cultures, transiently (4-day) exposed to 43 μM UBX0101, dramatically reduced the level of SnCs **(Fig. 4.17g)**, as determined by reduced SA-β-gal activity **(Fig. 4.17h)**. UBX0101 also reduced the levels of *cdkn2a, mmp3, il1β* and *il6* mRNAs and increased levels of *col2a1* and *acan* **(Fig. 4.17i)**. Similarly, UBX0101 decreased protein levels of $p16^{INK4a}$ and mmp13 and increased col2a1, proteoglycan and sulfated glycosaminoglycans (sGAG), confirming new cartilage growth **(Fig. 4.17i, j)**.

4.4 Conclusions

In summary, we report the development of SnCs after articular joint injury in the superficial layer of cartilage and the synovium. These cells express a SASP that includes inflammatory molecules and degradative enzymes. The removal of SnCs, either using a transgenic mouse models or through pharmaceutical intervention that targets SnCs, reduced the development of post-traumatic OA and related pain, and created a pro-chondrogenic environment. Aged animals had a higher senescence burden and developed more severe OA after injury. The relevance of our findings to human disease was validated using chondrocytes isolated from arthritic patients. These findings provide new insights into therapies targeting SnCs for treating trauma and age-related degenerative joint disease.

4.5 Figures

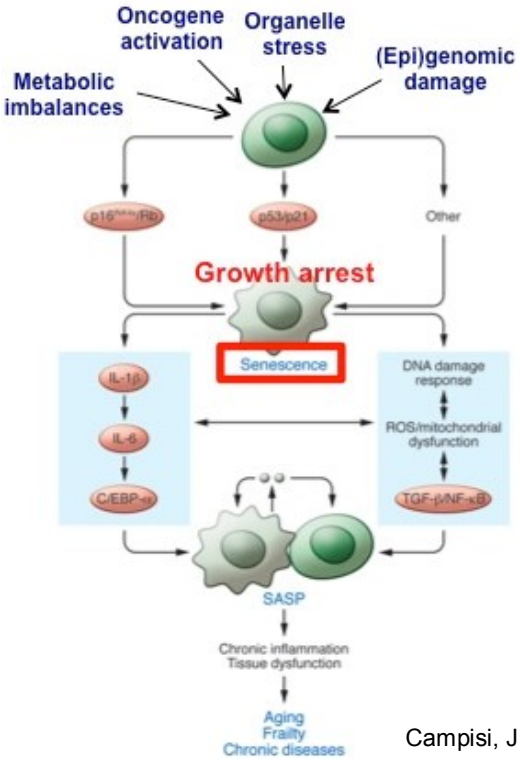

Campisi, J., *et al*., *J Clin Invest*, 2013

Figure 4.1 Cellular senescence (cellular aging). When cells are stressed by any kinds of genomic damages, they undergo this transition into senescence state via p16/Ratinoblastoma (RB), p53/p21, or others and develop Two distinct phenotypic changes that cells are adapted. One of them is an irreversible cellular growth arrest to prevent proliferation of damaged and dysfunctional cells.

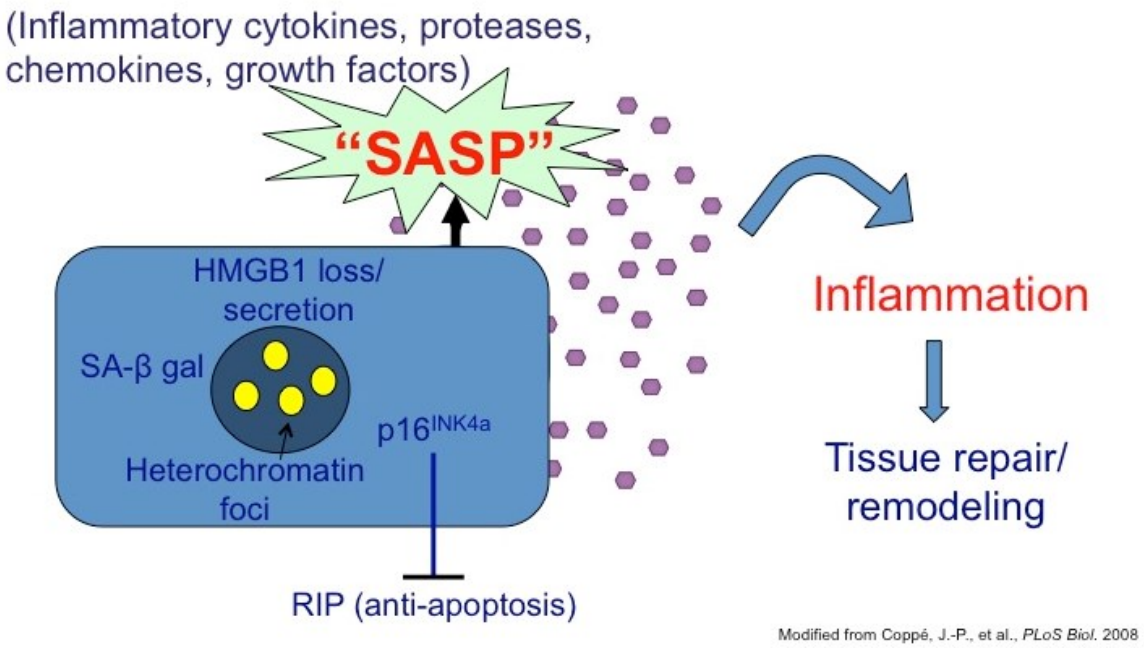

Figure 4.2 Senescent cells secrete senescent-associated secretory phenotypes (SASPs). Senescent cells express tumor suppressor proteins ($p16^{ink4a}$) and certain other markers and resist to apoptotic cell death. Senescent cells secrete SASPs into outside of cells including inflammatory cytokines, proteases, chemokines, and growth factors. These SASPs affect normal cells around senescence cells, which makes tissue function failed by driving inflammatory environment of tissues and subsequently affect tissue repair and remodeling.

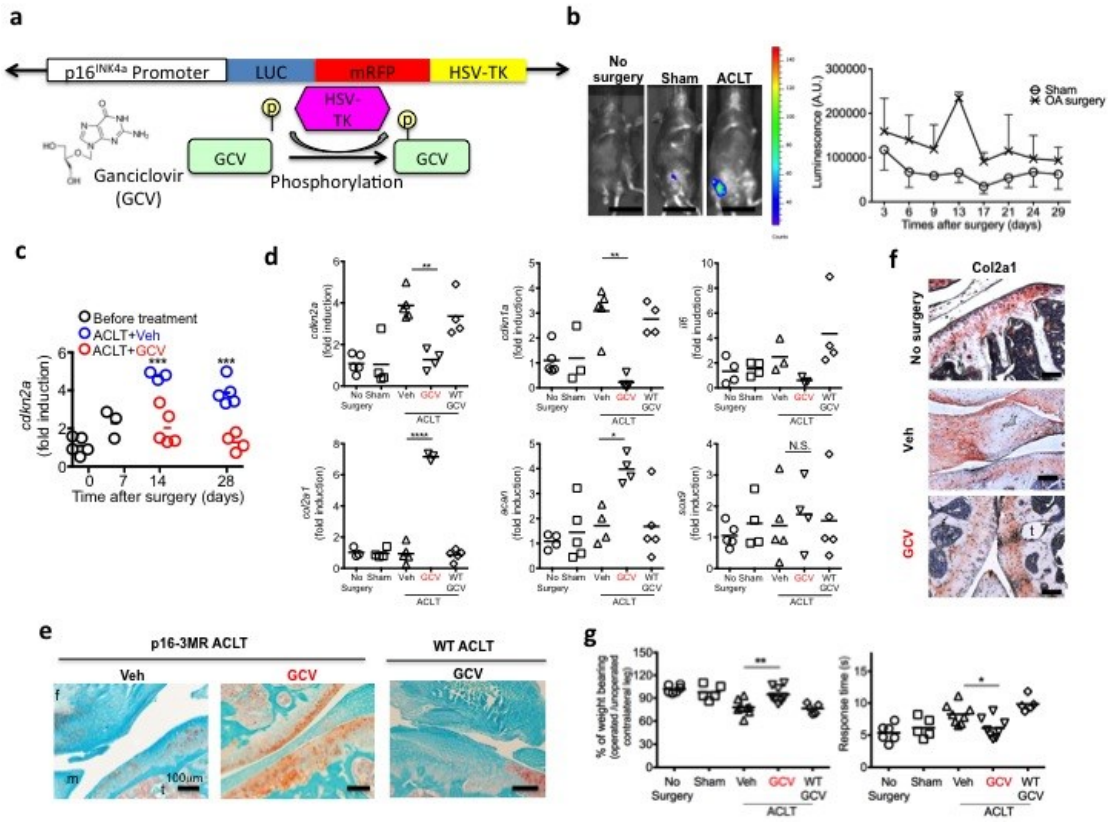

Figure 4.3 Kinetics of SnCs development in surgically-induced OA and effect of GCV-induced SnC clearance on OA disease progression in C57BL and p16-3MR mice. (a) Diagram depicting the p16-3MR transgene. (b) p16-3MR mice received vehicle (Veh, 10 µl saline) to the ACLT-operated or sham-operated knee by IA injection 8 days after the surgery for 5 consecutive days, with a 2nd treatment 21 days after post-surgery for 5 consecutive days. Shown are representative images of mice 28 days post-surgery and quantification of luminescence (in arbitrary units, A.U.) at the indicated time. $n = 4$ for each group. Scale bar, 2 cm. In c–g, we administered two cycles of GCV for 5 consecutive days (1 mM in 10 µl saline) starting at day 8 after surgery in p16-3MR or non-transgenic C57BL mice. (c) Quantification of mRNA expression for *cdkn2a* at indicated time and (d) *cdkn1a, il6, col2a1*, *acan* and *sox9* normalized to *β-actin* day 28 after surgery from p16-3MR mice articular joints that received Veh or GCV and non-transgenic C57BL mice that received GCV. (**e**) Representative images of Safranin-O/methyl green staining and (**f**) col2a1 immunohistochemistry. Scale bar, 100 µm and (**g**) the percentage of weight placed on the operated limb versus contralateral control limb and response time of mice after placement onto a 55°C hotplate. $*P < 0.05$, $**P < 0.01$, $***P < 0.001$ and N.S. (Not Significant); one-way ANOVA (Tukey's multiple comparison test) for **c**, **d**; unpaired t-test (two-tailed) for **g**. All data are expressed as mean and each data point represents an individual mouse.

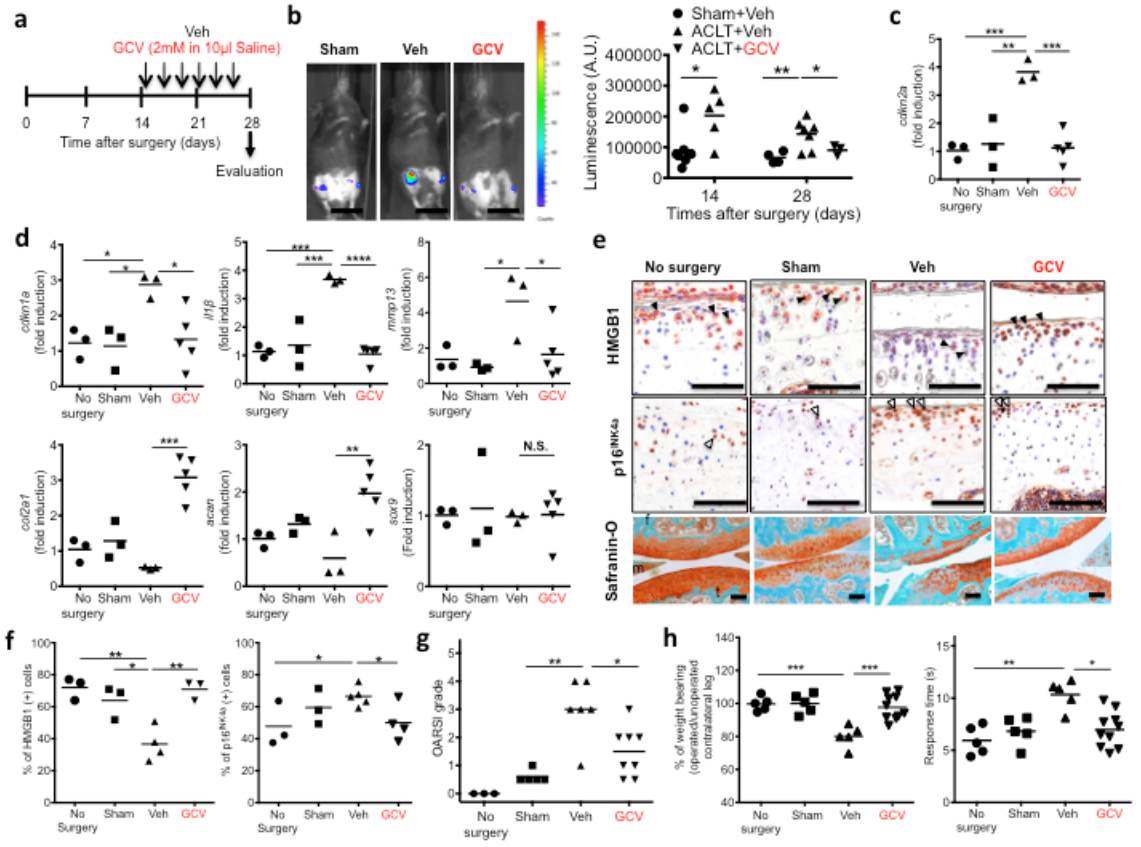

Figure 4.4 Clearance of SnCs by GCV reduces the development of post-traumatic OA. (**a**) Schematic of time course for experiments in **b**–**h**. p16-3MR male mice undergoing the anterior cruciate ligament transection (ACLT) were injected IA with vehicle (Veh) or ganciclovir (GCV) and evaluated as indicated. (**b**) Representative luminescence images of ACLT mice after Veh or GCV treatment on day 28 post-surgery (left) and quantification of the luminescence (right) at the indicated time (in arbitrary units, A.U.). Scale bar, 2 cm. (**c**) Quantification of mRNA expression for *cdkn2a* in the articular joints treated on day 28 post-surgery. (**d**) Quantification of mRNA expression for *cdkn1a, il1β, mmp13, col2a1, acan* and *sox9,* normalized to *β-actin* in joints from no surgery, sham operated, and ACLT mice treated as indicated. (**e**) Representative images of HMGB1 (brown, closed arrowheads) and $p16^{INK4a}$ (brown, open arrowheads) immunostaining and Safranin-O/methyl green in p16-3MR mice. f, femur; t, tibia; m, meniscus. Scale bar, 100 µm. (**f**) Quantification of non-SnCs with positive nuclear HMGB1 and SnCs with positive $p16^{INK4a}$ in articular cartilage. (**g**) The medial tibial plateau joint score in p16-3MR mice, based on the OARSI scoring system. (**h**) The percentage of weight placed on the operated limb versus contralateral control (top) and response time of mice after placement onto a 55°C hotplate (bottom). All data are expressed as mean and each data point represents an individual mouse. $*P < 0.05$, $**P < 0.01$, $***P < 0.001$, $****P < 0.0001$ and N.S. (Not Significant); one-way analysis of variance (ANOVA) with Tukey's multiple comparison test for **c**, **d**; two-tailed t-test (unpaired) for **b**, **f**-**h**.

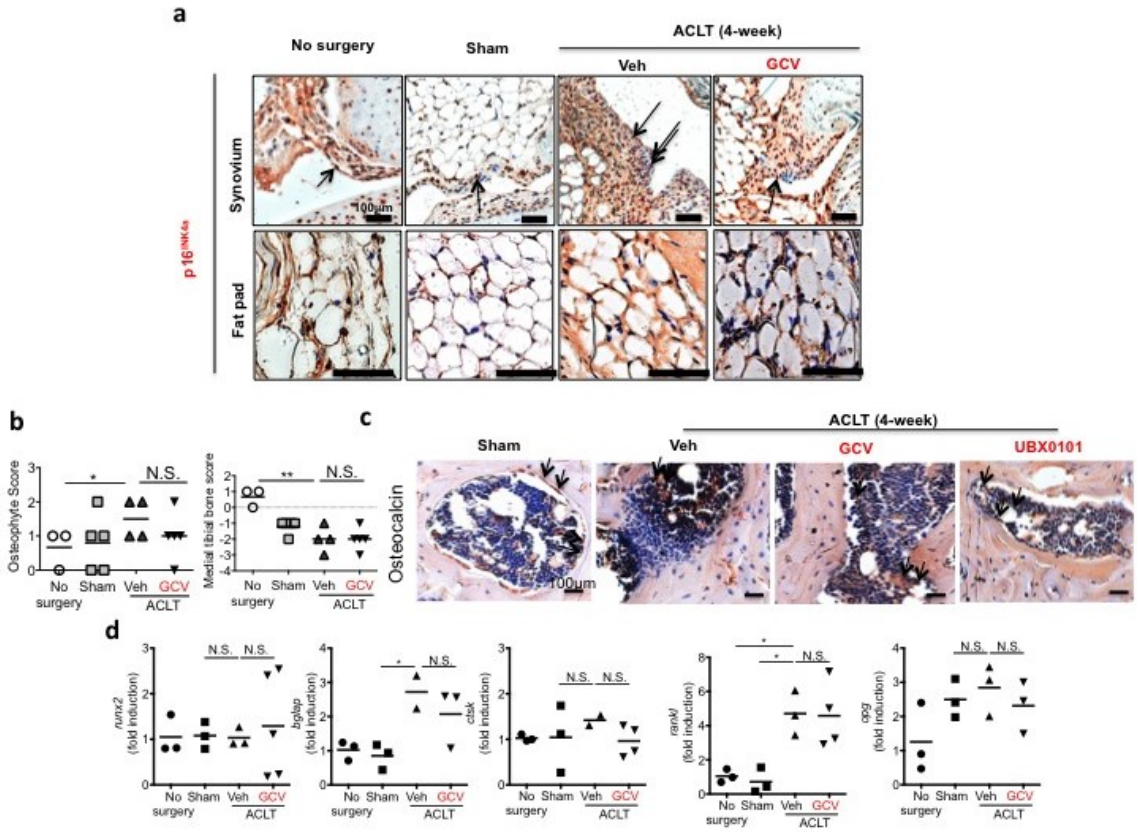

Figure 4.5 The presence of SnCs in the synovium and infrapatellar fat pad, and characterization of subchondral bone changes in p16-3MR mice after vehicle or GCV-treatment. (**a**) Representative images of $p16^{INK4a}$-positive SnCs in the synovium and infrapatellar fat pad. Scale bar, 100 μm (**b**) Scores for osteophyte formation and medial tibial bone loss. **(c**) Representative images of osteocalcin. There was an increase in abnormal osteocalcin-positive osteoblasts (arrows) in the marrow area of the tibial subchondral bone are increased in abnormal in Veh, GCV and UBX0101-treated p16-3MR with ACLT surgery. In contrast, these cells were located on the bone surface of sham-operated controls. Scale bar, 100 μm (**d**) Quantification of mRNA expression for *runx2* and *bglap* (osteocalcin) as bone formation markers and *ctsk*, *rankl*, and *opg* (osteoprotegerin) as bone turnover markers normalized to *β-actin* in joints. In (**b**) and (**d**), $*P < 0.05$, $**P < 0.01$, and N.S. (Not Significant); unpaired t-test (two-tailed) for **b**; one-way ANOVA (Tukey's multiple comparisons test) for **d**. All data are expressed as mean and each data point represents an individual mouse.

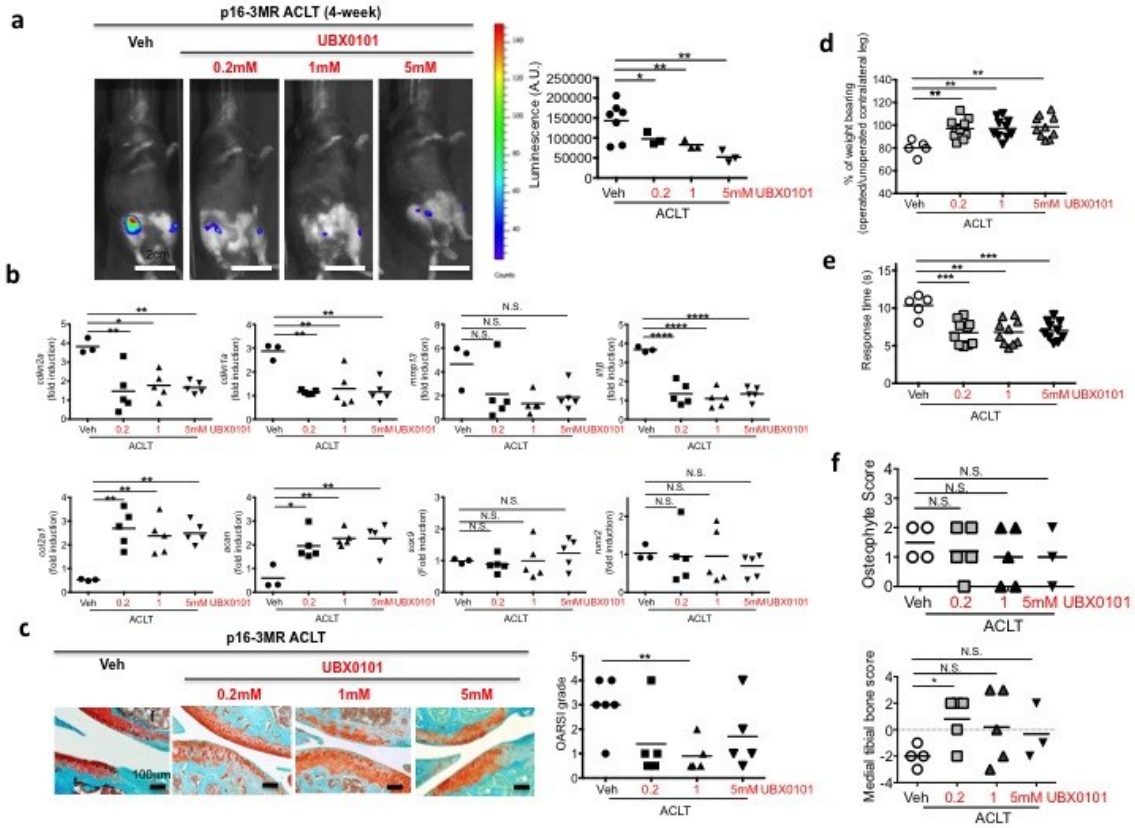

Figure 4.6 UBX0101 dose–dependent elimination of SnCs induced by post-traumatic OA in p16-3MR mice and resulting changes in progression of post-traumatic OA. (**a**) Representative whole body luminescent images of vehicle (Veh) or 0.2, 1, and 5 mM of UBX0101-treated p16–3MR mice 28 days following IA injection once every two days over 2 weeks starting 14 days post-surgery (left). Quantification of luminescence (right). Scale bar, 2 cm. (**b**) Quantification of mRNAs expression for *cdkn2a, cdkn1a, mmp13, il1β, col2a1, acan, sox9* and *runx2* normalized to *β-actin*. (**c**) Representative images of Safranin-O/methyl green and comparison of Veh or 0.2, 1, and 5 mM of UBX0101-treated p16–3MR mice knee joints by OARSI grade. Scale bar, 100 μm. (**d**) Weight bearing test (top) and (**e**) hotplate analysis (bottom) upon UBX0101 treatment. (**f**) Scores for osteophyte formation and local medial tibial bone density on day 28 after surgery. **P* < 0.05, ***P* < 0.01, ****P* < 0.001, *****P* < 0.0001 and N.S. (Not Significant); one-way ANOVA (Tukey's multiple comparisons test) for **b**; unpaired t-test (two-tailed) for **a** and **c**–**f**. All data are expressed as mean and each data point represents an individual mouse.

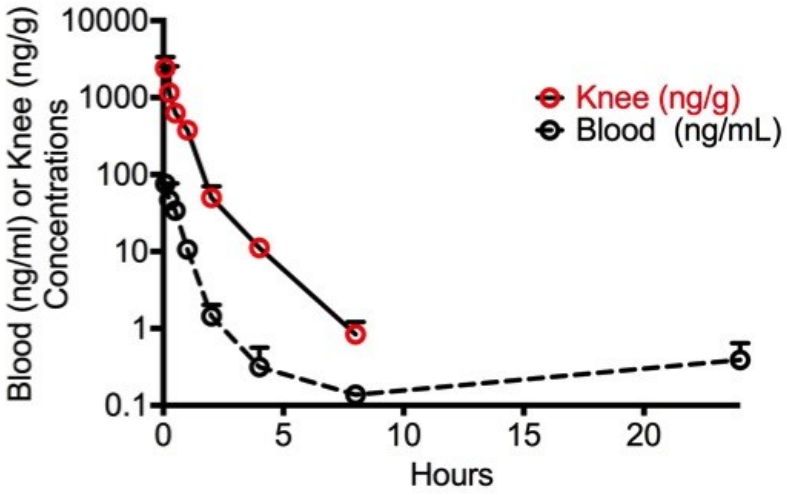

Figure 4.7 Local and blood pharmacokinetics (PK) of UBX0101 after IA injection. C57BL mice were injected IA with 1 mM UBX0101 (in 10 µl of saline per knee, $n = 2$ mice per time point). The initial dose of UBX0101 falls below the IC50 1.5 hours following IA injection. Approximately $1/30^{th}$ of the initial dose reaches the circulation and the IC50 is never reached in the circulation.

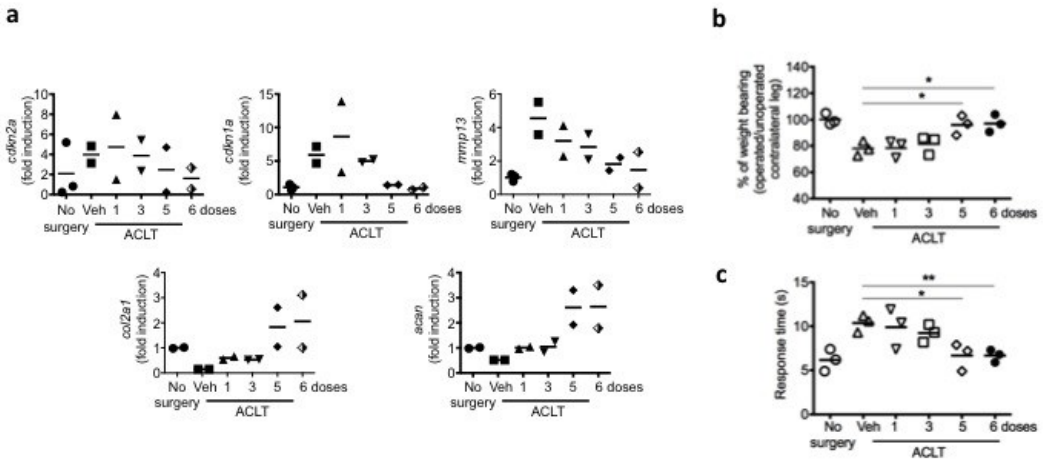

Figure 4.8 Efficacy of increasing UBX0101 injections on OA progression. C57BL mice that underwent the ACLT in one rear limb to induce OA were treated every other day with vehicle (Veh) or different numbers of UBX0101 IA injections (1 mM in 10 µl saline, 1 to 6 injections) for 2 weeks starting 14 days post-surgery. (a) Quantification of mRNA expression for *cdkn2a*, *cdkn1a mmp13*, *il1β, col2a1* and *acan* normalized to *β-actin* in joints 28 days after ACLT; $n = 2$ for each group. No statistical analysis. (b) The percentage of weight placed on the operated limb versus the contralateral control limb, and (c) response time after placement on a 55°C platform on day 28 after ACLT surgery. $*P < 0.05$ and $**P < 0.01$; two-tailed t tests (unpaired). All data are expressed as mean and each data point represents an individual mouse.

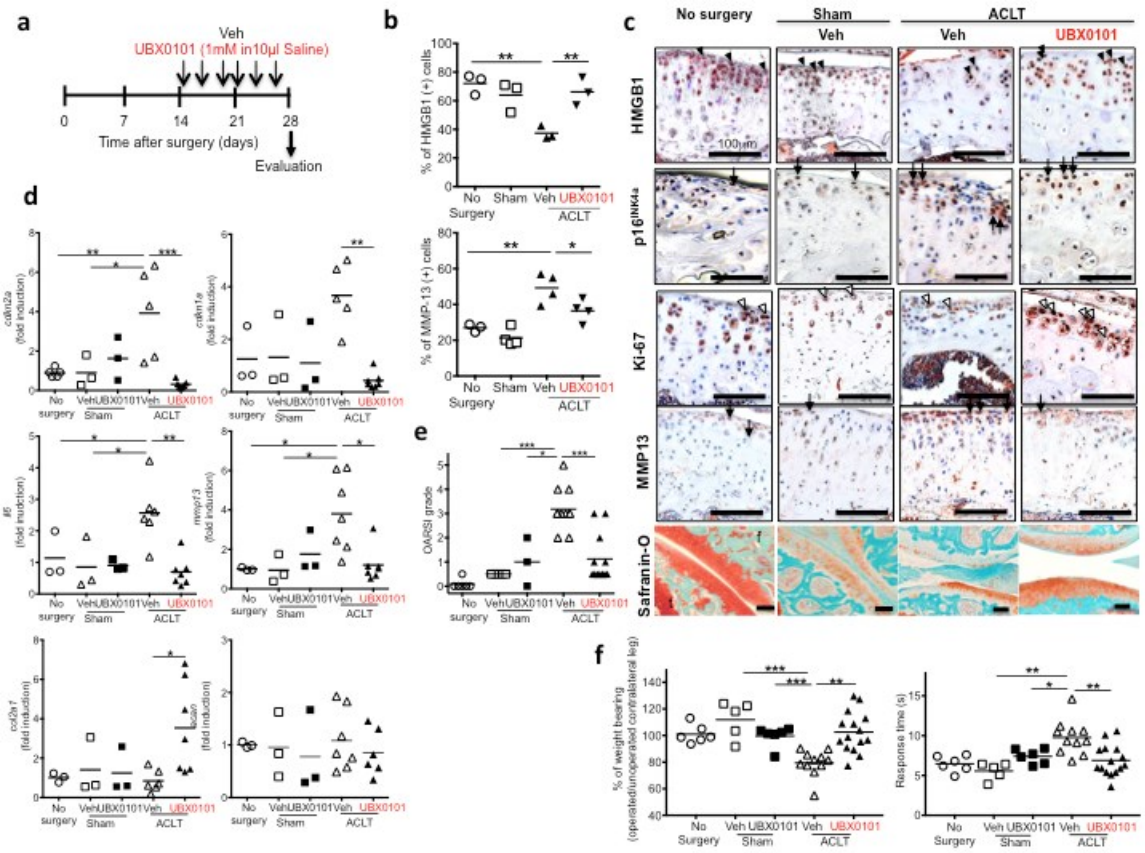

Figure 4.9 Senescent cell clearance by UBX0101 attenuates post-traumatic OA and creates a pro-chondrogenic environment. (**a**) Schematic of time course for experiments in **b**–**f**. C57BL male mice that underwent ACLT were injected IA every other day with vehicle (Veh) or UBX0101 and evaluated as indicated. (**b**) Quantification of nuclear HMGB1-positive non SnCs and mmp13 immunostaining and (**c**) representative images of HMGB1 (brown, closed arrowheads), $p16^{INK4a}$ (brown, closed arrowheads), Ki-67 (brown, open arrowheads), and mmp13 (brown, closed arrowheads) immunostaining and the medial tibial plateau stained with Safranin-O/methyl green in articular cartilage from no surgery, sham operated, and ACLT mice treated as indicated. f, femur; t, tibia; m, meniscus. Scale bar, 100 µm. (**d**) Quantification of mRNA expression for *cdkn2a, cdkn1a, il6, mmp13, col2a1* and *acan* normalized to *β-actin* in joints. (**e**) OARSI scores of articular joints. (**f**) The percentage of weight placed on the operated limb versus contralateral control limb (left) and response time after placement onto a 55°C platform (right). All data are expressed as mean and each data point represents an individual mouse. $*P < 0.05$, $**P < 0.01$, $***P < 0.001$ and N.S. (Not Significant); one-way ANOVA with Tukey's multiple comparison test for **d**; two-tailed t-test (unpaired) for **b**, **e**-**f**.

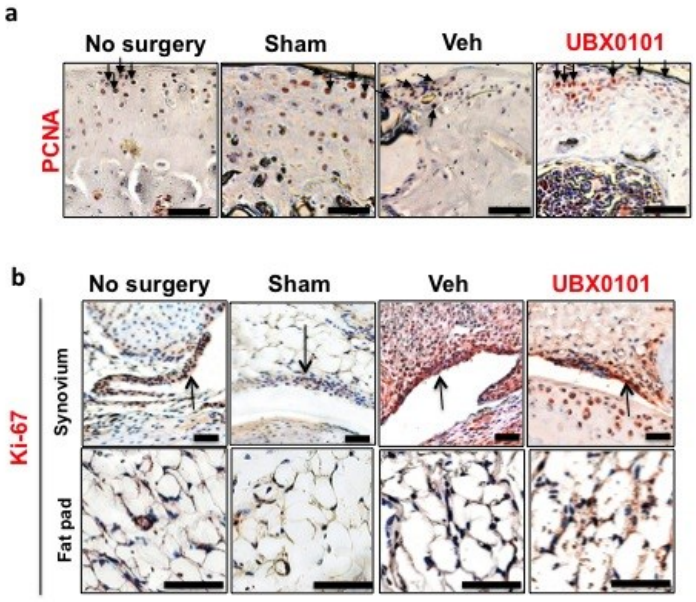

Figure 4.10 The PCNA-positive non-SnCs in cartilage and Ki67 positive non-SnCs in other joint compartments after vehicle or UBX0101-treated C57BL mice. (**a**) Representative images of PCNA expression by immunohistochemistry (brown staining at arrows). There were fewer PCNA-expressing non-SnCs in the articular cartilage of vehicle (Veh)-treated C57BL mice, whereas increased number of PCNA positive proliferating cells in those of UBX0101-treated mice 4 weeks after ACLT. Scale bar, 100 μm. (**b**) Representative images of Ki-67 expression (brown staining at arrows). In Veh-treated C57BL mice, fewer Ki-67-expressing cells (hyperplastic synovial membrane, brown staining at arrows) were detected in the synovium, consistent with the presence of SnCs, which was abrogated by UBX0101 treatment. Scale bar, 100 μm.

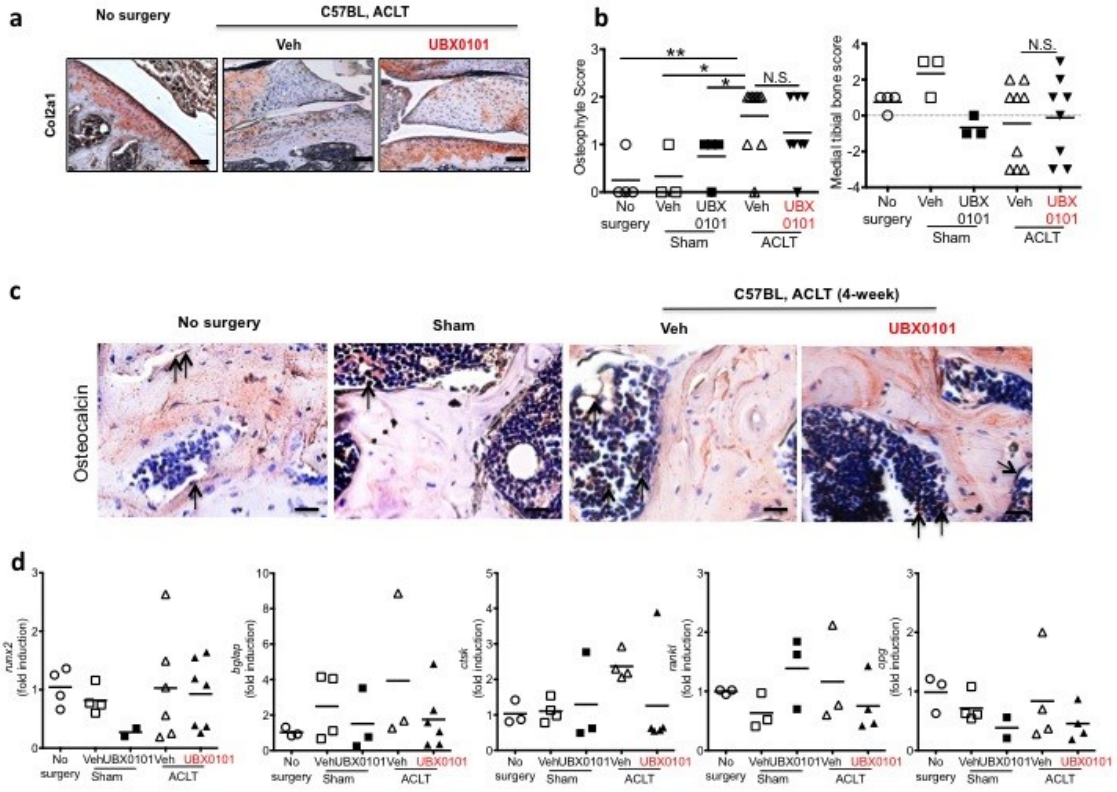

Figure 4.11 UBX0101 treatment increased type II collagen protein but did not significantly reduce subchondral bone changes in ACLT C57BL mice 28 days after the injury. (**a**) Immunohistochemical analyses showed that in UBX0101-treated C57BL mice, increased type II collagen protein was detected relative to vehicle (Veh)-treated ACLT mice. Scale bar, 100 μm (**b**) UBX0101 treatment did not significantly suppress osteophyte formation and the extent of subchondral bone loss in ACLT mice. (**c**) Osteocalcin-positive cells (arrows) in tibial subchondral bone marrow collected 28 days after ACLT surgery and treatment with Veh or UBX0101. Scale bar, 100 μm (**d**) Quantification of the levels of mRNAs encoding *runx2, bglap, ctsk*, *rankl* and *opg* normalized to *β-actin* in joints from C57BL mice that received Veh or UBX0101 on day 28 after surgery.

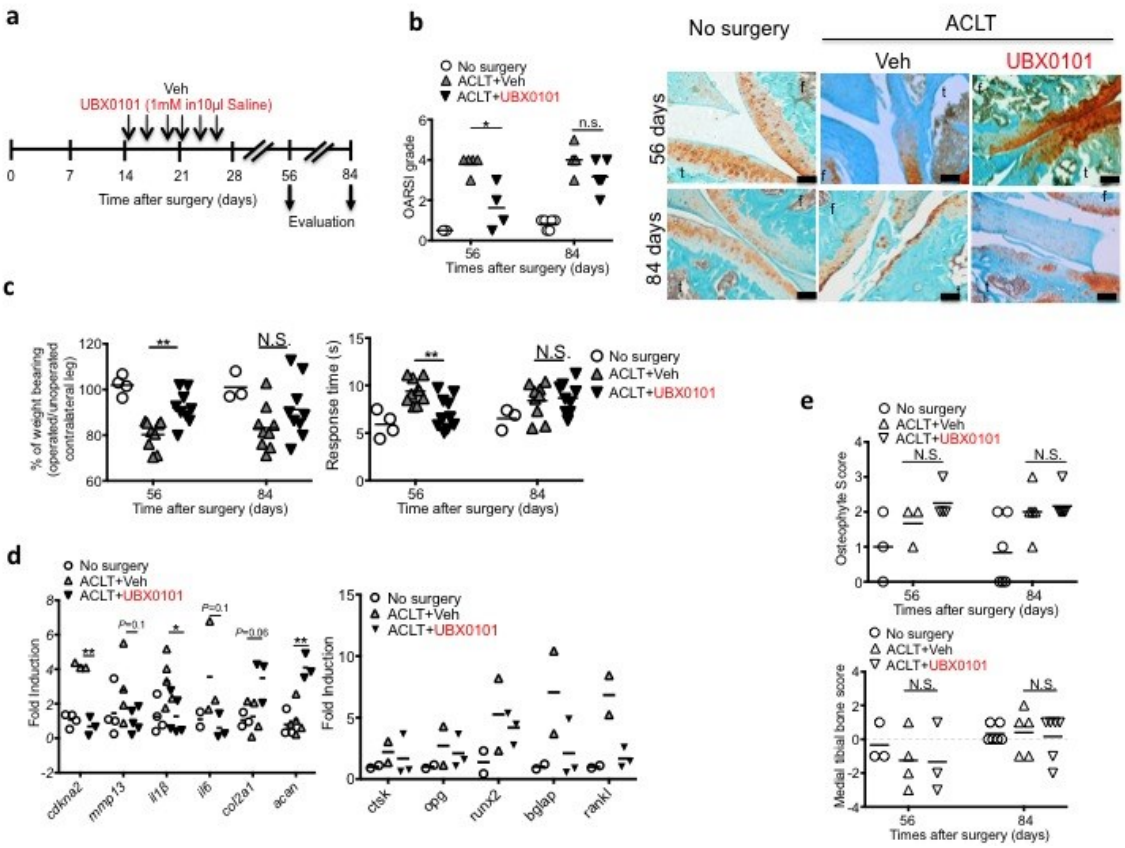

Figure 4.12 Long-term efficacy of UBX0101 in attenuating post-traumatic OA development. (**a**) Schematic of time course for experiments in **b** **e**. C57BL mice that underwent the ACLT of one rear limb were treated with vehicle (Veh) or UBX0101 (1 mM in 10 µl saline) once every two days over 2 weeks starting 14 days post-surgery. (**b**) Left: Comparison of vehicle-treated and UBX0101-treated knee joints 56 or 84 days after surgery by OARSI grade. Right: Representative images of Safranin-O/methyl green staining of the medial compartment as indicated time. Scale bar, 100 µm. (**c**) Percentage of weight placed on the operated limb versus contralateral control limb (left) and response time after placement onto a 55° C platform (right). (**d**) Quantification of mRNA expression for *cdkn2a*, *mmp13*, *il1β, il6, col2a1, acan, ctsk*, *opg*, *runx2, bglap* and *rankl* normalized to *β-actin* in joints 56 days after ACLT. (**e**) Histological analysis of subchondral bone changes as confirmed by osteophyte formation and bone sclerosis score. All data are expressed as mean and each data point represents an individual mouse. **P* < 0.05, ***P* < 0.01, and N.S. (Not Significant); one-way ANOVA (Tukey's multiple comparison test) for **d**; two-tailed t tests (unpaired) for **b, c,** and **e**.

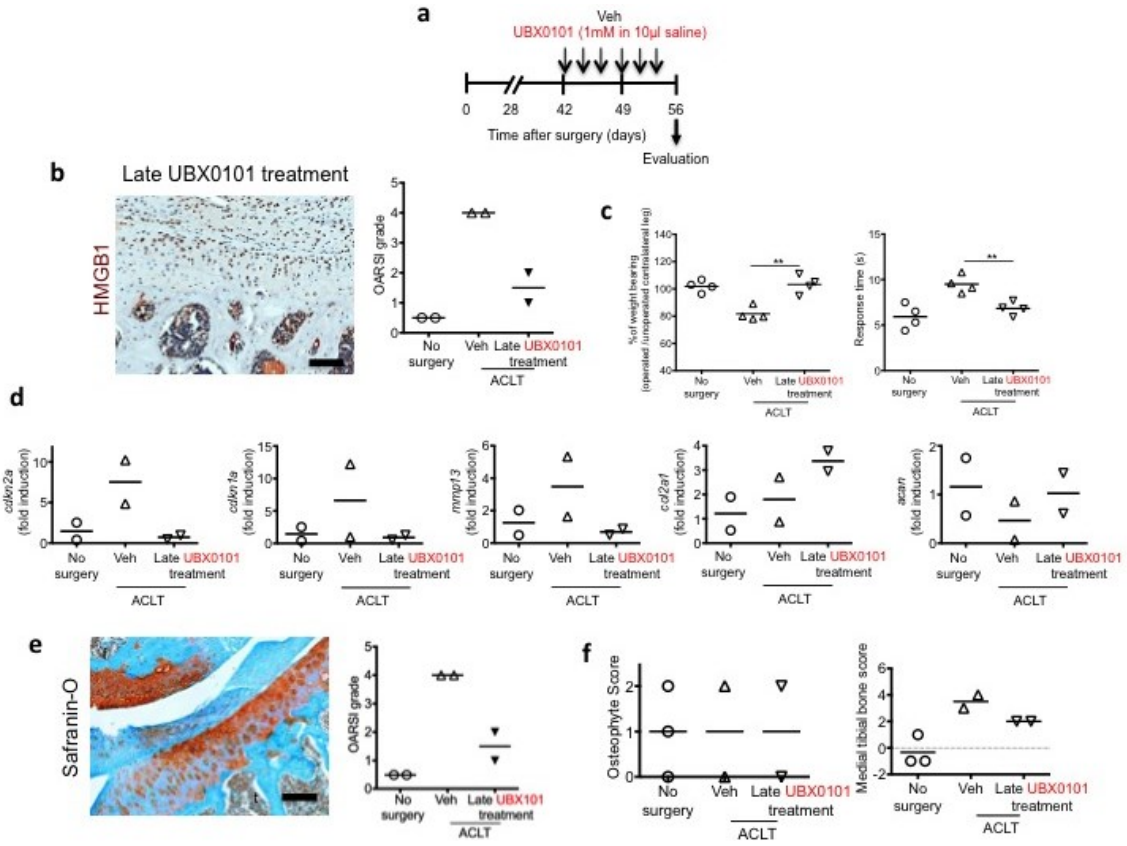

Figure 4.13 Efficacy of UBX0101 for treating advanced post-traumatic OA. (**a**) Schematic of experiment for **b**–**e**. C57BL mice underwent ACLT of one rear limb to induce OA and were injected IA once every two days with vehicle (Veh) or UBX0101 (1 mM in 10 µl saline) during 6 and 7 weeks post-surgery for 2 weeks. (**b**) Representative images of cells for nuclear HMGB1 by immunohistochemistry (left) and quantification of HMGB1-positive non-SnCs in articular cartilage (right). Scale bar, 100 µm. (**c**) Weight bearing and hot plate analyses on day 56 after ACLT surgery. (**d**) Quantification of mRNAs expression *cdkn2a, cdkn1a, mmp13, il1β, col2a1* and *acan* normalized to *β-actin* in joints as indicated. (**e**) Representative images of Safranin-O/methyl green staining and OARSI scores. Scale bar, 100 µm. (**f**) Osteophyte formation and medial tibial bone score as indicated at 56 days post ACLT surgery. All data are expressed as mean and each data point represents an individual mouse. No statistical analysis.

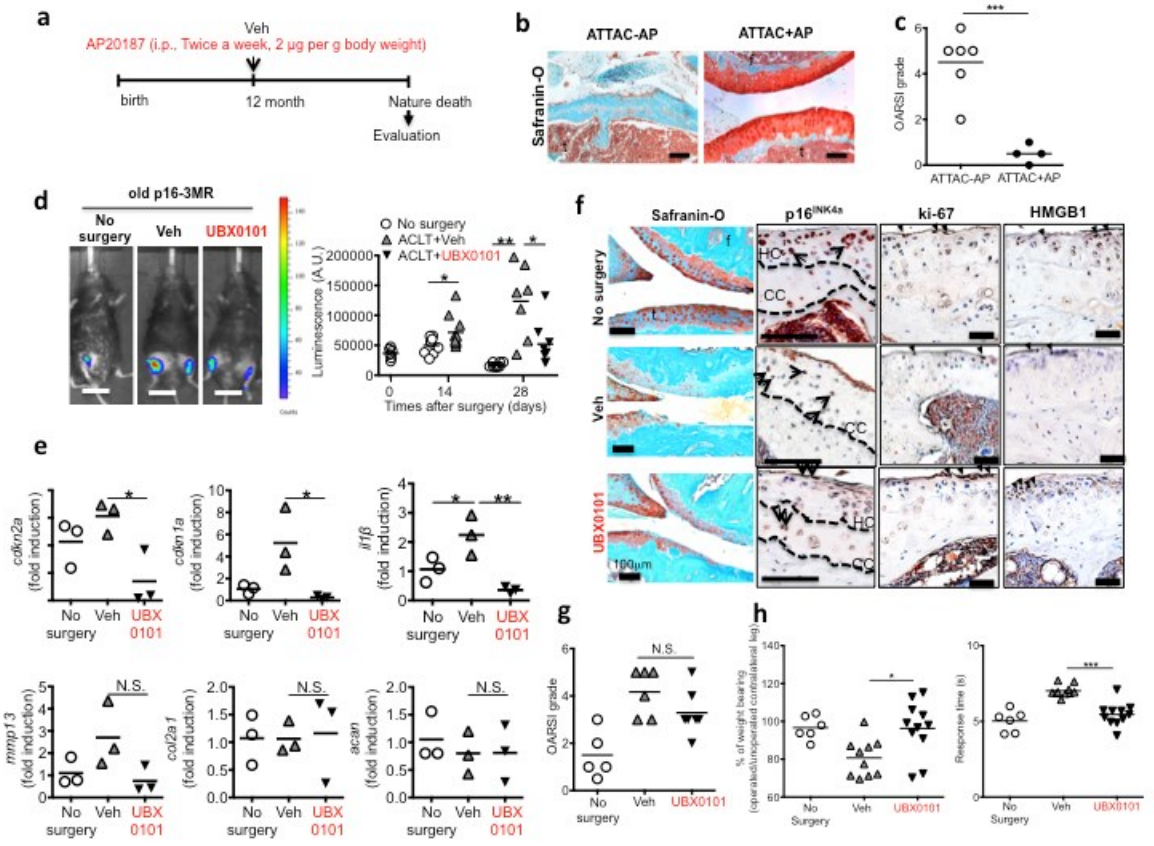

Figure 4.14 Clearance of SnCs slows the development of naturally occurring OA and post-traumatic OA in old mice. (**a**) Study design for clearance of naturally occurring p16^{INK4a}-positive SnCs in INK-ATTAC female mice. AP20187 (AP) was administrated intraperitoneal (i.p.) twice a week starting at 12 months of age. (**b**) Representative images of Safranin-O/methyl green staining from vehicle-treated (-AP) and AP-treated (+AP) mice. f, femur; t, tibia. Scale bar, 100 μm. (**c**) OARSI grade; veh-treated, 20, 21, 25, 28, 28 and 32-months-old; AP-treated, 21, 28, 28 and 34-months-old. ***$P < 0.001$; two-tailed t tests (unpaired). (**d**) Representative whole-body luminescence images (left) on day 28 after ACLT surgery and quantification of luminescence (right; in arbitrary units, A.U.) at the indicated time after the surgery of 19- to 20-month-old male p16–3MR mice treated as indicated in Figure 2a. Scale bar, 2 cm. (**e**) Quantification of mRNA expression for *cdkn2a, cdkn1a, mmp13, col2a1* and *acan* normalized to *β-actin* in joints 28 days after ACLT. (**f**) Representative images of Safranin-O/methyl green staining and p16^{INK4a} (brown, arrows), Ki-67 and HMGB1 (brown, arrowheads) immunostaining on the articular cartilages. HC, hyaline cartilage; CC, calcified cartilage. Scale bar, 100 μm. (**g**) OARSI grade. (**h**) The percentage of weight placed on the operated limb versus contralateral control (left) and response time of mice after placement onto a 55°C platform (right). All data are expressed as mean and each data point represents an individual mouse. *$P < 0.05$, **$P < 0.01$, ***$P < 0.001$ and N.S., (Not Significant); one-way ANOVA with Tukey's multiple comparison test for **e**; two-tailed t-test (unpaired) for **c**–**d** and **g**–**h**.

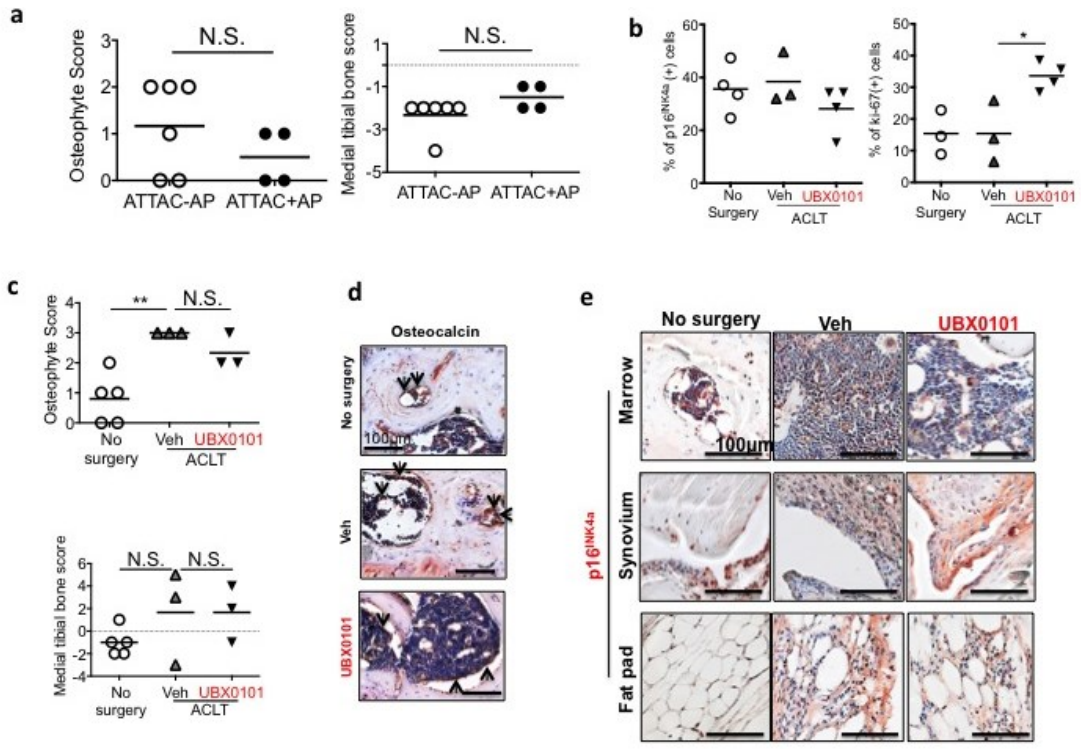

Figure 4.15 Characterization of bone and other joint tissue changes after SnC clearance in naturally-occurring or surgically-induced INK-ATTAC or p16-3MR aged mice. (**a**) Subchondral bone damage scores for osteophyte formation and medial tibial bone sclerosis in INK-ATTAC female mice that received vehicle (-AP, n = 6) or AP (+AP, n = 4) according to the scheme shown in **Figure 4.14a**. (**b**) Quantification of $p16^{INK4a}$-positive SnCs and Ki-67-positive non-SnCs staining in articular cartilage. (**c**) Scores for osteophyte formation and medial tibial bone sclerosis and (**d**) osteocalcin-positive cells in subchondral bone marrows (brown, arrows) by IHC of 20-month-old p16-3MR male mice with ACLT surgery treated with vehicle (Veh) or UBX0101 (1 mM in 10 µl saline, once every 2 days over 2 weeks starting 14 days post-surgery). (**e**) The presence of $p16^{INK4a}$-positive cells in the subchondral bone marrow, synovium and fat pad (brown) of p16-3MR mice shown by immunostaining and their changes after UBX0101 treatment. *P < 0.05, **P < 0.01 and N.S. (Not Significant); two-tailed t tests (unpaired).

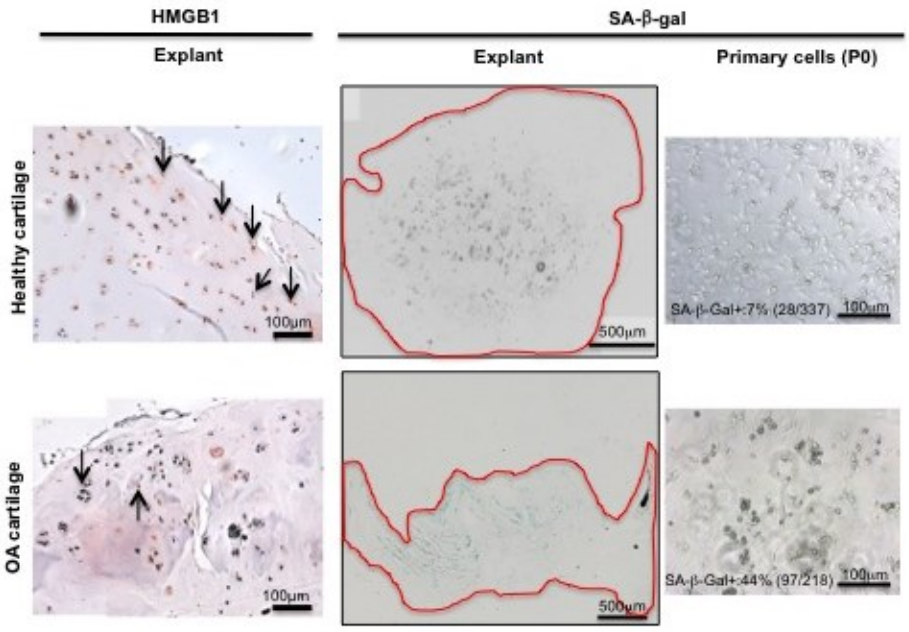

Figure 4.16 Presence of SnCs in human healthy and osteoarthritic articular cartilage. Representative images of HMGB1-positive non-SnCs (brown staining at arrows) by immunohistochemistry and SA-β-gal-positive SnCs expression on the articular cartilage. SA-β-gal-positive SnCs were observed throughout the depth of osteoarthritic cartilage (donor: 65-years-old, Male), but were sparsely present in healthy cartilage (donor: 62-years-old, Male). A range of 7-15% SA-β-gal-positive SnCs were observed in primary chondrocytes isolated from healthy cartilage and 41–50% SA-β-gal-positive SnCs were detected in the chondrocytes from osteoarthritic cartilage (passage 0).

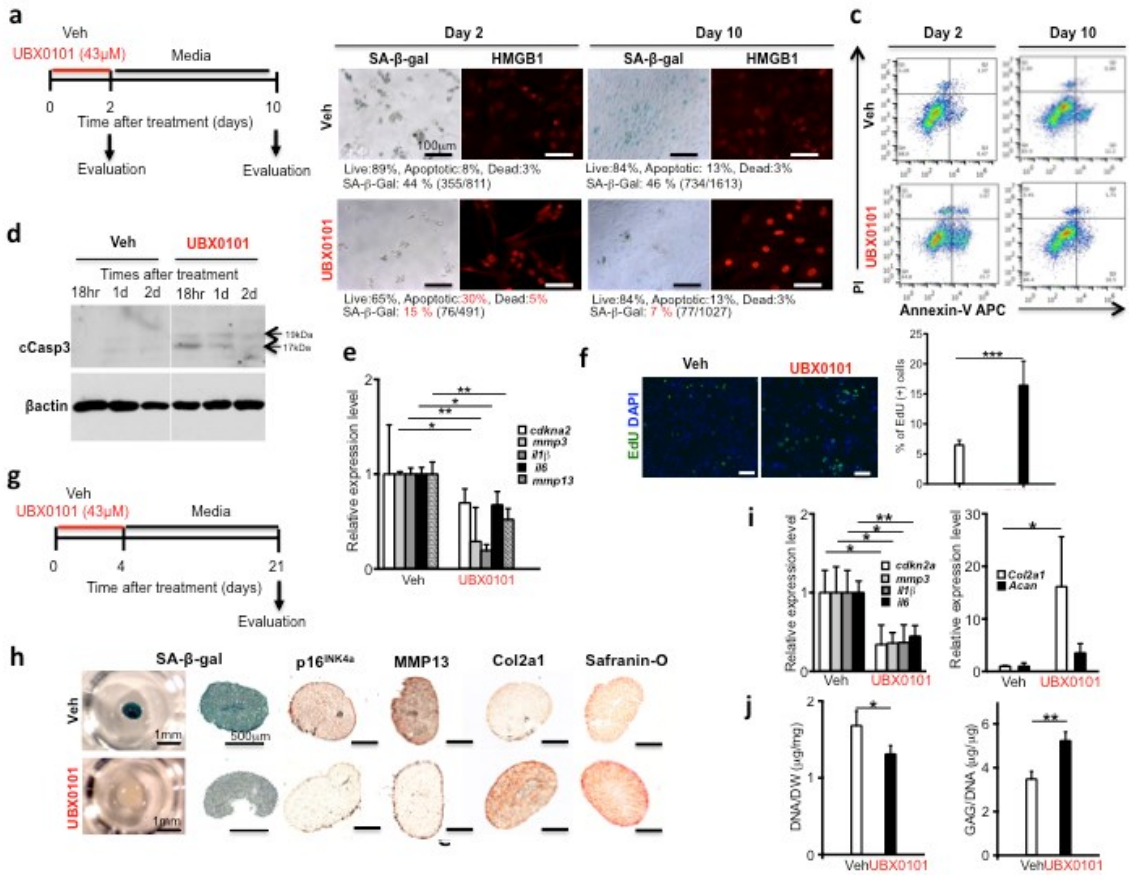

Figure 4.17 UBX0101 clears SnCs by inducing apoptosis and improves cartilage tissue forming ability of chondrocytes from human OA tissue. (**a**) Schematic for monolayer experiment in **b**–**e**. (**b**) Quantification of SA-β-gal-positive cells and the percentage of live (gate Q2: PI^-Annexin V^-), apoptotic (gate Q3: PI^-Annexin V^+ and Q4: PI^+Annexin V^+), and dead (gate Q1: PI^+Annexin V^-) SnCs in monolayer cultured human OA chondrocytes treated with vehicle (Veh) or 43 μM of UBX0101. Representative images of cells with nuclear HMGB1 (red) by immunostaining. (**c**) Representative flow cytometric plots to measure apoptosis from 3 independent experiments. (**d**) Western blot analysis of cleaved caspase3 (cCasp3) and actin in human OA chondrocytes 18h, 1 and 2 days after incubation with Veh or 43 μM UBX0101. (**e**) Quantification of mRNAs expression for *cdkn2a*, *mmp3, il1β, il6* and *mmp13* normalized to *β-actin* in cultures described in (a); $n = 3$ for each group. (**f**) Representative 5-ethynyl-20-deoxyuridine (EdU) staining (left; green) and quantification of the percentage of EdU-positive cells (right) after removing SnCs from human OA chondrocyte cultures by UBX0101; $n = 5$ for each group. (**g**) Schematic for 3D cultured pellets experiment in **h**-**j**. (**h**) SA-β-gal (left) and sectioned images (right) immunostained for $p16^{INK4a}$, mmp13 and col2a1 and stained for Safranin-O of 3D cultured pellets of the human OA chondrocytes treated with Veh or 43 μM of UBX0101; $n = 3$ for each group. (**i**) Quantification of mRNAs expression for *cdkn2a*, *mmp3, il1β, il6*, *col2a1*, and *acan* normalized to *β-actin*; $n = 3$ for each group. (**j**) DNA contents normalized to dry weight and sulfated glycosoaminoglycans (sGAGs) normalized to the DNA content. In (**e**–**f**) and (**i**–**j**), data are averages ± S.D. $*P < 0.05$, $**P < 0.01$, $***P < 0.001$; two-tailed t tests (unpaired).

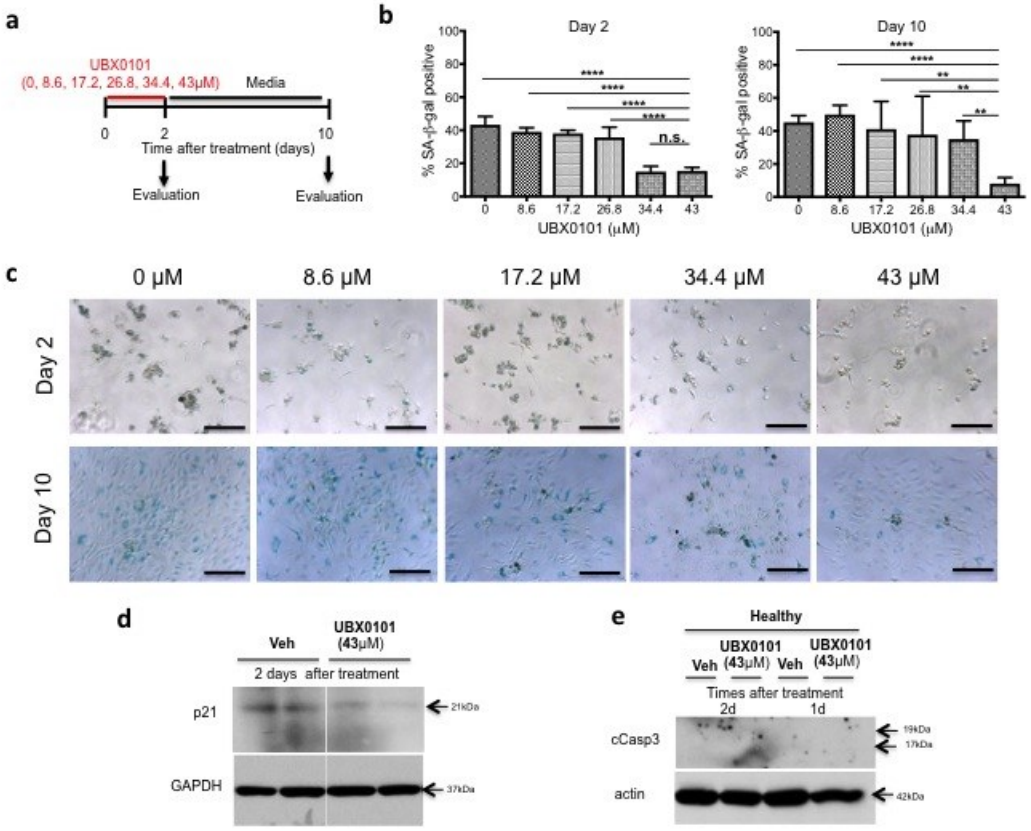

Figure 4.18 Dose-dependent elimination of senescent chondrocytes isolated from human OA tissue by UBX0101 treatment. (**a**) Schematic of experiment for **b**–**c**. (**b**) SA-β-gal positive cells were quantified 2 and 8 days following treatment with increasing concentrations of UBX0101. A dose of 43 μM and a short treatment time (2 days) selectively eliminated SA-β-gal positive senescent chondrocytes. Data are averages ± S.D. $*P < 0.05$, $**P < 0.01$, $***P < 0.001$ and n.s (Not Significant); two-tailed t tests (unpaired). $n = 5$ for 0, 8.6 and 12.2 μM; $n = 6$ for 34.4 and 43 μM. (**c**) Representative images of cells with SA-β-gal staining. Scale bar, 100 (**d**) Western blot analysis of p21 and GAPDH in OA chondrocytes 2 days after treatment with vehicle or 43 μM UBX0101. (**e**) Activated caspase-3 (cCasp-3) and actin in healthy chondrocytes (Non-SnCs) and actin in OA and healthy chondrocytes 1 or 2 days after treatment with vehicle or 43 μM UBX0101. Scale bar, 100 μm.

4.6 References

[1] J. Martel-Pelletier, A.J. Barr, F.M. Cicuttini, P.G. Conaghan, C. Cooper, M.B. Goldring, S.R. Goldring, G. Jones, A.J. Teichtahl, J.P. Pelletier, Osteoarthritis, Nat Rev Dis Primers 2 (2016) 16072.

[2] F.J. Blanco, C. Ruiz-Romero, New targets for disease modifying osteoarthritis drugs: chondrogenesis and Runx1, Ann Rheum Dis 72(5) (2013) 631-634.

[3] J.P. Pelletier, Rationale for the use of structure-modifying drugs and agents in the treatment of osteoarthritis, Osteoarthritis Cartilage 12 Suppl A (2004) S63-8.

[4] H.A. Wieland, M. Michaelis, B.J. Kirschbaum, K.A. Rudolphi, Osteoarthritis - an untreatable disease?, Nat Rev Drug Discov 4(4) (2005) 331-44.

[5] J. Campisi, Cancer, aging and cellular senescence, In Vivo 14(1) (2000) 183-8.

[6] P.D. Adams, Healing and hurting: molecular mechanisms, functions, and pathologies of cellular senescence, Mol Cell 36(1) (2009) 2-14.

[7] J.M. van Deursen, The role of senescent cells in ageing, Nature 509(7501) (2014) 439-46.

[8] J.P. Coppe, P.Y. Desprez, A. Krtolica, J. Campisi, The senescence-associated secretory phenotype: the dark side of tumor suppression, Annu Rev Pathol 5 (2010) 99-118.

[9] J.C. Acosta, A. Banito, T. Wuestefeld, A. Georgilis, P. Janich, J.P. Morton, D. Athineos, T.W. Kang, F. Lasitschka, M. Andrulis, G. Pascual, K.J. Morris, S. Khan, H. Jin, G. Dharmalingam, A.P. Snijders, T. Carroll, D. Capper, C. Pritchard, G.J. Inman, T. Longerich, O.J. Sansom, S.A. Benitah, L. Zender, J. Gil, A complex secretory program orchestrated by the inflammasome controls paracrine senescence, Nat Cell Biol 15(8) (2013) 978-90.

[10] D.J. Baker, B.G. Childs, M. Durik, M.E. Wijers, C.J. Sieben, J. Zhong, A.S. R, K.B. Jeganathan, G.C. Verzosa, A. Pezeshki, K. Khazaie, J.D. Miller, J.M. van Deursen, Naturally occurring p16-positive cells shorten healthy lifespan, Nature (2016).

[11] D.J. Baker, T. Wijshake, T. Tchkonia, N.K. LeBrasseur, B.G. Childs, B. van de Sluis, J.L. Kirkland, J.M. van Deursen, Clearance of p16Ink4a-positive senescent cells delays ageing-associated disorders, Nature 479(7372) (2011) 232-6.

[12] R. Salama, M. Sadaie, M. Hoare, M. Narita, Cellular senescence and its effector programs, Genes Dev 28(2) (2014) 99-114.
[13] N.E. Sharpless, C.J. Sherr, Forging a signature of in vivo senescence, Nat Rev Cancer 15(7) (2015) 397-408.
[14] D. Munoz-Espin, M. Canamero, A. Maraver, G. Gomez-Lopez, J. Contreras, S. Murillo-Cuesta, A. Rodriguez-Baeza, I. Varela-Nieto, J. Ruberte, M. Collado, M. Serrano, Programmed cell senescence during mammalian embryonic development, Cell 155(5) (2013) 1104-18.
[15] J.I. Jun, L.F. Lau, The matricellular protein CCN1 induces fibroblast senescence and restricts fibrosis in cutaneous wound healing, Nat Cell Biol 12(7) (2010) 676-85.
[16] M. Demaria, N. Ohtani, S.A. Youssef, F. Rodier, W. Toussaint, J.R. Mitchell, R.M. Laberge, J. Vijg, H. Van Steeg, M.E. Dolle, J.H. Hoeijmakers, A. de Bruin, E. Hara, J. Campisi, An essential role for senescent cells in optimal wound healing through secretion of PDGF-AA, Dev Cell 31(6) (2014) 722-33.
[17] A. Helman, A. Klochendler, N. Azazmeh, Y. Gabai, E. Horwitz, S. Anzi, A. Swisa, R. Condiotti, R.Z. Granit, Y. Nevo, Y. Fixler, D. Shreibman, A. Zamir, S. Tornovsky-Babeay, C. Dai, B. Glaser, A.C. Powers, A.M. Shapiro, M.A. Magnuson, Y. Dor, I. Ben-Porath, p16(Ink4a)-induced senescence of pancreatic beta cells enhances insulin secretion, Nat Med 22(4) (2016) 412-20.
[18] J.S. Price, J.G. Waters, C. Darrah, C. Pennington, D.R. Edwards, S.T. Donell, I.M. Clark, The role of chondrocyte senescence in osteoarthritis, Aging Cell 1(1) (2002) 57-65.
[19] D. Philipot, D. Guerit, D. Platano, P. Chuchana, E. Olivotto, F. Espinoza, A. Dorandeu, Y.M. Pers, J. Piette, R.M. Borzi, C. Jorgensen, D. Noel, J.M. Brondello, p16INK4a and its regulator miR-24 link senescence and chondrocyte terminal differentiation-associated matrix remodeling in osteoarthritis, Arthritis Res Ther 16(1) (2014) R58.
[20] J.A. Martin, T. Brown, A. Heiner, J.A. Buckwalter, Post-traumatic osteoarthritis: the role of accelerated chondrocyte senescence, Biorheology 41(3-4) (2004) 479-91.
[21] I. Sekiya, J.T. Vuoristo, B.L. Larson, D.J. Prockop, In vitro cartilage formation by human adult stem cells from bone marrow stroma defines the sequence of cellular and

molecular events during chondrogenesis, Proc Natl Acad Sci U S A 99(7) (2002) 4397-402.

[22] S.S. Glasson, M.G. Chambers, W.B. Van Den Berg, C.B. Little, The OARSI histopathology initiative - recommendations for histological assessments of osteoarthritis in the mouse, Osteoarthritis Cartilage 18 Suppl 3 (2010) S17-23.

[23] S. Schreiber, M.M. Backer, J. Yanai, C.G. Pick, The antinociceptive effect of fluvoxamine, Eur Neuropsychopharmacol 6(4) (1996) 281-4.

[24] N. Ohtani, K. Yamakoshi, A. Takahashi, E. Hara, The p16INK4a-RB pathway: molecular link between cellular senescence and tumor suppression, J Med Invest 51(3-4) (2004) 146-53.

[25] J. Chang, Y. Wang, L. Shao, R.M. Laberge, M. Demaria, J. Campisi, K. Janakiraman, N.E. Sharpless, S. Ding, W. Feng, Y. Luo, X. Wang, N. Aykin-Burns, K. Krager, U. Ponnappan, M. Hauer-Jensen, A. Meng, D. Zhou, Clearance of senescent cells by ABT263 rejuvenates aged hematopoietic stem cells in mice, Nat Med 22(1) (2016) 78-83.

[26] U. Holmlund, H. Wahamaa, N. Bachmayer, K. Bremme, E. Sverremark-Ekstrom, K. Palmblad, The novel inflammatory cytokine high mobility group box protein 1 (HMGB1) is expressed by human term placenta, Immunology 122(3) (2007) 430-7.

[27] A.R. Davalos, M. Kawahara, G.K. Malhotra, N. Schaum, J. Huang, U. Ved, C.M. Beausejour, J.P. Coppe, F. Rodier, J. Campisi, p53-dependent release of Alarmin HMGB1 is a central mediator of senescent phenotypes, J Cell Biol 201(4) (2013) 613-29.

[28] J. Sellam, F. Berenbaum, The role of synovitis in pathophysiology and clinical symptoms of osteoarthritis, Nat Rev Rheumatol 6(11) (2010) 625-35.

[29] G.P. Dowthwaite, J.C. Bishop, S.N. Redman, I.M. Khan, P. Rooney, D.J. Evans, L. Haughton, Z. Bayram, S. Boyer, B. Thomson, M.S. Wolfe, C.W. Archer, The surface of articular cartilage contains a progenitor cell population, J Cell Sci 117(Pt 6) (2004) 889-97.

[30] B. Sharma, S. Fermanian, M. Gibson, S. Unterman, D.A. Herzka, B. Cascio, J. Coburn, A.Y. Hui, N. Marcus, G.E. Gold, J.H. Elisseeff, Human cartilage repair with a photoreactive adhesive-hydrogel composite, Sci Transl Med 5(167) (2013) 167ra6.

[31] R.M. Laberge, D. Adler, M. DeMaria, N. Mechtouf, R. Teachenor, G.B. Cardin, P.Y. Desprez, J. Campisi, F. Rodier, Mitochondrial DNA damage induces apoptosis in senescent cells, Cell Death Dis 4 (2013) e727.

[32] M.B. Goldring, M. Otero, Inflammation in osteoarthritis, Curr Opin Rheumatol 23(5) (2011) 471-8.

[33] D.B. Burr, M.A. Gallant, Bone remodelling in osteoarthritis, Nat Rev Rheumatol 8(11) (2012) 665-73.

[34] Y. Zhu, T. Tchkonia, H. Fuhrmann-Stroissnigg, H.M.M. Dai, Y.Y.Y. Ling, M.B. Stout, T. Pirtskhalava, N. Giorgadze, K.O. Johnson, C.B. Giles, J.D. Wren, L.J. Niedernhofer, P.D. Robbins, J.L. Kirkland, Identification of a novel senolytic agent, navitoclax, targeting the Bcl-2 family of anti-apoptotic factors, Aging Cell 15(3) (2016) 428-435.

[35] T. Komori, Signaling networks in RUNX2-dependent bone development, J Cell Biochem 112(3) (2011) 750-5.

[36] M.Z. Ruan, A. Erez, K. Guse, B. Dawson, T. Bertin, Y. Chen, M.M. Jiang, J. Yustein, F. Gannon, B.H. Lee, Proteoglycan 4 expression protects against the development of osteoarthritis, Sci Transl Med 5(176) (2013) 176ra34.

[37] R.F. Loeser, A.L. Olex, M.A. McNulty, C.S. Carlson, M.F. Callahan, C.M. Ferguson, J. Chou, X. Leng, J.S. Fetrow, Microarray analysis reveals age-related differences in gene expression during the development of osteoarthritis in mice, Arthritis Rheum 64(3) (2012) 705-17.

[38] R.F. Loeser, Aging and osteoarthritis: the role of chondrocyte senescence and aging changes in the cartilage matrix, Osteoarthritis Cartilage 17(8) (2009) 971-9.

Chapter 5: Curriculum Vitae

Ok Hee Jeon, MS

Ph.D. in Biomedical engineering, Laboratory of Dr. Jennifer Elisseeff, Translational Tissue Engineering Center, 5001 Smith Building 400 N. Broadway Baltimore, MD 21231
Phone: (410)-622-2755; Email: ojeon2@jhmi.edu

EDUCATION

Ph.D. Biomedical Engineering, Johns Hopkins University, U.S.A. 2012 – present

M.S. Biomedical Engineering, Yonsei University, Korea 2011

- Thesis entitled "Role of Primary Cilia in Bone Cell Mechanotransduction"
- 33 Credits in 5 semesters, GPA 4.03/4.30

Exchange Student Health Science, Copenhagen University, Denmark 2006 – 2007

B.S. Biomedical Engineering, Yonsei University, Korea 2009

- Thesis entitled "Optical Tweezers for Force Measurements"
- 143 Credits in 9 semesters, GPA 3.71/4.30

REARCH EXPERIENCE

Laboratory of Dr. Jennifer Elisseeff, PhD 2013 – present
Translational Tissue Engineering Center, Biomedical Engineering, Johns Hopkins University, MD

- Demonstrating therapeutic utility of *senescent cells* elimination in osteoarthritis (OA) and biomarkers in *extracellular vehicles* of senescent cells induced in OA joints
  - Induction of post-traumatic OA in mice and rats by anterior cruciate ligament transection surgery and Intra-articular injection of small molecules
  - Examination of OA disease change in animal by histologic staining, immunolabeling techniques, and qPCR for cartilage/bone degeneration and functional behavioral tests for OA-induced pain
  - Screening small molecules on 2D and 3D pellet systems with human OA chondrocytes by staining senescent cells and apoptosis assays

- Extraction and Characterization of exosomes from biofluidics and analyze miRNA/protein

- *Locally delivering a carbohydrate*-based OA modifying drug candidate for cartilage repair
  - Identification of underlying mechanism by which a sugar analog promotes chondrogenesis of human MSC and reduces inflammation of human OA chondrocytes

- Engineering bone substitutes using human induced pluripotent stem cells (*hiPSCs*)-derived osteoblasts and osteoclasts and *3D biomaterials*
  - Development of 3D coculture systems (PLLA/PLGA with hydroxyapatite) with Hematopoietic and mesenchymal stem cell
  - Osteoblast/osteoclast differentiation from hiPSCs and analysis of their bone forming and resorptive activities in vitro and in vivo (flow cytometry, qRT-PCR, and histologic staining)

Laboratory of Dr. Chi Hyun Kim, Ph.D. 2009 - 2012

Cell and Tissue MechanoBiology Lab, Biomedical Engineering, Yonsei University, Korea

- Understanding the role of *primary cilia* on bone mechanotransduction
  - Identification of the role of focal adhesions in primary cilia-mediated osteogenic responses to fluid flow shear stress in pre-osteoblasts by immunocytochemistry for cell-matrix interaction and investigation of signaling pathways involved this mechanism by qPCR and Western blotting

- Investigating *osteoclastic bone resorption* in response to mechanical stimulation
  - Examination of (1) how osteoclastic bone resorption pits are generated by focusing on the changes in osteoclasts numbers, (2) increases in area, depth, and volume, and (3) how osteoclastic bone resorption can be controlled by mechanical stimulus using staining and engineering techniques

- Understanding mechanobiology in the *degenerated intervertebral disc*
  - Examination of changes in morphological and measured stiffness in degenerated intervetebral disc induced by calcium free diet and ovariectomy using AFM
  - Studying in the effects of mechanical stimulus in chondrocytes isolated from osteoporotic intervertebral disc on chondrogenic gene and protein expressions and cell-matrix interaction

- Analyzing alternations of mechanical characteristic determined by bone quality (microarchitecture and mineralization) on trabecular bone due to *metastatic bone tumor*
    - Development of animal model for study of metastatic bone tumor (injection of cancer cells to intercondylar notch of rats)

WORKING EXPERIENCE

Researcher 2009 - 2010

Green Chemistry &Manufacturing System Division/Gerontechnology Center, Korea

- Participated in the development of the new animal model for metastatic bone tumor

Undergraduate Research Assistant 2005 – 2006 and 2008

Cell and Tissue MechanoBiology Lab, Biomedical Engineering, Yonsei University, Korea

- Assisted in bone cell culture and analysis of osteogenic gene and protein expressions by using RT-PCR and immunoassay techniques

TEACHING EXPERIENCE

- **Mentor,** Biomedical Engineering, Johns Hopkins University, U.S.A 2013-2017
  - Directed research for undergraduates (Lucy Oh, Do Hun Kim, Jae Wook Chung, and Yoonki Joo)
- **Teaching Assistant,** Biomedical Engineering, Johns Hopkins University, U.S.A 2015
  - Classes: "Tissue engineering" and "Cells and Molecules"
- **Teaching Assistant,** Biomedical Engineering, Yonsei University, Korea 2011
  - Supervised undergraduate thesis. Thesis title: The Role of Primary Cilia in ATDC5 cells Stimulated by Chloral Hydrate and Fluid Flow, received participation award
- **Advisor**, Biomedical Engineering, Yonsei University, Korea 2010
  - Directed government-supported Women Into Science and Engineering program for high school students. Taught how to culture cells, slice bone using a microtome, and apply stress to cells
- **Teaching Assistant,** Biomedical Engineering, Yonsei University, Korea 2009 - 2010

- Assisted professor in teaching Biomaterials and Cell Mechanics for undergraduate class. Prepared lectures, exams, homework assignments, and answer keys; manage graders.

- **Advisor and Mentor**, Biomedical Engineering, Yonsei University, Korea 2009 - 2010
  - Directed government-supported Research and Education program for a group of 5 GangWon science high school students (Project title: The Effects of Cell Movement on Bone Formation) and Designed experimental schedule and give students advices to problem solve the project work.

AWARDS AND HONORS

- Mogam Science Scholarship for 2016
- Fulbright Graduate Study Award in the fields of Science and Engineering for 2012-2014
- Teaching Assistant scholarship, Biomedical Engineering, Yonsei University, Korea 2009 - 2011
- Government Supported-Brain Korea 21 Fellowship, Biomedical Engineering, Yonsei University, Korea 2009 - 2011
- Best Paper Award, Undergraduate Thesis Competition, Biomedical Engineering, Yonsei University, Korea - Paper Title: "Optical Tweezers for Force Measurements" 2008
- Government Supported-Nuri Scholarship for the highest GPA, Yonsei University, 2006 - 2008
- Honors students for the highest GPA, Yonsei University, Korea 2005 and 2008

PUBLICATIONS

O. H. Jeon, L. M. Panicker, Q. L, J. J. Chae, R. A. Feldman, J. H. Elisseeff. "Human iPSC-derived osteoblasts and osteoclasts together promote bone regeneration in 3D biomaterials", *Scientific Report*. 2016, 26(6).

O. H. Jeon, J. H. Elisseeff, "Orthopedic tissue regeneration: cells, scaffolds, and small molecules", *Drug Delivery and Translational Research*. 2016, 6(2):105-20.

C. Kim, L. Shores, Q. Guo, A. Aly, ***O. H. Jeon***, D. H. Kim, N. Bernstein, R. Bhattacharya, J. J. Chae, K. J. Yarema, and J. H. Elisseeff. "Electrospun Microfiber

Scaffolds with Anti-Inflammatory Tributanoylated N-Acetyl-d-Glucosamine Promote Cartilage Regeneration", *Tissue Engineering Part A*. 2016, 22(7-8): 689-697.

C. Kim+, ***O. H. Jeon*** +, D. H. Kim, J. J. Chae, L. Shores, N. Bernstein, R. Bhattacharya, J. M. Coburn, K. J. Yarema, J. H. Elisseeff, "Local delivery of a carbohydrate analog for reducing arthritic inflammation and rebuilding cartilage", *Biomaterials*. 2016, 83:93-101.

O. H. Jeon, S. H. Jeong, Y-M. Yoo, K. H. Kim, D. S. Yoon, C. H. Kim, "Quantification of temporal changes in 3D osteoclastic resorption pit using confocal laser scanning microscopy", *Tissue Engineering and Regenerative Medicine*, 2012, 9(1):29-35

O. H. Jeon, Y-M Yoo, K. H. Kim, C. R. Jacobs, C. H. Kim, "Primary Cilia-mediated Osteogenic Response to Fluid Flow Occurs via Increases in Focal Adhesion and Akt Signaling Pathway in MC3T3-E1 Osteoblastic Cells", *Cellular and Molecular Bioengineering*, 2011, 4(3):379-388

C-H. Kim, D-G. Woo, J-H. Park, ***O. H. Jeon***, S-H Lee, C. H. Kim, D-S. Yoon and H-S. Kim, "Mechanical analysis of knee chondrocyte on hormone efficiency of growing rat using atomic force microscopy", *Tissue Engineering and Regenerative Medicine*, 2010, 7(4):381-387

S. Park, ***O. H. Jeon***, C. H. Kim, H. S. Kim, K. J. Chun, D. H. Lim, "Development and validation of animal model for study of metastatic bone tumor", *Tissue Engineering and Regenerative Medicine*, 2010, 7(1):16-23

J. H. Kwag, ***O. H. Jeon***, D. Y. Kang, H. Ryu, K. H. Kim, B. J. Jung, C. H. Kim, "Effect of low-energy laser irradiation on the proliferation and gene expression of myoblast cells", *Journal biomedical engineering research*, 2010, 31(1):81-86

S. Park, ***O. H. Jeon***, C-Y. Ko, C. H. Kim, H. S. Kim, K. J. Chun, D. H. Lim, "Longitudinal alterations of microarchitecture and mineralization distribution on trabecular bone due to metastatic bone tumor", *Journal biomedical engineering research*, 2009, 30(5):444-481

Patents and patent applications

R-M. Laberge, J. Campisi, A. Davalos, M, Demaria, N, Davi, A. P. Vasserot, J. D. Baker, G. B. Childs, L. J. Kirkland, T. Tchkonia, J. V. Deursen, Y. Zhu, J. Elisseeff, C. Kim, ***O. H. Jeon***. "Methods and compositions for killing senescent cells and for treating senescence-associated diseases and disorders" 2016, U.S.A. International patent appl. PCT/US2015/013387

INTERNATIONAL PRESENTATIONS

O. H. Jeon, C. Kim, S. Rathod, A. Vasserot, R.-M. Laberge, J. Campisi, and J. H. Elisseeff, "Clearance of senescent cells prevents the development of post-traumatic osteoarthritis", International Cartilage Repair Society, Sorrento, Italy, Sep 23-27, 2016

O. H. Jeon, L. M. Panicker, R. A. Feldman, J. H. Elisseeff, "Well-orchestrated Coupling Of Osteoblast To Osteoclast Derived From Human iPSCs Promotes Bone Regeneration", Orthopedic Research Society, Orlando, U.S.A., Mar 5-8, 2016

O. H. Jeon, L. M. Panicker, R. A. Feldman, J. Elisseeff, "3D Co-culture of Monocytes/macrophages and Mesenchymal Stem Cells Derived from Human Induced Pluripotent Stem Cells for Bone Tissue Engineering", TERMIS-WC, Boston, U.S.A., Sep 8-11,2015

O. H. Jeon, L. M. Panicker, R. A. Feldman, J. Elisseeff, "Engineering bone substitute to modulate bone homeostasis with biomaterial using human induced pluripotent stem cells", TERMIS-AM, Washington D.C., U.S.A., Dec 13-16, 2014

O. H. Jeon, Y.-M. Yoo, C. H. Kim, "The role of focal adhesion in primary cilia-mediated mechanotransduction in MC3T3-E1 pre-osteoblastic cells", ASBMR, Toronto, Canada, Oct 15-20, 2010

O. H. Jeon, Y.-M. Yoo, C. H. Kim, "Formation of focal adhesion mediates primary cilia-involved mechanotransduction in MC3T3-E1 pre-osteoblastic cells", WMICS, Kyoto, Japan, Sep 8-11, 2010

O. H. Jeon, J. H. Kwag, Y.-M. Yoo, C. H. Kim. "Primary cilia-mediated

mechanotransduction in bone via focal adhesion", 8th international conference on bone and mineral research, April 16-19, Beijing, China, 2010

O. H. Jeon, S. H. Lee, D. W. Kim, C. H. Im, S. W. Lee, D. S. Yoon, C. H. Kim. "Quantification of osteoblasticresorption pit volume using AFM", 4th ICEM, Nov 18-20, Singapore, 2009